Control of Hand Transmitted Vibration through Development and Analysis of a Human Hand-Arm-Isolator Model

Thomas Cherian

A Thesis
in
The Department
of
Mechanical Engineering

Presented in Partial Fulfillment of the Requirements
for
the Degree of Master of Applied Science
at
Concordia University
Montreal, Quebec, Canada

March 1994

ISBN 0-315-90826-2

Canada

Abstract

Control of Hand Transmitted Vibration through Development and Analysis of a Human Hand-Arm-Isolator Model

Thomas Cherian

The operators of hand-held power tools are exposed to high levels of hand-transmitted vibration arising from the tool-workpiece interaction. Prolonged exposure to such vibration has been related to many occupational, neural and muscular disorders. The most severe symptom of prolonged exposure to hand-transmitted vibration is the Vibration Induced White Finger (VWF) disease. In this thesis, the tool vibration transmitted to the operator hand and arm are investigated through analytical and experimental means. The human hand-arm system subjected to longitudinal tool vibration is characterized by an in-plane dynamical system model with five-degrees of freedom. The parameters of the bio-mechanical hand-arm vibration model are identified from the measured vibration transmitted to different locations of the hand-arm system. A complex eigenvalue analysis is performed to identify the damped natural frequencies of the human hand-arm. The deflection modes of the human-arm, derived from the modal analysis, are discussed to enhance an understanding of the bio-dynamic response of the hand-arm. The analytical models, derived for light finger grip and high palm grip are validated using the measured data. The influence of grip type, grip force and elbow angle on the hand-transmitted vibration is investigated for deterministic sinusoidal excitation. The hand-transmitted vibration under field measured stochastic excitations is evaluated, and assessed using proposed dose-response relationship. The analysis revealed that the hand-transmitted vibration can exceed the safety limits and pose a high risk of acquiring VWF. A vibration isolator, based upon the concept of energy flow divider, is proposed and analyzed for its potential benefits in reducing the hand-transmitted vibration. An assessment of the

coupled hand-arm-isolator model revealed that the proposed isolator effectively reduces the health and safety risks associated with the hand-transmitted vibration. The weighted acceleration of hand-transmitted vibration reduces by 40% and 22% for light finger and high palm grip conditions, respectively. The corresponding levels of vibration transmitted to the fore-arm and elbow, however, increase.

Acknowledgments

The author is sincerely grateful to his supervisors Dr. Subhash Rakheja and Dr. R.B. Bhat for their enthusiastic guidance and continuous encouragement during the course of this work.

The help and assistance provided at various stages of this work by Dr. Raghu Gurram is greatly acknowledged. Also I would like to thank my colleagues and friends, especially Mr. M. Balike, Mr. Gegi George and Mr. Suresh Kumar for their help and useful discussions throughout this work.

The Financial support by the Mechanical Engineering Department at Concordia University through the Natural sciences and Engineering Research Council and Institut de recherche en santé et en Sécurité du travail du Québec grants is further acknowledged.

Last but not least, I would like to thank my family members for their moral support throughout the course of this investigation.

Contents

List of Figures

List of Tables

Nomenclature

X_h	Vertical direction of vibration
Y_h	Lateral direction of vibration
Z_h	Longitudinal direction of vibration
DOF	Degrees of freedom
VWF	Vibration White Finger
M_i	Mass
K_i	Stiffness coefficients
C_i	Damping coefficients
K_{t_i}	Torsional Stiffness coefficients
C_{t_i}	Torsional Damping coefficients
$x_i, \dot{x}_i, \ddot{x}_i$	Displacement, velocity and acceleration response in X_h direction
$z_i, \dot{z}_i, \ddot{z}_i$	Displacement, velocity and acceleration response in Z_h direction
$z_o, \dot{z}_o, \ddot{z}_o$	Displacement, velocity and acceleration excitation in Z_h direction
$\theta_i, \dot{\theta}_i, \ddot{\theta}_i$	Pitch rotational response of displacement, velocity and acceleration
J_c	Effective moment of inertia of the upper arm about the c.g
l	Total length of the upper-arm
l_1	Distance of c.g of the upper-arm from the elbow joint
γ	Inclination of the upper-arm with respect to horizontal axis passing through the fore-arm
kg	Kilogram
ISO	International Standards Organization
ϕ	Transmissibility phase angle
$E(\overline{\chi})$	Objective function for the minimization of the transmissibility error
T_i	Analytical transmissibilities
T_{m_i}	Experimental transmissibilities
ω_i	Discrete frequencies

w_j	Weighting factors used for the optimization of the transmissibility error function
ω_{n_i}	Undamped natural frequency
ω_{d_i}	Damped natural frequency
ζ_i	Damping ratio
λ_i	Eigenvalues
$[M]$	Mass matrix
$[C]$	Damping matrix
$[K]$	Stiffness matrix
$[\phi]$	Modal matrix
q_i	Modal co-ordinates
H_i	Transformed force vector
RMS	Root mean square
$\{h(j\omega)\}$	Complex transmissibility vector
k_j	Weighting factors proposed by ISO
$a_{h,j}$	Weighted acceleration at the hand in the j^{th} octave band
$S_0(\omega)$	RMS acceleration of the handle vibration
$\{S_r(\omega)\}$	Vector of generalized RMS acceleration response of the HAV model
$\{S_p(\omega)\}$	Vector of RMS acceleration response of the shoulder joint
M^*	Mass of the flow divider
K^*	Total stiffness value of the flow divider system
C^*	Total damping value of the flow divider system
z^*	Response of the flow divider mass
α_i	Weighting factors used for the optimization of the flow divider parameters
W_i	Overall weighted accelerations
$F(\overline{X})$	Objective function for the tuning of flow divider parameters

Chapter 1

Introduction, Literature Review and Thesis Objectives

1.1 Introduction

Operators of hand-held power tools are exposed to high levels of vibration, predominant in a wide frequency range of 10-2000 Hz, arising from the dynamic interactions between the tool and the workpiece. These high amplitude vibrations are primarily absorbed by the hands and arms of the operators. Prolonged exposure to such hand-arm vibration has been related to many occupational health disorders, such as tingling, numbness and blanching of the fingers. The Epidemiological studies have established a strong relationship between the exposure to hand-transmitted vibration and white finger attacks, often referred to as "Vibration Induced White Finger (VWF)" or hand-arm vibration syndrome or as the "Traumatic Vasospastic Disease (TVD)".

The hand-arm vibration syndrome is related to many occupational, neural and muscular disorders which develop in a gradual manner over the years of exposure. The Vibration White Finger (VWF) is perhaps the most severe symptom caused by prolonged exposure to vibration. The VWF disease among the operators is initially observed as

intermittent tingling and numbness of the fingers. The intermittent tingling is followed by an attack of finger blanching confined to the tips of one or more fingers with continued exposure to hand-transmitted vibration. With further occupational exposure to the vibration, the finger blanching propagates to the base of the hand. An attack usually lasts 15-60 minutes but in advanced cases it may last for 1-2 hours. Continued exposure to vibration in the advanced stages causes nutritional changes in the finger pulps leading to the formation of areas of skin necrosis at the finger tips.

The dose-response relations developed to study the health risks associated with hand-arm vibration have established that the risk of occurrence of VWF disease is directly related to the dose or magnitude of vibration and the years of exposure. While many studies have been carried out to reduce the magnitude of hand-transmitted vibration, considerable research efforts have been mounted to establish hand-arm vibration syndrome etiology, dose-response standards and bio-dynamic response characteristics of the human hand-arm. The relevant studies on symptoms and effects of prolonged exposure to hand-arm vibration, characterization of hand-transmitted vibration and attenuation of transmitted vibration, are briefly reviewed in the following sections.

1.2 Effects of Hand-Transmitted Vibration

It has been established that prevalence of cumulative trauma disorders among the power tool operators is correlated with the prolonged vibration exposure of the hand-arm. The term **Hand-Arm Vibration Syndrome** is often used collectively for the symptoms associated with prolonged and repeated exposure to hand tool vibration. These symptoms include bone alterations, joint deformations, neurological disturbances and soft tissue damage which restrict the blood flow to the affected area.

Vibration Induced White Finger

Operators of chain saws, rock drills, chipping hammers, pedestal grinders and of many other power tools and machines have long been aware of tingling, numbness and blanching of their fingers. Episodes of *white fingers*, *dead fingers*, or *dead hand* were first reported in literature between 1911 and 1920, in studies by Loriga [1], Hamilton [2], Rothstein [3] and Leake [4]. The spasm of the arteries in the fingers was correctly attributed to vibration of the rotary-percussive air-driven drills commonly used by stonecutters and rock miners at that time. The close association between white finger attacks and vibration entering the hands was responsible for the introduction of the term *Vibration Induced White finger* (VWF), though the condition is still known as *Traumatic Vasospastic Disease* (TVD) in parts of Europe.

The first symptoms of the disease are intermittent tingling and numbness of the fingers followed later by an attack of finger blanching confined in the first instance to a finger tip and subsequently, with further vibration exposure, extending to the base. The provocative agent is cold but there are other factors involved in the trigger mechanism, e.g. central body temperature, metabolic rate and emotional state [5]. With further vibration exposure the number of blanching attacks is reduced to be replaced by a darkish, cyanotic appearance of the digits leading to nutritional changes in the finger pulps and finally small areas of skin necrosis at the finger tips.

Peripheral Neural and Vascular Effects

Neurological disorders, such as disturbances in the sense of touch, increased sensitivity to cold, as well as ulnar paresis and paralysis, acroparesthesia accompanied by cramp-like pains in the extremities and fatigue have been observed in workers exposed to vibration. The carpal tunnel syndrome, usually attributed to compression of the median

nerve, has been associated with the use of vibrating hand tools, and position of the hand and wrist while operating the tool [6,7]. Workers using hand held vibration tools commonly experience numbness and pain in the arms and hand which are also considered to disturb operator's sleep rhythm [8]. The earliest signs of peripheral vascular changes in the hand-arm system are observed by the attacks of fingertip blanching. These attacks usually occur during exposure to cold [9,10]. With the continued exposure to vibration, the frequency and severity of episodes of white finger increase until the blanching extends to the base of the fingers. A finger blanching may then also occur in the warm weather. The time between the first use of vibrating tools and the first appearance of episodic finger blanching is designated as the latent period. This period appears to vary with intensity of vibration, and other factors such as hand grip force, push-pull force, hand-arm posture and protective gear [10]. During VWF attacks, blood flow to the affected segments of the fingers is reduced by the contraction of the muscles, causing severe pain.

Effects on Muscle Force and Muscle Fatigue

Teleky [11] has reported degeneration in the muscle tissues in the hands of workers using vibratory tools. Similar studies conducted by Banister and Farkkila [12,13] showed that the use of vibratory tools causes significant decrease in manipulative skills and grip strength. Taylor [5] reported that due to repeated ischemic attacks in advanced cases, touch and temperature sensation are impaired. The operators thus experience a loss of dexterity and an inability to do fine work.

Effects on Bones and Joints

Radiographic studies of the wrist, elbow, shoulder and the cervical vertebrae of workers with weakened grip revealed abnormal findings in the elbows [14]. Kumlin *et*

al. [15] observed vacuoles in the carpal and metacarpal bones and phalanges in workers who had been exposed to chain saw vibration over long periods of time. In a study of Italian ship yard workers by Bovenzi [16] about 31% of 169 caulkers who worked with vibrating tools were reported to have bone cysts or vacuoles. It is reported that these injuries influence the performance and productivity of the worker and often force the operators to change occupation.

Effects on the Central Nervous System (CNS)

Although the hand-arm vibration syndrome is characterized by the vascular and peripheral nervous symptoms, the evidences of nervous disorders indicating involvement of central nervous system among the operators of vibrating tools have also been reported [17]. Griffin [18] reported that hand-arm vibration can impair CNS function through damage to the autonomic centers in the brain. The symptomology alleged to be associated with vibration induced disturbances of the central nervous system, includes anxiety, depression, insomnia, headache, palm sweating, irritability and emotional instability [19]. These signs and symptoms, derived from the subjective studies have not been objectively assessed and are not considered specific to a single stressor, such as vibration.

1.2.1 Epidemiological Studies

Of the estimated 8 million vibration exposed workers in the United States approximately 7 millions are exposed to whole body and 1 million are exposed to hand-arm vibration [20]. In Canada an estimate made by National Research Council of Canada [21] indicates that approximately 200,000 workers are exposed to hand-arm vibration. Numerous cross-sectional and longitudinal epidemiological studies of workers using hand held vibrating tools have been conducted in several countries all over the world. The cross

sectional studies involved examination of a group of workers using hand-held vibrating tools in an industry at one particular time to determine the proportion of workers with HAV syndrome, while the longitudinal studies examined a group of workers at more than one point in time. Traditionally cross-sectional and longitudinal epidemiological studies have concentrated on three classes of tools: (a) pneumatic tools (chippers, grinders, jack-hammers, riveters, drills etc.); (b) electrically operated tools (sanders, pedestal grinders, swagers, impact hammers, etc.); and (c) chain saws. Results of these studies indicated VWF prevalence rates ranging from 6 % to 100 %. Based on clinical observations and subjective evaluations, the severity of the VWF was characterized by a grading system in the Table1.1 [5]. Of the various stages indicated, the VWF stages 2, 3 and 4 have been related to interference with work, social activities and hobbies. Subjects with symptoms in these stages usually are advised to change their occupation. In summary epidemiological studies provide ample evidence that the use of vibrating producing tools is associated with the development of HAV syndrome.

1.2.2 Factors which Influence the Severity of Hand-Arm Vibration

The magnitude, frequency range and direction of hand-transmitted vibration are strongly related to many tool and operating factors. The results of numerous field measurements of hand-transmitted vibration characteristics, summarized by Gurram [22], reveal that the magnitude of acceleration levels of different tools vary in the 10-2014 m/s^2 range. The dominant frequencies of vibration of different tools were observed in the 25-320 Hz range, while the vibration occurred in all the three orthogonal axes (X_h, Y_h, Z_h) specified in the ISO 5349 [23]. Brammer and Taylor [24] identified various physical, bio-dynamic and individual factors that affect the hand-transmitted vibration and the severity of exposure. These factors are summarized in the Table 1.2 [24].

Table 1.1: Stages of Raynaud's phenomenon [5]

Stage	Condition of Digits	Work and Social interference
O	No blanching of digits	No complaints
OT	Intermittent tingling	No interference with activities
ON	Intermittent numbness	No interference with activities
1	Blanching of one or more fingertips with or without tingling and numbness	No interference with activities
2	Blanching of one or more fingers with numbness.Usually confined to Winter	Slight interference with home and social activities
3	Extensive blanching frequent episodes summer as well as winter	Definite interference at work, home and with social activities. Restriction of hobbies
4	Extensive blanching. Most fingers.Frequent attacks	Occupation changed to avoid further vibration exposure because of severity of signs and symptoms

Griffin [25] presented a list of extrinsic and intrinsic variables that influence an individual's mechanical and subjective response to hand induced vibration. The extrinsic variables include frequency of vibration, amplitude of vibration, time history of vibration exposure, direction of vibration, type of grip used to clasp a vibrating tool, tightness of grip and clothing. The intrinsic variables include body size, body posture and muscle

tension etc.. Reynolds [26] concluded that the extrinsic variables strongly influence the operator response to vibration exposure.

Table 1.2: Summary of factors affecting hand-transmitted vibration [24]

Physical	• Dominant vibration amplitudes entering hand. • Dominant vibration frequencies entering hand. • Years of employment involving vibration exposure. • Total duration of exposure each work day. • Temporal pattern of exposure each work day. • Dominant vibration direction relative to the hand. • Non occupational exposure to hand.
Biodynamic	• Hand grip forces. • Surface area, location and mass of parts of the hand in contact with source of vibration. • Posture. • Other factors influencing the coupling of vibration into the hand (e.g. texture of handle etc.)
Individual	• Factors influencing source intensity and exposure duration (e.g. state of tool maintenance, operator control of tool,machine work rate, skill and productivity). • Biological susceptibility to vibration. • Vasoconstrictive agents affecting the peripheral circulation (e.g. smoking, drugs, etc.). • Predisposing disease or prior injury to the fingers hands. • Hand size and weight.

The determination of vibration dosage and exposure requires measurement of vibration amplitudes and frequencies entering the hand from all directions as a function of time for hand grip forces in well defined postures. The monitoring of all these factors for each worker is clearly impractical. It is therefore necessary to reduce the problem to manageable proportions, by identifying those factors that significantly contribute to the severity of vibration exposure.

1.2.3 HAV Standards

In view of the severe effects of hand-arm vibration, efforts have been mounted to develop standards to assess the vibration dosage and the severity of hand-transmitted vibration. These efforts however, have achieved only moderate success due to lack of understanding of the etiology of VWF. While the relationship between the vibration dosage associated with vibration intensity, frequency and cumulative exposure duration, and the symptoms are not exactly known, certain norms on measurements, evaluations and reporting procedures have been established. Figure 1.1 illustrates the hand-arm reference co-ordinate system, outlined in ISO 5349 [23], for reporting the HAV data. All standards suggest that vibration exposure be expressed in terms of rms acceleration in m/s^2 in the 1/3 octave band spectrum with center frequencies ranging from 6.3 Hz to 1250 Hz. Figure 1.3 shows the threshold values recommended by International Standard Organization (ISO) 1986, British Standards Institute (BSI) 1987, American National Standard Institute (ANSI) 1986 and American Conference of Governmental Industrial Hygienist (ACGIH) 1990. It is considered that acceleration levels that fall below the recommended curves for a specified duration of exposure are considered to be acceptable.

The International Standards Organization(ISO) has proposed exposure limits for hand-transmitted vibration based upon the data from both practical experience and laboratory experimentation, derived primarily from subjective human response to hand-

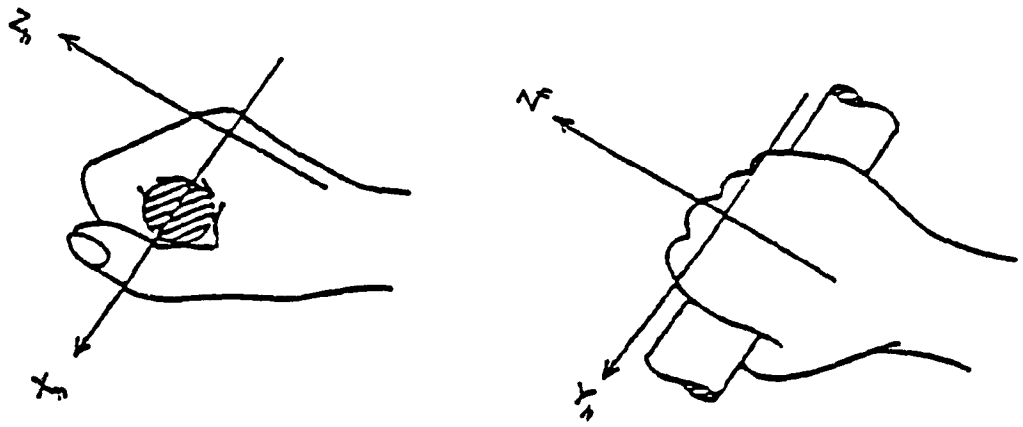

Figure 1.1: Hand-arm vibration coordinate system (ISO 5349) [23]

transmitted vibration and mechanical behaviour of the hand-arm system. The exposure limits are specified in terms of vibration acceleration, daily exposure time and direction of vibration relative to the hand as shown in Figures 1.1 and 1.2. The recommended exposure limits represent the safe daily occupational exposure to hand-transmitted vibration in terms of rms acceleration measured in one-third octave band spectra.

Using the results of several epidemiological studies, ISO 5349 [23], proposed a dose-response relationship in terms of frequency weighted energy equivalent acceleration for a period of 4 hrs. The relationship was derived from the results of 40 studies of populations of workers exposed to hand-transmitted vibration in their occupations for periods of up to 25 years. Each study involved workers who normally work all day with only one type of power tool or an industrial process throughout the year.

The dose-response relationship, presented in Figure 1.4, describes the number of years of exposure to hand-transmitted vibration that may lead to the onset of vascular

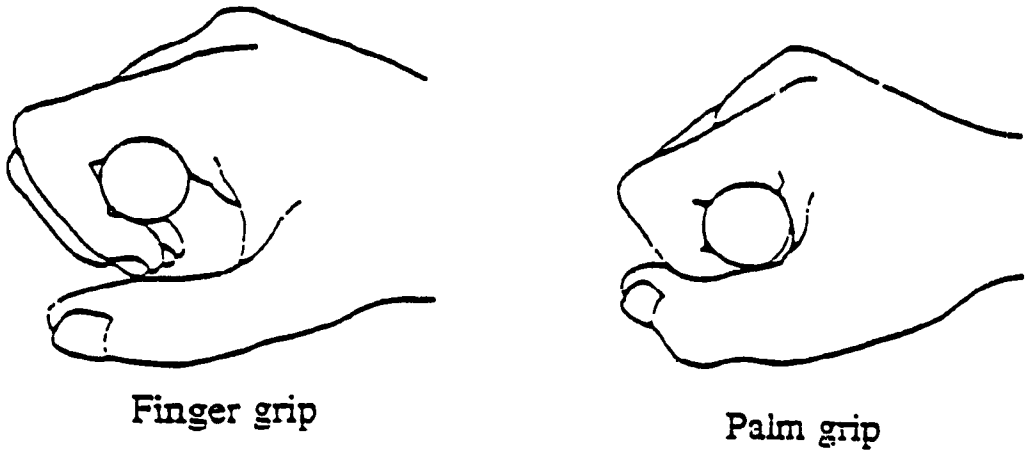

Figure 1.2: Different types of grips

symptoms, characterized by finger blanching, as a function of rms weighted acceleration. The dose-response relationship for different percentile of population is also summarized in Table 1.3. The dose-response relationship, as an example, reveals that 4 hours daily exposure to hand-transmitted vibration of 10 m/s^2 weighted rms acceleration, will cause HAV syndrome among 10% of the exposed population in a period of less than 3 years or among 20% of the population in nearly 4 years.

1.2.4 HAV Models

The severe health and safety risks posed by prolonged exposure to hand held power-tool vibration have prompted many research efforts to enhance an understanding of the vibration response characteristics of the hand-arm system. The epidemiological studies have identified the high prevalence rates of vibration syndrome among the operators of power tools, typical offending tools and their vibration levels [27,28]. Although

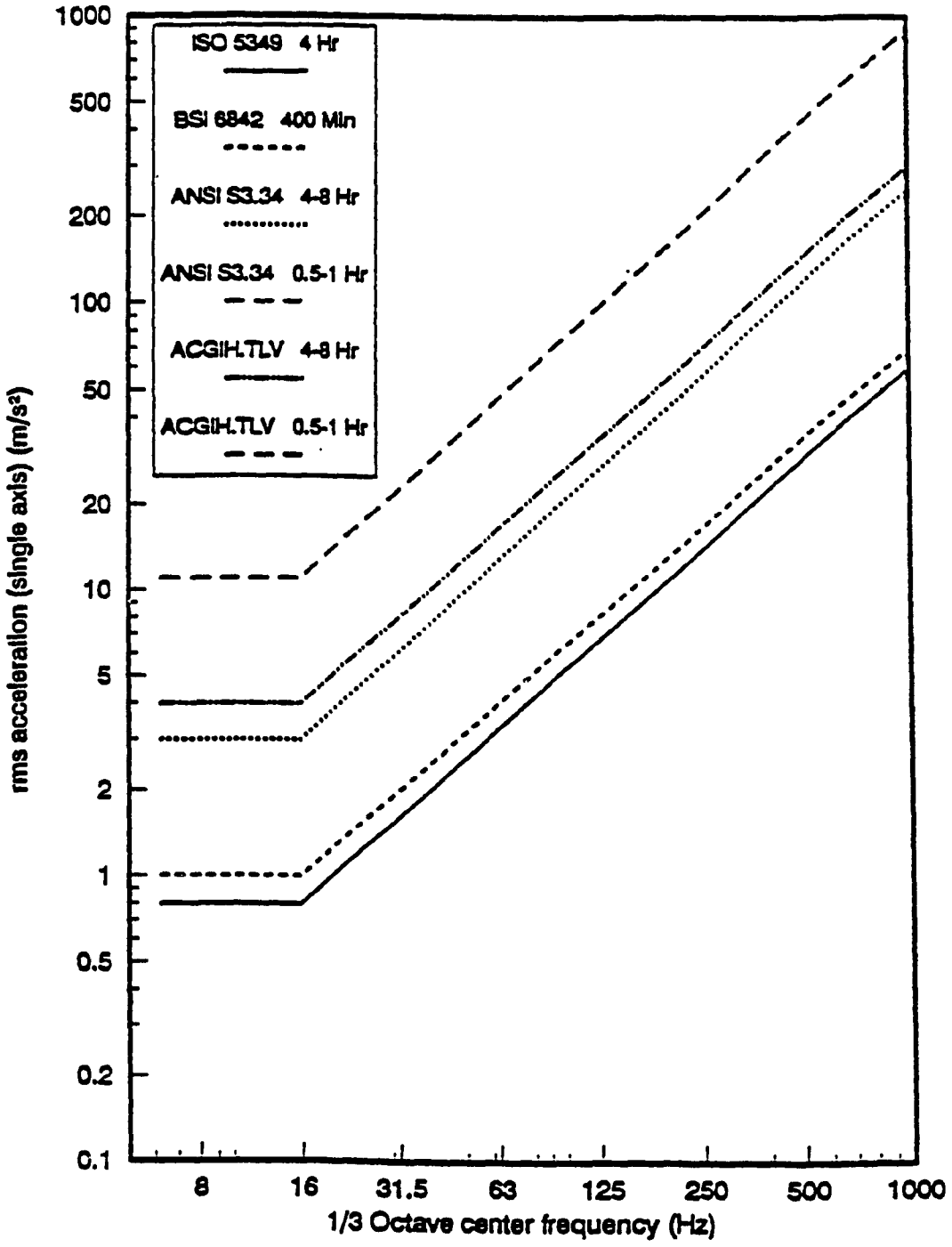

Figure 1.3: Hand-arm vibration standards proposed by different organizations [22]

Table 1.3: Exposure time in years for different percentile of a population for various weighted accelerations [23]

Weighted acceleration $m.s^{-2}$	Percentile of population				
	10	20	30	40	50
	Exposure time, years				
2	15	23	> 25	> 25	> 25
5	6	9	11	12	14
10	3	4	5	6	7
20	1	2	2	3	3
50	< 1	< 1	< 1	1	1

many subjective and objective clinical studies have identified various HAV symptoms, the primary injury mechanisms are not yet well known. The engineering studies have concentrated on design of effective protective devices and tools [29,30]. All the studies however, have emphasized the need to enhance a thorough understanding of the bio-dynamic response behaviour of the hand-arm system.

Many analytical and experimental studies have thus been undertaken to characterize the vibration response behaviour of the human hand-arm system. The hand-arm system in majority of these studies has been characterized by its impedance or apparent mass properties. Various lumped-parameter mechanical impedance models, ranging from simple single degree-of-freedom (DOF) to many DOF, have been developed. Majority of these HAV models are derived from the driving-point impedance measurements performed in the laboratory, and do not represent the bio-mechanical properties of the human hand-arm. While the impedance models provide considerable insight into the influence of various design and operating factors, such as grip force, handle size, direction and magnitude of vibration, push-pull force and posture, these models fail to characterize the vibration transmitted to the hand and the arm.

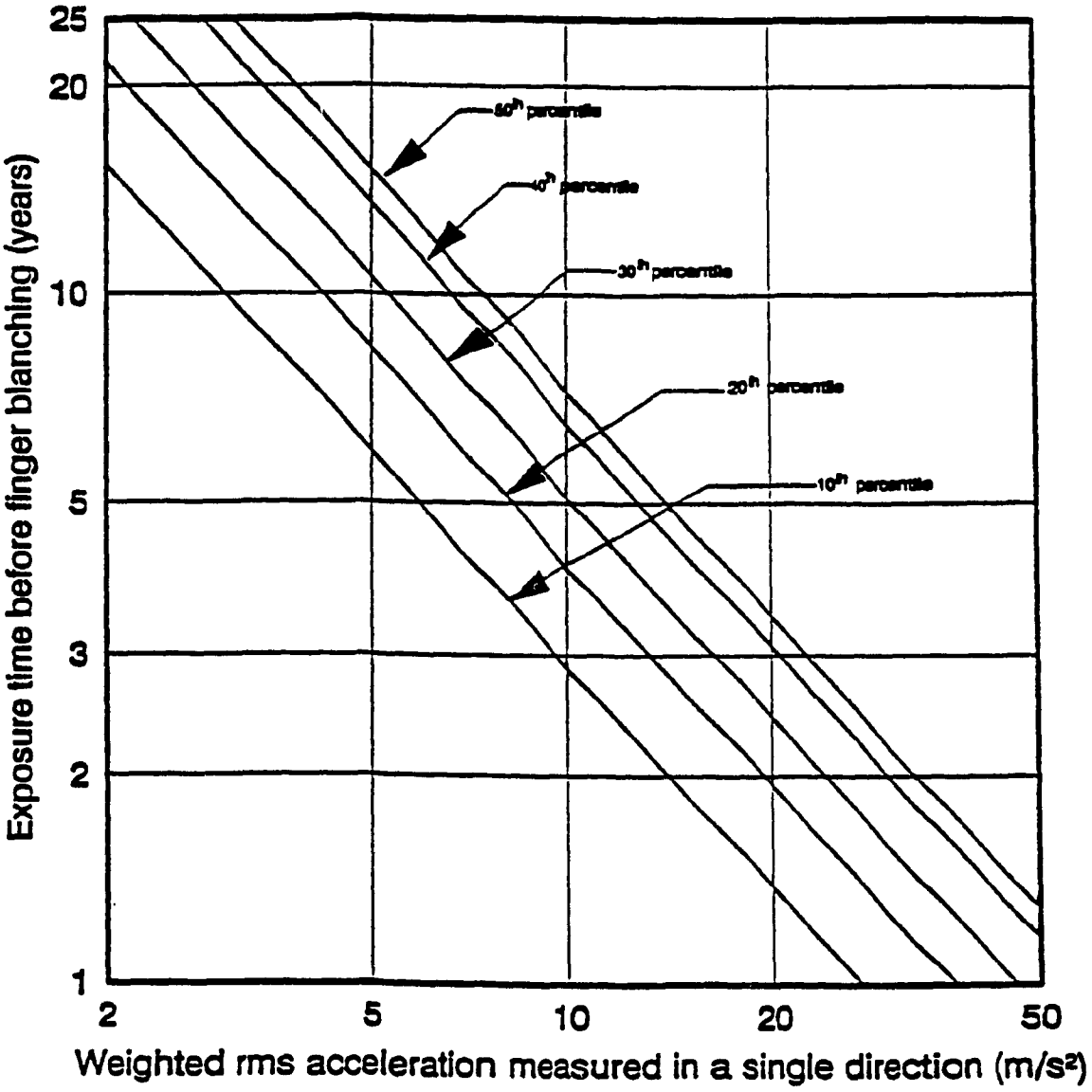

Figure 1.4: Exposure time for different percentile of a population group exposed to vibration in three coordinate axes [23]

The direct relationship between the severity of HAV syndrome and the characteristics of hand-transmitted vibration have prompted a strong desire to (i) enhance an understanding of the vibration transmission characteristics of the hand-arm system; and (ii) design vibration attenuating protective devices and tools. Although many studies have been performed to assess the vibration isolation performance of protective devices, only limited efforts have been mounted to investigate the vibration transmission characteristics of the hand-arm system [22,31,32,33,34]. Sub-mininature accelerometers and laser based sensors have been employed to measure the vibration transmitted to the hand, fore-arm and upper-arm [22,31]. The vibration transmitted to various locations of the hand-arm system have been measured on a cadaver arm by Abrams [35,36], and live subjects by Gurram [22] and Reynolds and Angevine [31]. Lumped parameter models with linear restoring and dissipative properties have been proposed to assess the vibration attenuation performance of protective gloves and to derive the hand-transmitted vibration [37]. These models, similar to the mechanical impedance models, do not represent the bio-mechanics of the human hand-arm system and thus cannot be used to derive the vibration transmitted to different segments. Table 1.4 summarizes some of the mechanical impedance and transmissibility models presented in the literature.

1.2.5 Control of Hand-Arm Vibrations

High levels of hand-held power tool vibration, high rates of prevalence of VWF symptoms among the exposed workers and severe health effects, have all prompted a strong desire to reduce the magnitudes of hand-transmitted vibration. The control of hand-transmitted vibration in general, is achieved through reduction of the source vibration and the use of vibration isolators. The reduction in vibration at the source can be realized by operating the tool at suitable speed, maintaining the tool and the drive, and through improved design of the drives [45]. Attenuation of hand-transmitted vibration is primarily attained using two methods. In the first method, the tool handle is isolated from

Table 1.4: Summary of hand-arm vibration models

Researcher	Type of Model	Measurements used for developing the model	Directions considered (type of grip)	Grip force used	Frequency range (Hz)
Abrams [38]	One DOF lumped-parameter	Driving point impedance	X_h, Y_h, Z_h (Palm)	16.0 N	(70-1670)
Reynolds [39, 40]	One,three and four DOF lumped parameter	Driving point impedance	X_h, Y_h, Z_h (Palm & Finger)	8.9,25.4 and 35.6 N	(20-2000)
Mishoe [41]	Three dof lumped-parameter	Driving point impedance	X_h, Y_h, Z_h (Palm)	13,27 and 40 N	(30-1000)
L.A.Wood [42]	Lumped as well as distributed - parameter	Driving point impedance	X_h (Palm)	not known	(30-1000)
Meltzer [43]	Three DOF lumped-parameter	Driving point impedance	Z_h (Palm)	not known	(10-500)
Fritz [44]	Nine dof Bio-mechanical lumped-parameter	Driving point impedance	Z_h (Palm)	not known	(20-100)
Gurram [22]	2 DOF lumped parameter	Transmissibility	X_h (Palm)	10,25 and 50 N	(10-500)
Gurram [22]	Three and Four DOF lumped parameter	Driving point impedance	X_h, Y_h, Z_h (Finger & Palm)	10,25 and 50 N	(10-1000)

the vibrating source, while the hand is isolated from the vibrating handle in the second method [30,35,46]. Tool handle isolators, successfully integrated within certain tools, have proven to be effective in attenuating the handle vibration [35]. The general implementation of these isolators, however has been limited due to design complexities of many tools and associated costs [46]. Alternatively, handle grips and anti-vibration gloves have been proposed to isolate the hand from the vibrating handle.

The vibration attenuation properties of different types of visco-elastic glove materials have been investigated in many studies [30,47,48]. Isolators, comprising rubber or metal springs, are currently being used by the operators of chain saws [49] and many

other hand-held power tools [45, 50]. It has been established that these isolators effectively attenuate the high frequency vibrations. The low frequency vibration is transmitted to the handle with only little attenuation or amplification in certain cases. A study on vibration transmissibility characteristics of industrial gloves concluded that these gloves do not attenuate vibration to protect the hand from hazardous levels of HAV encountered in the industry [51].

Numerous anti-vibration gloves comprising natural rubber, neoprene, sorbothane, plastic foam, air-filled alveolar, etc. have been commercially developed to isolate the hand from the vibrating handle [30,52,53]. Table 1.5 summarizes the construction of some of the commercially available gloves. The vibration attenuation characteristics of many general purpose and anti-vibration gloves have been investigated through laboratory measurements [22,54].

Rens [54] reported that the gloves # 1,2,3,6 and 10 tend to amplify the hand vibration below 400-500 Hz, and the attenuation approaches 5 db at certain frequencies. These gloves, however, attenuate vibration at higher frequencies with 15-20 db attenuation at 1000 Hz. The vibration amplification of the gloves # 4,5,7 and 9 is not pronounced at frequencies below 250 Hz, and the attenuation at higher frequencies up to 750 Hz is insignificant. The glove # 8 provided amplification of vibration in the 250-1000 Hz frequency range with no attenuation or amplification of vibration below 250 Hz. The glove # 11 was observed to yield amplification of vibration at frequencies below 130 Hz with attenuation increasing progressively at higher frequencies, approaching 25 db at 1000 Hz. The general purpose or anti-vibration gloves are, in general, considered ineffective to attenuate the hand-transmitted vibration. The vibration attenuation performance of the gloves can be improved at the expense of high dexterity loss.

Table 1.5: Characteristics of different gloves [54]

No.	Type of Gloves	Materials	Weight (g)	Thickness (mm)	Dexterity loss
1	Moufle VDP-Thermox-TB	KEVLAR boucle nomex felt lining	38	10	Very high
2	Polysafe Multi	KEVLAR knitting waterproof neopren lining	115	6.5	Very high
3	Winter Monkey Grip 23-193	PVC, foam, cotton	95	5.5	High
4	Seams-Rite/H 20-105	PVC, felt	55	2.5	Low
5	Hycron/M Tric/H 27-600	Nitril rubber,cotton	50	2.5	Medium
6	Crusader 42-325L	Nitril rubber,cotton	68	3	High
7	Therm-a-Grip 44-315M	PVC, felt	60	5	Medium
8	Terrytect Verrier	Boucle+cotton knitting	75	3.5	Low
9	Worker Soudeur Top	Leather, felt	102	6	Very high
10	Safety Robusta Buffle	Leather, cotton	85	3	Medium
11	Cut-Grp Verrier	Natural rubber,cotton	82	3.5	High

1.3 Scope and Objectives of the Dissertation Research

Numerous subjective and objective studies, reviewed in the previous sections, have identified several health risks associated with prolonged exposure to hand-held power tool vibration. The studies on dose-response relationships have demonstrated a strong relationship between the magnitude of hand-transmitted vibration and the onset of VWF symptoms among the operators. It is thus extremely vital to control the levels of hand-transmitted vibration to reduce the health risks associated with operation of

power tools. Although a number of handle and hand isolators have been developed to reduce the transmitted vibration, they have met only marginal success due to difficulties in implementation of handle isolators. The commercially available gloves have been considered ineffective due to their poor vibration isolation performance and associated dexterity loss. The control of hand-transmitted vibration further necessitates an enhanced understanding of the vibration transmission characteristics of the human hand-arm system.

The scope and objectives of this thesis research are:

a. Establish vibration transmissibility characteristics of the human hand-arm through laboratory measurements.

b. Develop a bio-mechanical HAV model and identify the system parameters from the measured data.

c. Perform modal analysis of the HAV model to enhance the vibration response behaviour of the human hand-arm.

d. Evaluate the hand-transmitted vibration characteristics of representative power tools and perform an assessment using the dose-response relationship.

e. Investigate the vibration attenuation performance of a new concept in vibration isolator through development and analysis of coupled isolator-hand-arm model.

f. Determine the optimal parameters of the isolator for the power tool considered and investigate the effectiveness of the isolator.

1.4 Overview of the Thesis

The human hand-arm system characterized by a five-DOF lumped parameter model is described in Chapter 2. The model, comprising the masses due to the hand, fore-arm

and upper-arm and linear visco-elastic properties, is configured to determine the vibration transmissibility characteristics of different segments of the hand-arm. The model parameters are identified from the measured transmissibilities using a curve fitting algorithm based on non-linear optimization technique. The influence of elbow angle on the vibration transmission characteristics is further described.

In Chapter 3, a complex eigenvalue analysis is performed to describe the modal behaviour of the heavily damped hand-arm system. The modal deflection patterns of the hand-arm system are derived from the complex eigenvectors. The deflection behaviour of the human hand-arm system is discussed using the mode shapes. The vibration response of the hand-arm system to deterministic vibration is obtained using the mode summation and numerical integration techniques. The frequency response characteristics of the hand-arm system are derived and discussed.

In Chapter 4, hand-arm model is analyzed for stochastic excitations arising from a power tool. The vibration excitation due to the selected power tool is derived from the field measured data reported in the literature. The hand-arm vibration response characteristics are assessed using the recommended exposure limits, and the severity of hand-transmitted vibration of the selected power tool is discussed. A concept of vibration isolator is proposed and analytically modeled. The coupled hand-arm-isolator model is analyzed for stochastic excitation. A parametric study is performed to select near optimal parameters of the isolator for the selected power tool. The relative performance benefits of the proposed isolator are discussed using the analytical results.

The conclusions drawn and recommendations for the future work are finally described in Chapter 5.

Chapter 2

Development of a HAV Model

The severe nature of hand-transmitted vibration from hand operated tools and associated health hazards due to prolonged exposures have all prompted several experimental and analytical studies on dynamic characterization of the hand-arm system. Various studies have established that the electrical activity of different hand-arm muscles and the health risks are directly related to frequency and magnitude of hand-transmitted vibration [22]. An assessment of power-tool vibration thus necessitates an estimation of the hand-transmitted vibration and a thorough understanding of the vibration transmission characteristics. A study of vibration transmission characteristics can provide vital knowledge related to the HAV response and may contribute to the design of effective vibration isolators. The vibration transmissibility can further provide the vibration levels transmitted to various parts of the hand-arm and their relative response.

The vibration transmissibility characteristics of the hand-arm system have been analyzed through laboratory measurements in only limited number of studies [22,31,32,33,34]. The lack of appropriate sensors, and standardized measurement and assessment procedures have severely limited such studies. Abrams [36] measured the vibration transmissibility of a cadaver arm by mounting the accelerometers directly on the bones. Pyykkö [32] measured the longitudinal (Z_h) vibration transmitted to the wrist, elbow and upper-

arm for excitations in 20-630 Hz frequency range, using miniature accelerometers. The study observed that for a constant grip force the vibration transmissibility characteristics of the hand-arm resemble that of a linear system. Reynolds [31] performed extensive measurements to characterize the vibration transmitted to different locations of the hand-arm, in X_h, Y_h and Z_h directions, under palm and finger types of grips. These studies concluded that vibration excitation at frequencies above 200 Hz remain limited to the hands.

The vibration transmissibility characteristics of the hand-arm system, alternatively, can be determined through development and analysis of an analytical model. An analytical model can be effectively used to assess the performance characteristics of vibration isolators and to investigate concepts in vibration control. Although numerous impedance models have been proposed to characterize the dynamic behaviour of the hand-arm system [22,38,39,42,43,44], only a few attempts have been made to derive vibration transmissibility model [22]. This has been primarily attributed to lack of reliable transmissibility data and the complexities of the human hand-arm. Human hand-arm system is a highly complex non-homogeneous continuous system comprising of visco-elastic properties of muscles, bones, skin etc. Dynamic characterization through an analytical bio-mechanical model necessitates identification of various visco-elastic and inertia properties of the model under typical operating conditions.

Analytical studies on the vibration transmission to the hand-arm system used model parameters that were derived by curve fitting the measured data.Two and three-DOF lumped-parameter models of the hand and the hand-glove system, respectively, have been proposed by Gurram [22] and Griffin [37]. These models do not relate to the bio-mechanical properties of the hand-arm and do not yield the vibration transmitted to different segments of the hand-arm.

In this Chapter, the vibration transmissibility characteristics of the hand-arm system,

measured in the laboratory, are discussed and compared to those reported by Reynolds [31]. The hand-arm system is represented by five-DOF bio-mechanical model and its parameters are identified from the measured data using an optimization based curve-fitting algorithm.

2.1 Development of the Model

Figure 2.1 illustrates the anatomical representation of the human hand-arm. It has been reported that majority of the power tools transmit severe vibration along the (Z_h) direction [60]. An in-plane five-degrees-of-freedom (DOF) model of the hand-arm is thus developed to determine its vibration transmissibility characteristics when subjected to longitudinal (Z_h) handle vibration. Figure 2.2 illustrates the in-plane lumped-parameter model of human hand-arm.

The hand, forearm and upper-arm are represented by lumped masses (m_1, m_2 and m_3) respectively. The visco-elastic properties of skin, muscle, bones etc. are represented by linear restoring and dissipative elements lumped at the joints connecting the different masses, as shown in Figure 2.2. The five DOF of the model include: longitudinal motions of the masses due to hand (z_1), fore-arm (z_2) and upper-arm (z_3) ; pitch rotation (θ_3) of the upper-arm with respect to the elbow joint; and vertical motion (x_3) of the elbow joint with respect to the longitudinal axis passing through the fore-arm. The assumptions and the highlights of the model are described below:

- The masses corresponding to hand and fore-arm are considered to move along the longitudinal co-ordinate depending on a specific posture assumed by the operator.
- The mass due to the upper-arm is considered to be of finite length of 0.298 m equal to the length derived from the 50^{th} percentile of the population of measurements

performed by Dempster [67]. The centre of gravity of upper-arm is assumed to be located away from the elbow joint at a distance of 0.6 times the length of the upper-arm [66,67].

- The visco-elastic properties of the palm or hand-handle interface and the wrist are characterized by combination of linear restoring and dissipative elements.
- The masses of hand, fore-arm and upper-arm are assumed to be 0.6%, 1.6% and 2.7%, respectively of the total mass of the body [66,67]. The total mass of the human body is assumed to be 70 kg, based upon the data reported in [66].
- The moment of inertia with respect to center of gravity of the upper-arm is taken around 0.0149 kg.m^2 based upon the measurements performed by Page[68].
- The upper-arm mass experiences longitudinal, vertical and pitch motions with respect to the longitudinal axis passing through the fore-arm.
- The upper-arm mass is connected to the upper body through the visco-elastic properties of the shoulder joint and the motion of the upper body is assumed to be insignificant.
- The visco-elastic properties of the shoulder joint are represented by the parallel combinations of springs and dampers constrained to move along the vertical (K_4, C_4), longitudinal (K_3, C_3) and pitch (K_{t_1}, C_{t_1}) co-ordinates.
- The visco-elastic properties of elbow joint are described by restoring and dissipative elements constrained to move along the longitudinal (K_2, C_2) and pitch (K_{t_2}, C_{t_2}) co-ordinates.
- The damped torsional springs at the elbow and shoulder joints represent the visco-elastic properties of muscles that develop torques around these joints.
- Pitch moment due to the weight of the upper-arm is considered negligible.

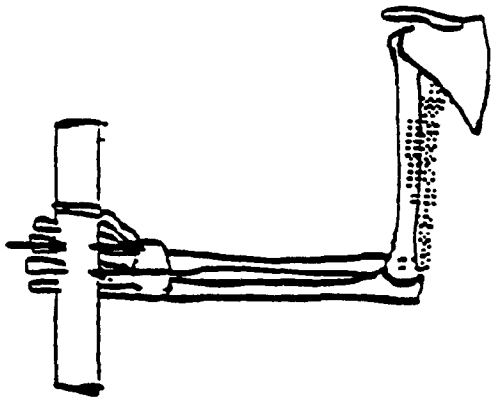

Figure 2.1: Anatomical structure of the hand-arm system [44]

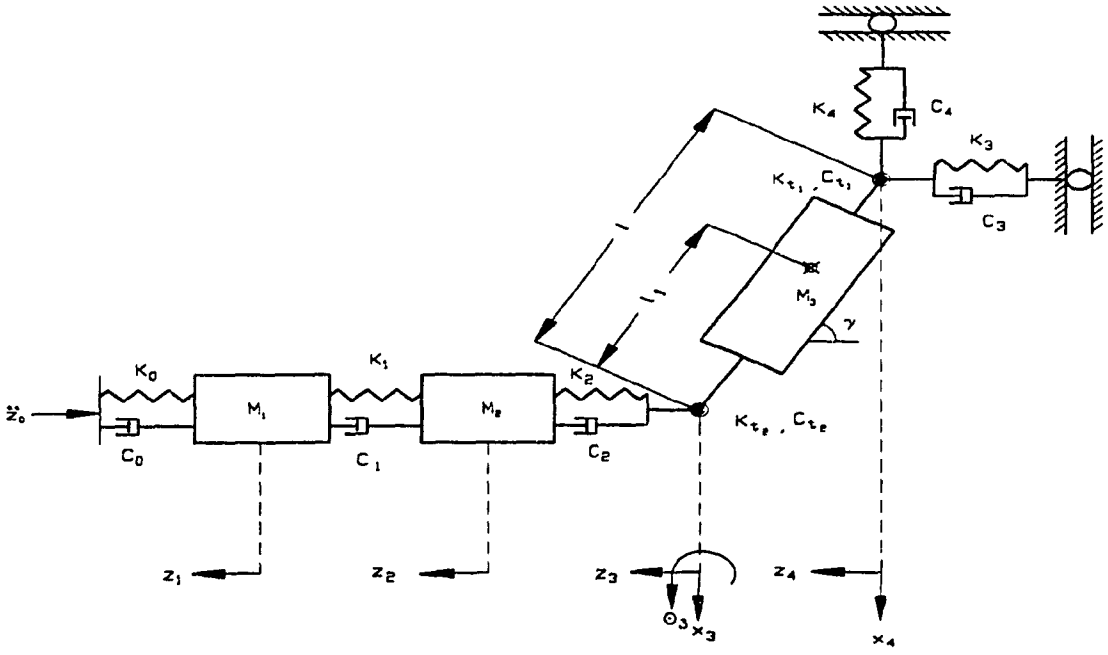

Figure 2.2: Schematic of the five DOF bio-mechanical hand-arm vibration model

- The elbow angle, (γ) is assumed to be constant representing the hand-arm position during a task.
- The handle vibrations along the vertical (X_h) and lateral (Y_h) co-ordinates are assumed to be small compared to those along the longitudinal axis (Z_h).

2.1.1 Equations of Motion

The equations of motion of the lumped-parameter five-DOF bio-mechanical model of the hand-arm, subject to longitudinal vibration of the handle, are derived using Langrange's equations. The coupled differential equations of motion are obtained as:

$$M_1\ddot{z}_1 + C_0\dot{z}_1 + C_1(\dot{z}_1 - \dot{z}_2) + K_0 z_1 + K_1(z_1 - z_2) = C_0\dot{z}_0 + K_0 z_0 \tag{2.1}$$

$$M_2\ddot{z}_2 + C_1(\dot{z}_2 - \dot{z}_1) + C_2(\dot{z}_2 - \dot{z}_3) + K_1(z_2 - z_1) + K_2(z_2 - z_3) = 0 \tag{2.2}$$

$$\begin{aligned} M_3\ddot{z}_3 + M_3 l_1\ddot{\theta}_3 sin\gamma + C_2(\dot{z}_3 - \dot{z}_2) + C_3(\dot{z}_3 + l\dot{\theta}_3 sin\gamma) \\ + K_2(z_3 - z_2) + K_3(z_3 + l\theta_3 sin\gamma) = 0 \end{aligned} \tag{2.3}$$

$$M_3\ddot{x}_3 - M_3 l_1\ddot{\theta}_3 cos\gamma + C_4(\dot{x}_3 - l\dot{\theta}_3 cos\gamma) + K_4(x_3 - l\theta_3 cos\gamma) = 0 \tag{2.4}$$

$$\begin{aligned} (J_c + M_3 l_1^2)\ddot{\theta}_3 + M_3 l_1\ddot{z}_3 sin\gamma - M_3 l_1\ddot{x}_3 cos\gamma + C_3 l sin\gamma\dot{z}_3 \\ - C_4 l cos\gamma\dot{x}_3 + \left[\left(C_3 sin^2\gamma + C_4 cos^2\gamma\right) l^2 + C_{t_1} + C_{t_2}\right]\dot{\theta}_3 \\ + K_3 l sin\gamma z_3 - K_4 l cos\gamma x_3 \\ + \left[\left(K_3 sin^2\gamma + K_4 cos^2\gamma\right) l^2 + K_{t_1} + K_{t_2}\right]\theta_3 = 0 \end{aligned} \tag{2.5}$$

where l is length of the upper-arm, J_r is the mass moment of inertia of the upper arm about its center of gravity and l_1 is the distance between the center of gravity of the mass of the upper-arm from the elbow joint. Also, z_1, z_2, and z_3 are the longitudinal motions of the hand mass (m_1), fore-arm mass (m_2) and elbow joint, respectively. Angle θ_3 is the pitch motion of the upper arm mass (m_3) with respect to the elbow joint and x_3 is the vertical co-ordinate of the upper-arm mass taken at the elbow joint. Further, z_0 represents the displacement excitation at the handle, K_{t_1} and K_{t_2} are the torsional stiffness coefficients of the elbow and shoulder joints, respectively, and C_{t_1} and C_{t_2} are the damping coefficients of the elbow and shoulder joints, respectively.

Equations 2.1 to 2.5 describe the dynamics of the hand-arm subject to longitudinal handle vibration. While the masses/inertias in the model are selected as the mean values of the human hand-arm system, the stiffness and damping parameters are identified from the measured transmissibility characteristics.

2.2 Measurement of Transmitted Vibration

The vibration transmitted to the hand-arm was measured in the laboratory using a 38 mm diameter test handle, split along its axial direction. The handle was mounted on an electrodynamic exciter to deliver sinusoidal vibrations in the Z_h direction. The test handle used in this experiment behaved like a pure mass with no resonant frequencies in the frequency range of interest (10-200) Hz.

The vibration transmission characteristics of the hand-arm system are strongly related to grip force and excitation frequency. The laboratory tests are thus performed for nearly constant hand grip force in the 10-200 Hz frequency range. The hand-grip force is measured using strain gages mounted along the axial direction of the handle. The strain gages are calibrated by applying known loads at a specific position of the handle. The

measured strain gage signal was constantly displayed to the subject, through a digital voltmeter, to enable the subject to maintain nearly constant grip force during the test. An accelerometer was mounted on the handle to measure and control the excitation level.

Table 2.1: Range of selected test parameters for vibration transmissibility analysis

Direction of Vibration	Z_h
Frequency range	10-200 Hz
Excitation	0.5 g peak sinusoidal
Grip force	25.0 N
Push force	0 N
Elbow angle	90 degrees
Grip type	Palm grip using the dominant right hand
Body posture	Standing upright
Shoulder abduction	0 degrees
Handle size	38 mm diameter
Subject	One male subject

The instrumented handle was mounted on the vibration exciter such that subject's hand-arm was exposed to sinusoidal vibration along the Z_h direction, recommended by ISO -5349 [23]. The Figure 2.3 illustrates the hand-handle orientation for measuring the transmissibility characteristics in the Z_h direction. The Figure 2.4 illustrates the schematic representation of the test apparatus.

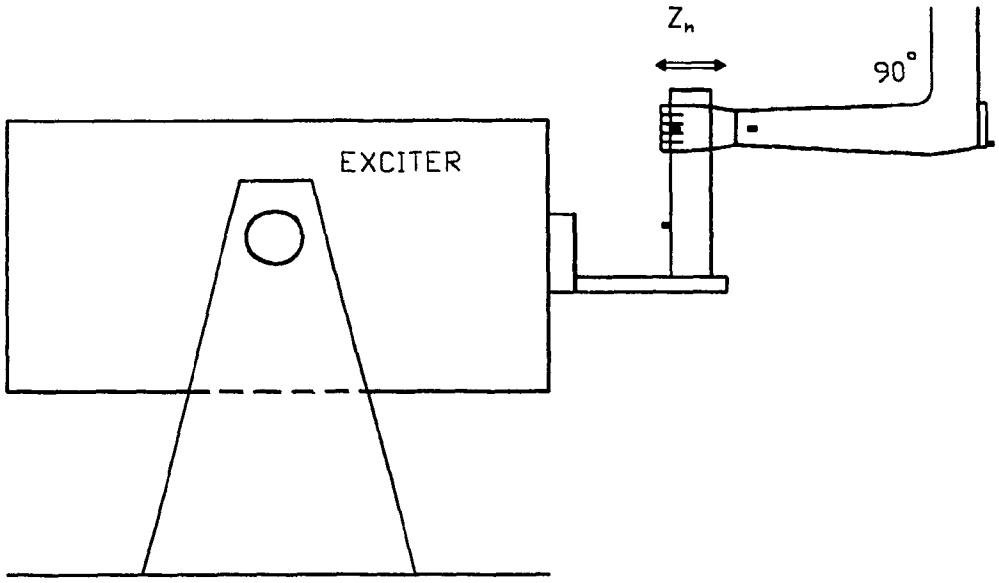

Figure 2.3: Location of accelerometers for transmissibility tests
(Black dots represents tiny accelerometers located to measure the acceleration)

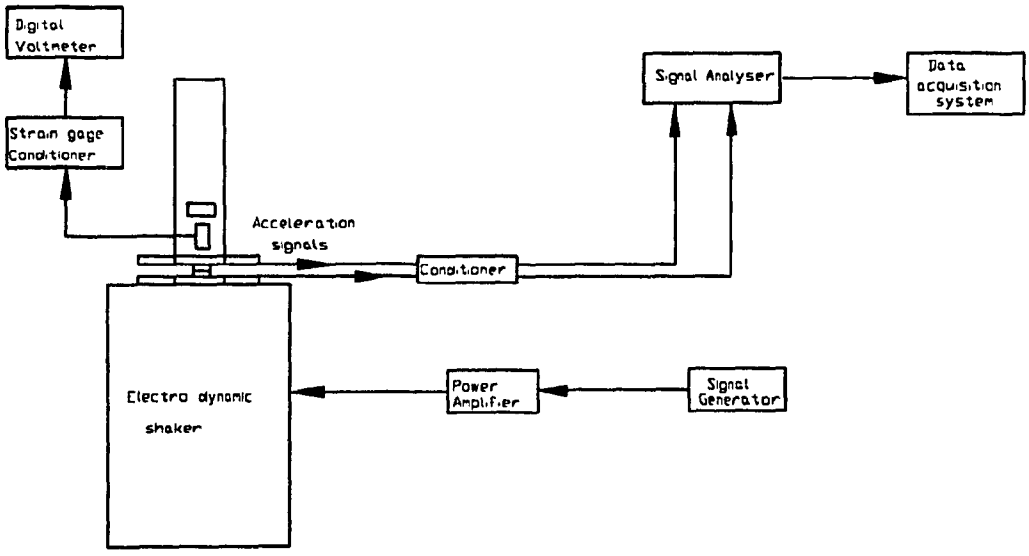

Figure 2.4: Schematic representation of the transmissibility measurement apparatus

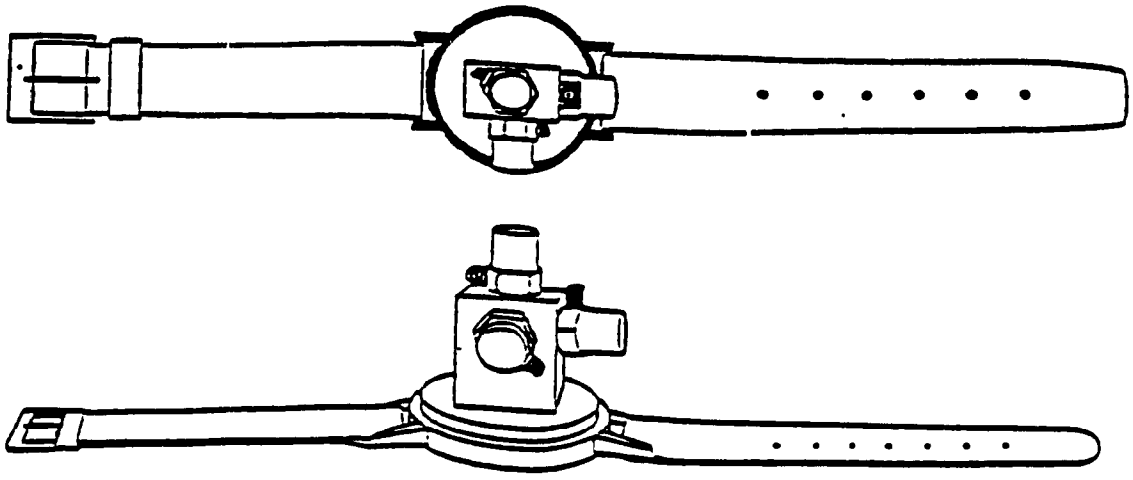

Figure 2.5: Schematic representation of the bracelet with accelerometers

The vibration transmissibility tests were performed on one subject in standing posture. The subject was advised to apply a desired grip force with his dominant right hand, and maintain an elbow angle of 90 degrees with zero shoulder abduction. The measurements were performed for constant sinusoidal acceleration excitations at 14 discrete frequencies in the 10-200 Hz frequency range.

Miniature accelerometers weighing 2.2 g were used to measure the vibration transmitted to the hand, fore-arm and elbow. The transmitted vibration to the hand was measured using an accelerometer mounted on a specially designed ring worn on the middle finger. A resonance test was performed to determine the resonant frequency of the ring, which was observed to be around 530 Hz. The vibration transmitted to the fore-arm was measured using an accelerometer mounted on a specially designed bracelet shown in Figure 2.5. Although the bracelet is designed to accommodate three miniature accelerometers oriented in three orthogonal directions, only one accelerometer was mounted to measure transmitted vibration in the Z_h direction. The resonant fre-

quency of the bracelet with the accelerometer was reported to be 1.2 kHz [64]. The bracelet was firmly fastened near the wrist with sufficiently large tension considered tolerable by the subject.

The vibration transmitted to the upper-arm, near the elbow joint, was measured using an accelerometer mounted on a light weight aluminium strip. The aluminium strip was held firmly with the upper-arm using an elbow pad. The pictorial views of the laboratory test set up are shown in Figure 2.6. The measured acceleration data were recorded and analyzed to yield the vibration transmissibility characteristics of the hand-arm. The test parameters are summarized in Table 2.1.

2.3 Transmissibility Characteristics of the Hand-Arm

The measured response characteristics were analyzed using a dual-channel analyzer to derive the acceleration transmissibility at each excitation frequency. The acceleration transmissibility is derived from the ratio of rms accelerations measured at a location on the hand-arm to that measured at the handle. The transmissibility data thus obtained in the 10-200 Hz frequency range are illustrated in Figure 2.7.

Transmissibility characteristics of the fore-arm measured near the wrist and the elbow, exhibit considerable attenuation of vibration at frequencies above 50 Hz. At excitation frequencies above 100 Hz, the transmissibility is observed to be below 0.2. At low excitation frequencies (below 20 Hz), the results reveal an amplification of vibration at hand, fore-arm and elbow which conforms with the conclusions of the study reported in [32]. Amplification of vibration at the hand, under palm grip, can be observed up to excitation frequencies of 80 Hz, which is quite similar to the results reported in the literature [22].

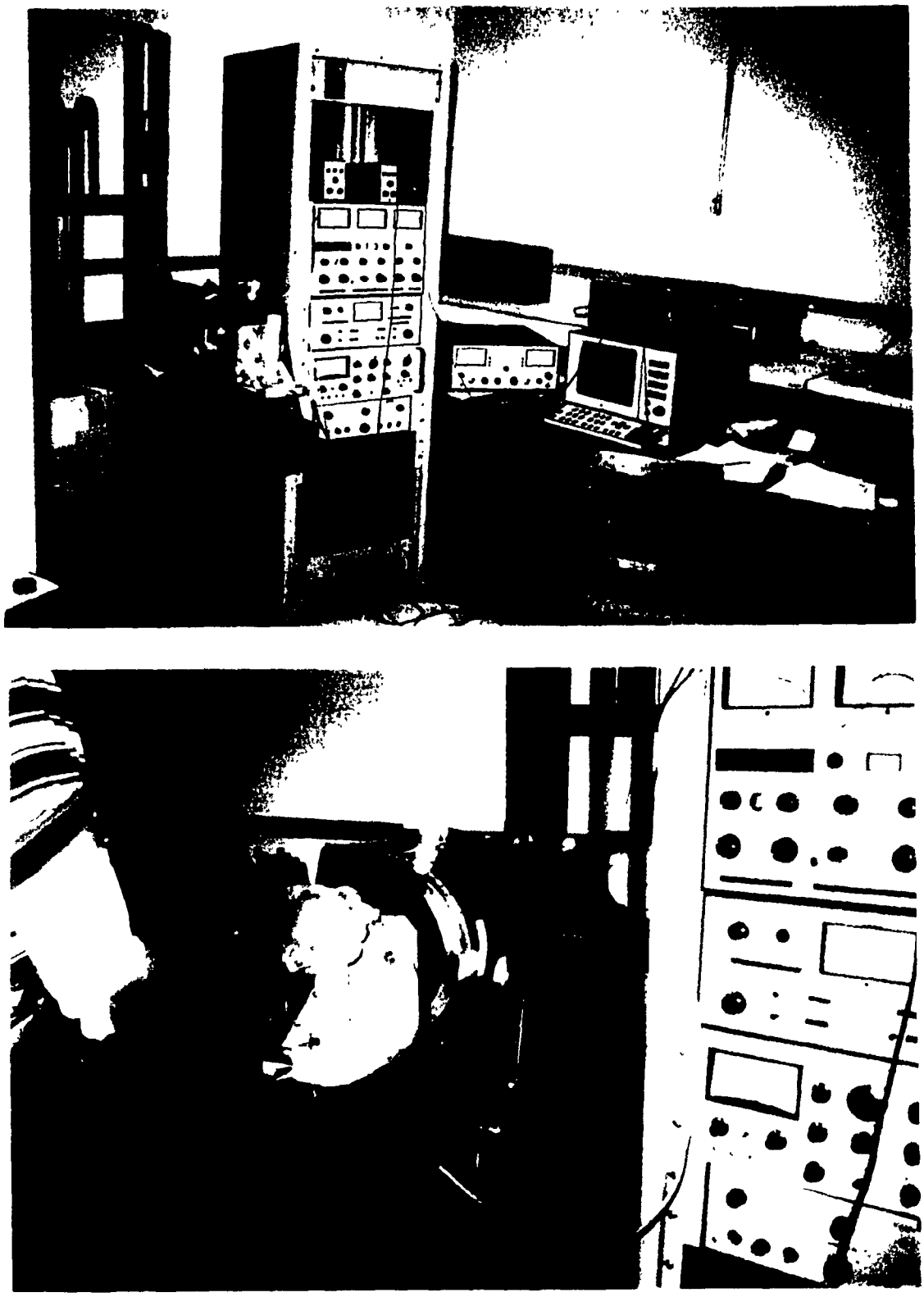

Figure 2.6: Photograph showing the experimental set up for measuring the transmissibility in the human hand-arm system

The vibration transmitted to the hand and fore-arm reveal peaks in the 20-30 Hz and 10-20 Hz frequency ranges, respectively. The measured vibration transmissibility at all locations, however, exhibit peaks in the 40-70 Hz and 80-150 Hz frequency ranges, indicating resonances of the hand-arm system in these two ranges of frequencies. The resonant frequency ranges, identified in this study, are further supported by the experimental results reported in the literature [22,32,33].

As discussed in section 2.1, the only comprehensive measurements of hand-arm vibration transmissibility, reported in the literature, were by Reynolds [31]. The vibration transmissibility data, derived from the present study, are thus compared to those reported in the literature. Reynolds [31] utilized miniature accelerometers, attached to the skin at various locations of the hand-arm, as shown in Figure 2.8. The human hand-arm was subject to sinusoidal vibration excitation through a T-bar handle mounted on an electro-mechanical exciter. The measurements were performed under a constant grip force of 8.9 N (2 lbf) in the 5-1000 Hz frequency range. The longitudinal vibration transmissibility measured at the middle finger (location 2), fore-arm (near wrist, location 5), upper-arm (near elbow joint, location 7), and the shoulder (location 8) are presented in Figure 2.9. A comparison of measured vibration transmissibility (Figure 2.7) and those reported by Reynolds (Figure 2.9) reveals quite similar patterns. The results clearly illustrate that the magnitude of vibration transmitted to the shoulder is insignificant. The shoulder vibration transmissibility is below 0.08 at frequencies above 10 Hz and below 0.01 at excitation frequencies above 100 Hz. The vibration transmitted to the fore-arm and upper arm also decreases rapidly at excitation frequencies beyond 20 Hz. The vibration transmitted to the hand, however, remains considerably large when compared to that transmitted to fore-arm and upper-arm.

The vibration transmissibility characteristics are further compared, as illustrated in Figures 2.10 to 2.12. While the vibration transmissibility characteristics measured at fore-arm and upper-arm are similar to those reported in [31], the hand transmissibility is

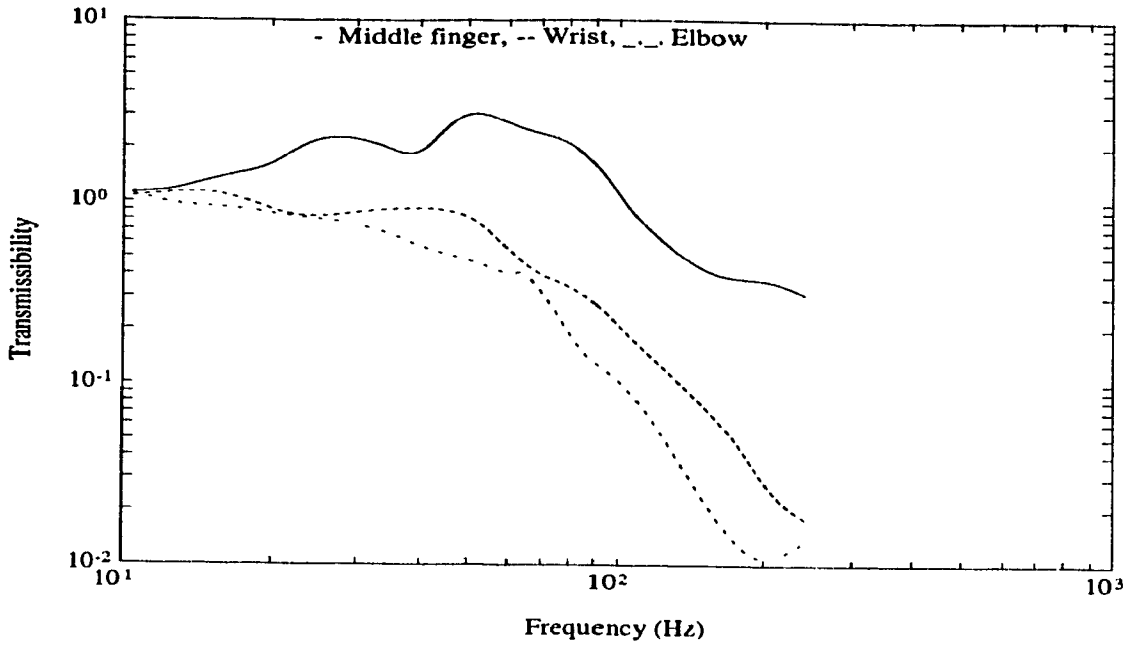

Figure 2.7: Acceleration transmissibility for longitudinal direction

quite different as shown in Figure 2.10. The measured hand transmissibility is considerably larger than that reported [31]. The large difference may be attributed to contact vibration of the metal ring bearing the accelerometer. The discrepancies, shown in Figure 2.10 to 2.12, are further attributed to the different grip force and type of grip used in the study. The vibration transmissibility characteristics reported in the literature were acquired for low levels of grip force, 8.9 N, and finger-type grip. The present study, on the other hand, was performed for palm-type grip and 25 N grip force. Studies conducted on hand-arm vibration have demonstrated an increase in transmitted vibration with increase in the grip force [22,34]. The transmissibility curves obtained by Reynolds [31], illustrate the resonances of the hand-arm system in the 5-20 Hz and 80-150 Hz frequency ranges respectively, in all of the curves. The vibration transmissibility measured near the wrist (location 5), further reveals a slight peak in the 50-70 Hz frequency range.

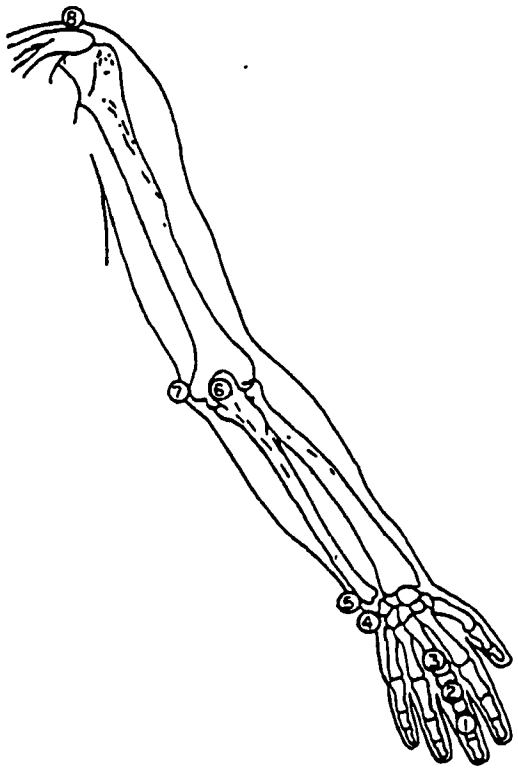

Figure 2.8: Location of accelerometers for transmissibility tests [31]

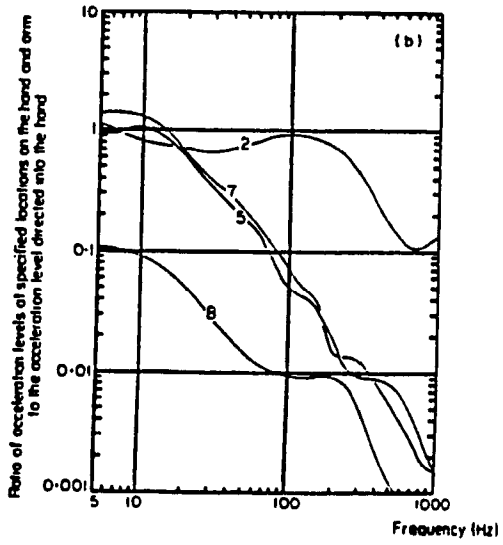

Figure 2.9: Acceleration transmissibility curve obtained for longitudinal direction [31] (2,5,7,8 locations representing hand, fore-arm, elbow and shoulder respectively)

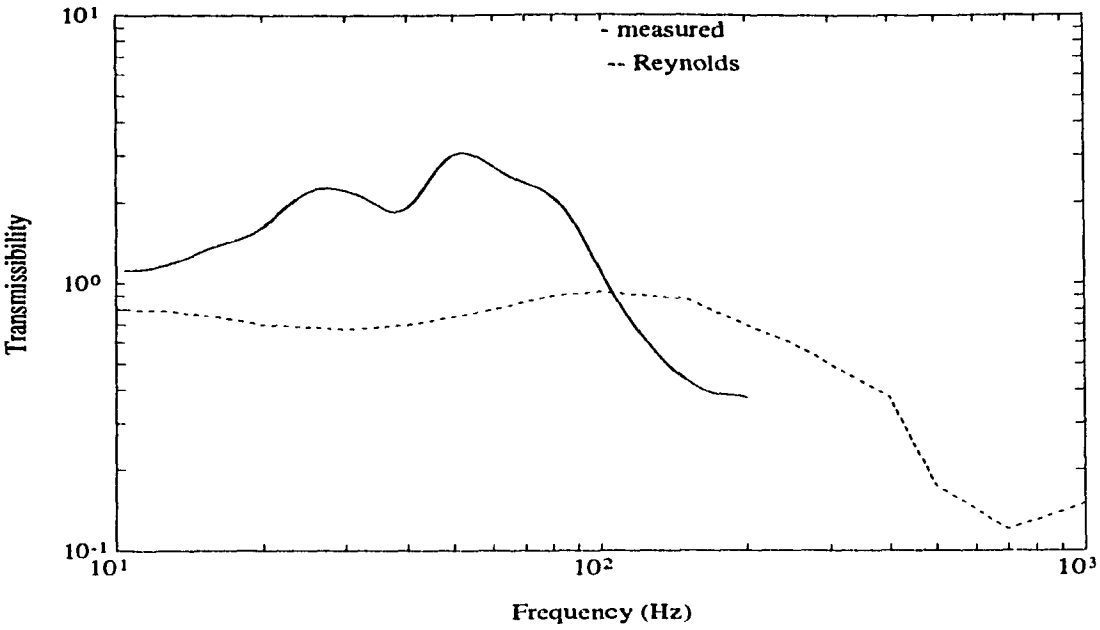

Figure 2.10: Hand transmissibility compared with that of Reynolds

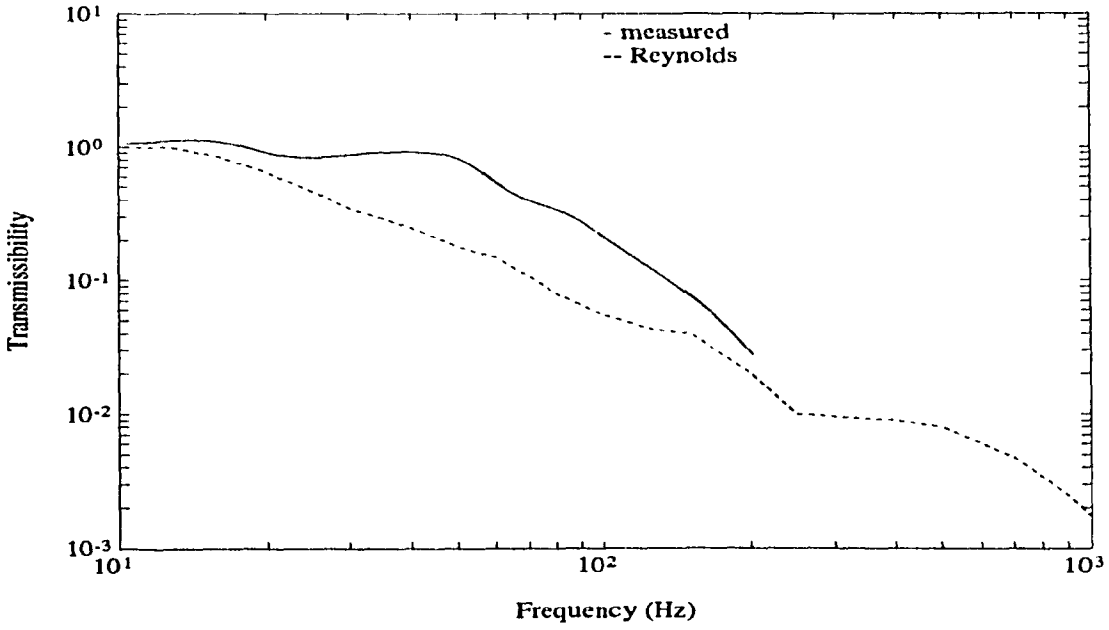

Figure 2.11: Forearm transmissibility compared with that of Reynolds

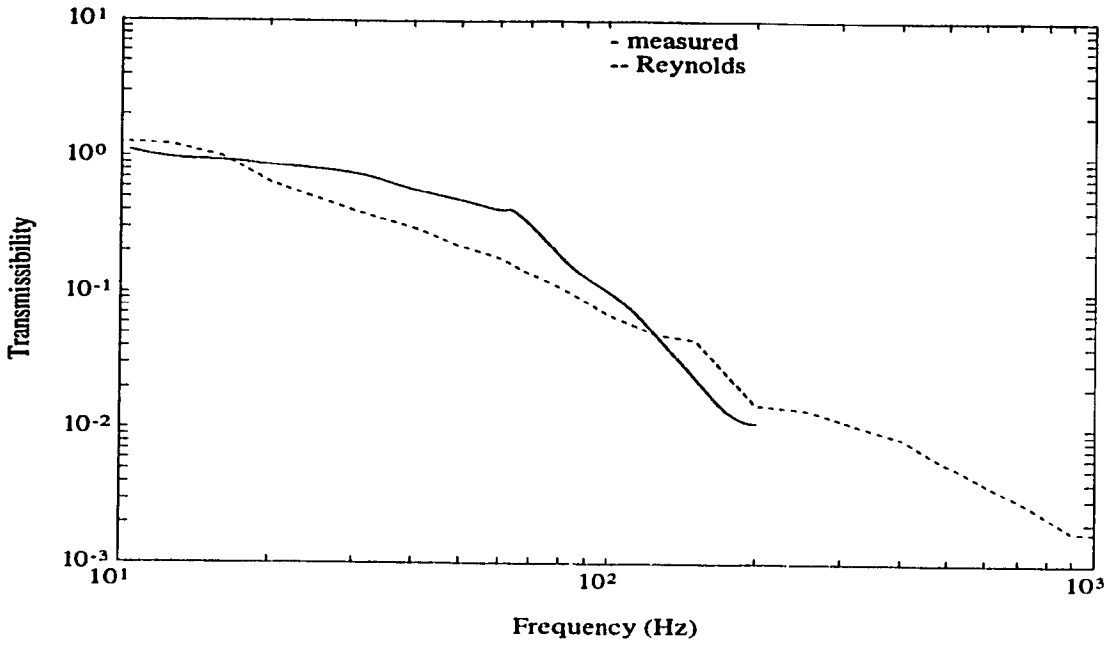

Figure 2.12: Elbow transmissibility compared with that of Reynolds

2.4 Identification of Model Parameters

The human hand-arm comprises a complex combination of skin, muscles, bones, joints, etc.. It is thus extremely difficult to identify the visco-elastic properties of the hand-arm vibration model. The model parameters are thus identified by curve fitting the measured data. Anthropometric data are used to derive the masses due to hand, fore-arm, upper-arm, and mass moment of inertia of the upper-arm [66,67,68]. The length of upper-arm and location of its c.g are further identified from the data. The lumped visco-elastic properties due to skin, muscles and joints are identified using an optimization based curve fitting algorithm. The uniqueness of the model parameters is enhanced by curve fitting the vibration transmissibility data measured at the hand, fore-arm and upper-arm.

2.4.1 The Curve Fitting Algorithm

The Equations 2.1 to 2.5 describing the vibration response characteristics of human hand-arm can be expressed in the following matrix form:

$$[M]\{\ddot{u}\} + [C]\{\dot{u}\} + [K]\{u\} = \{K_i\}\{z_0\} + \{C_i\}\{\dot{z}_0\} \tag{2.6}$$

where [M], [C] and [K] are (n × n) mass, damping and stiffness matrices, respectively, and {u} is a (n × 1) vector of displacement response quantities,

$\{u\}^T = \{z_1, z_2, z_3, x_3, \theta_3\}$ and n is the number of degrees of freedom (DOF)

$\{K_i\}$ and $\{C_i\}$ are (n × 1) forcing stiffness and damping vectors, given by:

$\{K_i\} = \{K_0, 0, 0, 0, 0\}^T$; and $\{C_i\} = \{C_0, 0, 0, 0, 0\}^T$

where 'T' indicates the transpose, and K_0 and C_0 represent the visco-elastic properties of the tissues of the palm which is at the hand-handle interface.

Fourier transform of Equation 2.6 yields the vibration transmissibility as follows:

$$\frac{\overline{U}_0}{Z_0}(j\omega) = \left[[K] - \omega^2[M] + j\omega[C]\right]^{-1} [\{K_i\} + j\omega\{C_i\}] \tag{2.7}$$

where Z_0 is amplitude of displacement excitation,

where $\{\overline{U}_0\} = \{\overline{U}_{01}, \overline{U}_{02}, \overline{U}_{03}, \overline{U}_{04}, \overline{U}_{05}\}$ is the complex amplitude of displacement response at the hand, forearm and elbow. The vibration transmissibilities of the hand mass (T_1), fore-arm (T_2), the elbow (T_3) and the shoulder joint (T_4) are then derived as:

$$T_1 = \frac{Z_1}{Z_0} = \frac{|\{\overline{U}_{01}\}|}{Z_0}$$

$$T_2 = \frac{Z_2}{Z_0} = \frac{|\{\overline{U}_{02}\}|}{Z_0}$$

$$T_3 = \frac{Z_3}{Z_0} = \frac{|\{\overline{U}_{03}\}|}{Z_0}$$

$$T_4 = \frac{Z_4}{Z_0}$$

where Z_1, Z_2, Z_3, Z_4 are the amplitudes of longitudinal displacement response at the hand, fore-arm, elbow and shoulder joint, respectively. The amplitude of longitudinal displacement at the shoulder joint, Z_4, is derived from:

$$Z_4 = |\{\overline{U}_{03} + l\sin\gamma\overline{U}_{05}\}|$$

The linear stiffness and damping coefficients of the bio-mechanical model are identified such that the analytical transmissibility characteristics are close to those measured in the laboratory. The error between the analytical and measured values is minimized using an optimization algorithm. An optimization function comprising of the sum of squared errors between the measured and analytical values of transmissibility corresponding to

14 discrete frequencies are selected in this study, such that it represents the measured transmissibility curve appropriately, in the frequency range considered.

Optimization function is thus formulated as the sum of squares of errors in the entire frequency range:

$$E(\overline{\chi}) \;=\; Minimize\left[\sum_{j=1}^{q}\sum_{i=1}^{p}\left[w_j\left\{T_j(\omega_i)-T_{m_j}(\omega_i)\right\}\right]^2\right] \tag{2.8}$$

where $E(\overline{\chi})$ is the transmissibility error function to be minimized, q is the number of transmissibility data considered in the analysis, and p is the number of discrete frequencies in the range of concern. w_j is the weighting factor and $T_j(\omega_i)$ is the vibration transmissibility of location j derived from the model at discrete frequencies ω_i. $T_{m_j}(\omega_i)$ is the corresponding measured vibration transmissibility and $(\overline{\chi})$ is a vector of model parameters, given by

$$\overline{\chi} = \{K_i, C_i\}; i = 1, ...r$$

where 'r' is the number of restoring and dissipative elements of the model. The optimization function, described in Equation 2.8, is subject to following equality and inequality constraints:

$$m_1 = 0.45kg,\ m_2 = 1.15kg,\ m_3 = 1.90kg \text{ and } J_c = 0.0149kg - m^2$$

$$K_i^L \leq K_i \leq K_i^U; i = 1, .., r$$

$$C_i^L \leq C_i \leq C_i^U; i = 1, .., r \tag{2.9}$$

The lower and upper limits in the inequality constraints are identified through a parametric study of the model.

2.4.2 Sensitivity Analysis of Model Parameters on Analytical Transmissibility

The sensitivity analysis is performed to establish the influence of each model parameter on the vibration transmissibility response. Sensitivity analysis will further provide the lower and upper limits on the design variable constraints, and their relative significance on different transmissibility data (T_1, T_2, T_3, T_4). The parametric study is performed by varying a single parameter at one time and the influence of each parameter on T_1, T_2, T_3 and T_4 is derived as a function of excitation frequency.

The results of the parametric study are summarized as follows:

- The influence of model damping parameters on the vibration transmissibility, in-general, is significant.
- The transmissibility of the hand mass (T_1) is greatly influenced by the properties at the hand-handle interface (K_0, C_0) and visco-elastic properties lumped at the wrist joint (K_1, C_1).
- The low frequency vibration transmissibility of the fore-arm (m_2) is mostly affected by the visco-elastic properties of the interface and the fore-arm lumped at the wrist joint (K_0, K_1, C_0, C_1).
- The interface properties (K_0, C_0) influence vibration transmissibility of all the masses.
- The restoring properties of the fore-arm, lumped at the wrist joint, affect all the transmissibility at low frequencies.

- The visco-elastic properties, lumped at the elbow joint, (K_2, C_2) influence the vibration transmissibility of the elbow (T_3) and the shoulder joints (T_4) significantly.

- The longitudinal stiffness and damping coefficients, represented at the shoulder joint (K_3, C_3), influence the vibration transmissibility of both the elbow and shoulder joints (T_3 and T_4).

- The influence of vertical stiffness and damping coefficients, represented at the shoulder joint, (K_4 and C_4) on all the vibration transmissibility is considerably small.

- The torsional stiffness and damping coefficients at the elbow and shoulder joints, primarily, influence the vibration transmissibility at these joints only.

From the parametric study, it was established that the vibration transmissibility response of the hand-arm model is strongly related to all the parameters, except K_4 and C_4. The values of K_4 and C_4 were thus identified and the design vector was appropriately modified to exclude these model parameters.

2.4.3 Optimization Algorithm

An optimization software, NCONF [75], based upon the sequential search algorithm, was employed to determine the model parameters by minimizing the function presented in Equation 2.8. In view of the differences between the measured and reported transmissibility data for the palm-type and finger-type grips, respectively, two different model parameters are identified. The parameters of model for finger-type grip, referred to as MODEL 1, are identified using the data reported by Reynolds [31] in the 10-1000 Hz frequency range. The transmissibility data, established through laboratory measurements for palm-type grip, are utilized to derive the corresponding model parameters, referred to

as MODEL 2. The parameters of this model are identified for the 10-200 Hz frequency range.

During each search, the errors between the computed and target transmissibility values for each location in the frequency range of interest are derived together with the total error using Equation 2.8. Since the vibration transmissibility of the shoulder is considerably small when compared to those of the hand and elbow joints, a weighting factor of 10 was used for the shoulder joint transmissibility error. The search was terminated when the error function approached its minimum value. Several simulation runs were performed with varying starting values of the model parameters to derive a near global solution. Majority of the simulation runs converged to almost identical model parameters listed in Table 2.2 and 2.3. An examination reveals that the stiffness parameters of the model parameters (K_2, K_3, K_4), representing the elasticity of the upper-arm, are considerably large when compared to K_0 and K_1 characterizing the elasticity of the interface and fore-arm. The low values of torsional stiffness and damping parameters reveal relatively soft joints. A comparison of the parameters for models 1 and 2 reveals that the type of grip and magnitude of grip force mostly influences the properties of the interface, and the damping properties lumped at the shoulder joint. The values of K_0, K_1, C_0 and C_1 indicate low stiffness with high dissipation for the tissues of the palm, skin, bones etc. of the hand. This shows that the hand acts as a low pass energy filter with most of the vibrational energy dissipated at the hand at higher frequencies, while passing vibrations to the other parts of the hand-arm system at lower frequencies. Generally the model parameters correlate reasonably well to explain the vibration transmission patterns occurring in the human hand-arm system. Therefore, these model parameters are considered for further analysis.

The model parameters $K_2, K_3, K_4, K_{t_1}, K_{t_2}, C_2, C_{t_1}$ and C_{t_2} are quite similar for both models. The increase in stiffness properties of the interface K_0, damping coefficient,

Table 2.2: Model parameters identified from optimization algorithm (Model 1 ; Finger-type grip ; 8.9 N Grip force)

Optimized model vectors				Fixed parameters			
K_0	=	44.0	kN/m	M_1	=	0.45	kg
K_1	=	23.6	kN/m	M_2	=	1.15	kg
K_2	=	444.6	kN/m	M_3	=	1.90	kg
K_3	=	415.4	kN/m	J_c	=	0.0149	$kg.m^2$
K_4	=	50.0	kN/m	l	=	0.298 m	
K_{t_1}	=	2.0	Nm/rad	$\frac{l_1}{l}$	=	0.6	
K_{t_2}	=	2.0	Nm/rad	γ	=	60^o	
C_0	=	408.7	Ns/m				
C_1	=	39.4	Ns/m				
C_2	=	470.2	Ns/m				
C_3	=	475.5	Ns/m				
C_4	=	500.0	Ns/m				
C_{t_1}	=	4.1	Nms/rad				
C_{t_2}	=	4.1	Nms/rad				

Table 2.3: Model parameters identified from optimization algorithm (Model 2 ; Palm-type ; 25.0 N Grip force)

Optimized model vectors				Fixed parameters			
K_0	=	155.8	kN/m	M_1	=	0.45	kg
K_1	=	23.6	kN/m	M_2	=	1.15	kg
K_2	=	444.6	kN/m	M_3	=	1.90	kg
K_3	=	415.4	kN/m	J_r	=	0.0149	$kg.m^2$
K_4	=	50.25	kN/m	l	=	0.298 m	
K_{t_1}	=	2.0	Nm/rad	$\frac{l_1}{l}$	=	0.6	
K_{t_2}	=	2.0	Nm/rad	γ	=	90^o	
C_0	=	30.0	Ns/m				
C_1	=	202.84	Ns/m				
C_2	=	500.0	Ns/m				
C_3	=	164.59	Ns/m				
C_4	=	49.99	Ns/m				
C_{t_1}	=	6.14	Nms/rad				
C_{t_2}	=	4.9	Nms/rad				

C_1 of the model 2 can be attributed to increase in the hand-grip force and the area of contact of the tissues of the palm with the vibrating handle. Also there is an overall reduction of dissipative properties of the hand-arm in the case of palm grip when compared with that of the finger grip. The considerably large grip force applied by the palm grip (25.0 N) compared to 10.0 N applied in the case of finger grip may be related to the reduction of the overall dissipative properties of the hand-arm. This observation further agrees with earlier studies reported in the literature [22,34].

2.5 Results and Discussion

The model parameters, identified from the solution of constrained error function, are used to derive the vibration transmissibility characteristics of the two models. The computed transmissibility characteristics for each model are compared to the measured data to verify the validity of the identified parameters. The computed and measured vibration transmissibilities of the hand mass (T_1), fore-arm (T_2), elbow joint (T_3) and shoulder joint (T_4) of the model 1 are compared in Figures 2.13 to Figures 2.16. The results show good agreement between the measured and computed values in the entire frequency range.

The measured vibration transmissibility at higher frequency range is observed to have low values, when compared with that at lower frequency range. The curve fitting algorithm is based upon reducing the error between the measured and analytical transmissibility values at discrete frequencies, ranging from low to high frequency range. Therefore the emphasis of error reduction shifts to the lower frequency range since it constitutes, numerically, a major portion of the total error. This may be attributed, in general, to the reasonably good curve fitting in the lower frequency range compared to that in the upper range as revealed in Figures 2.13 to 2.16.

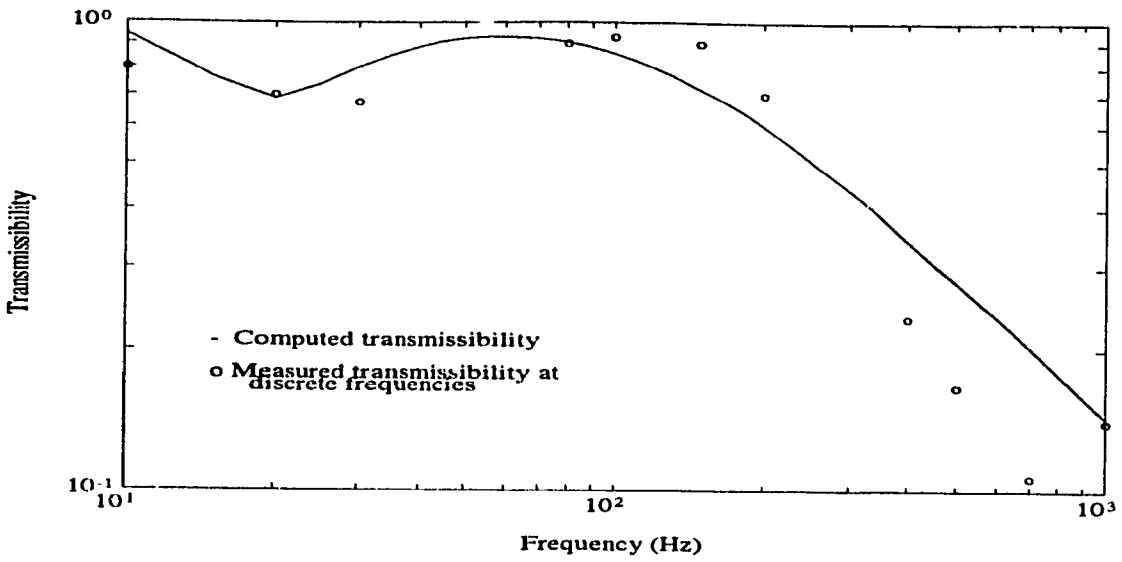

Figure 2.13: Comparison of computed vibration transmissibility at hand (T_1) with the measured data (Model 1) [31]

Figures 2.17 to 2.19 present a comparison of vibration transmissibility response of model 2 with the measured data in the 10-200 Hz frequency range. The vibration transmissibility of the fore-arm and the elbow joint agree well with measured data as shown in Figure 2.18 and 2.19. The hand vibration transmissibility response, however, deviates significantly from the measured data, as illustrated in Figure 2.17. This discrepancy may be attributed to the contact vibration of the ring with the handle. The vibration transmissibility above 80 Hz, however, agrees well with the measured data.

The experimental transmissibility curves obtained in this study as well as those reported by Reynolds [31], reveal resonance in the 80-150 Hz frequency range based on the peak observed in all of the curves. Also the peak is observed in all of the transmissibility curves reported by Reynolds [31], in the frequency range (5-20) Hz whereas similar trend is observed in (40-70) Hz frequency range for the measurements performed in this study. The observed peak in the respective frequency ranges for both the measured data, reveals the resonances of the hand-arm system occurring in the corresponding frequency ranges. The shift of the resonant frequency to a higher

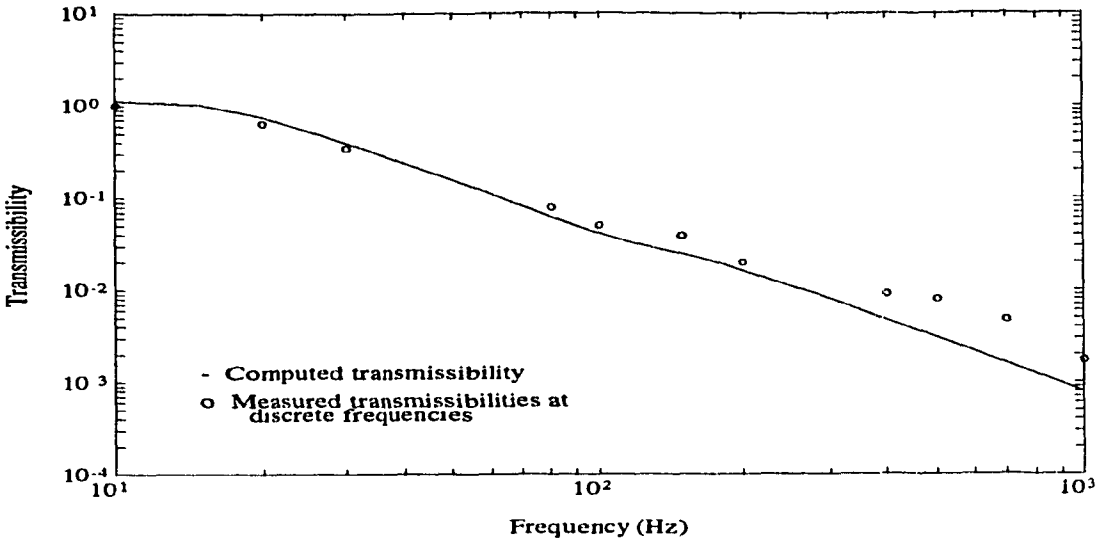

Figure 2.14: Comparison of computed vibration transmissibility at fore-arm (T_2) with the measured data (Model 1) [31]

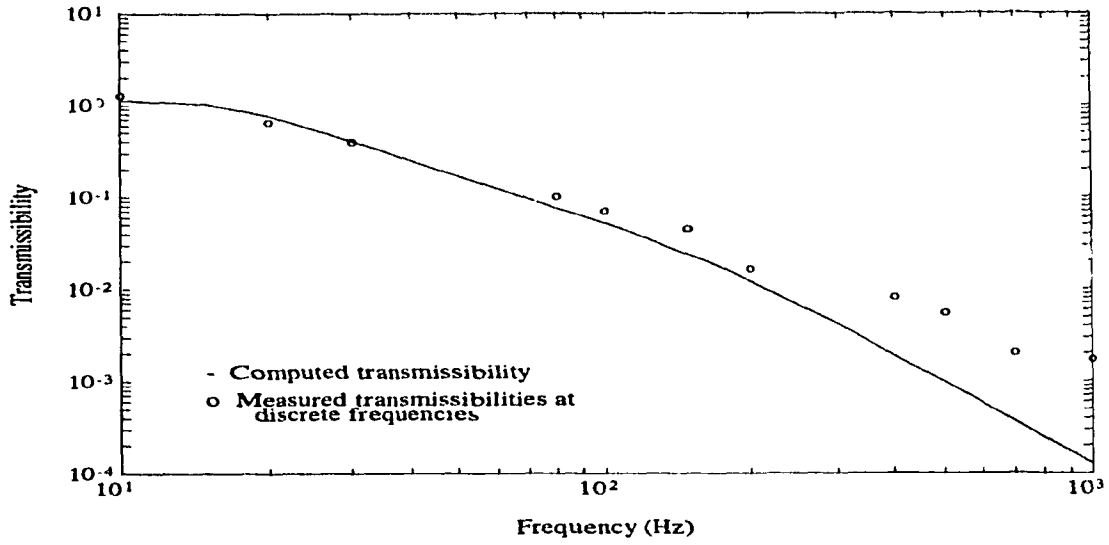

Figure 2.15: Comparison of computed vibration transmissibility at elbow (T_3) with the measured data (Model 1) [31]

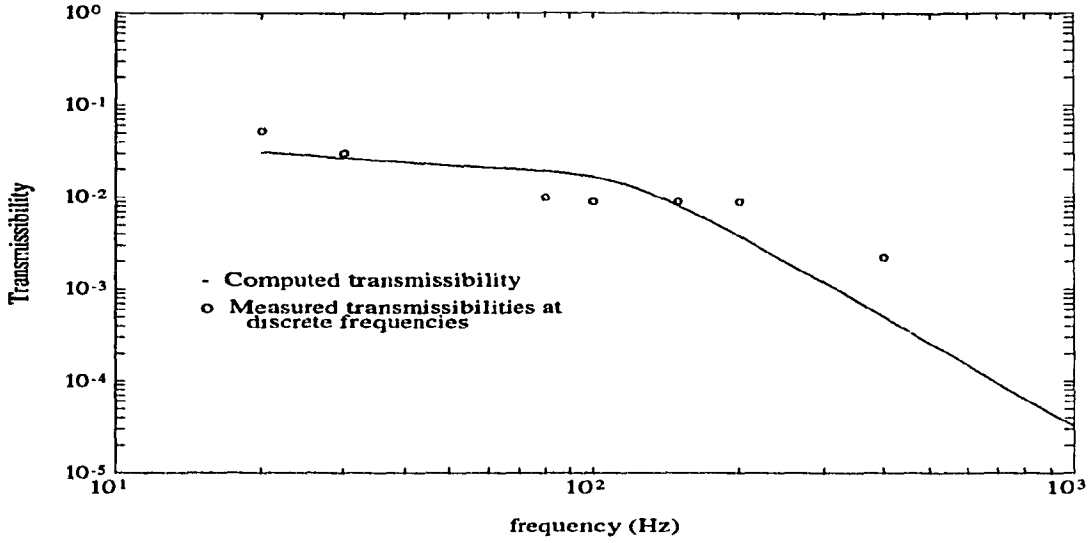

Figure 2.16: Comparison of computed vibration transmissibility at shoulder (T_4) with the measured data (Model 2) [31]

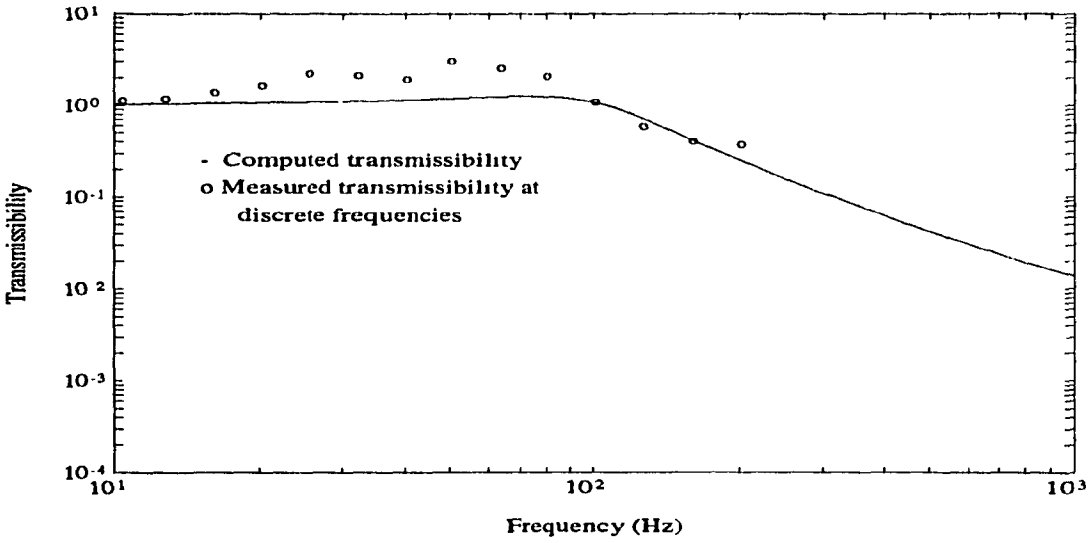

Figure 2.17: Comparison of computed vibration transmissibility at hand (T_1) with the measured data (Model 2)

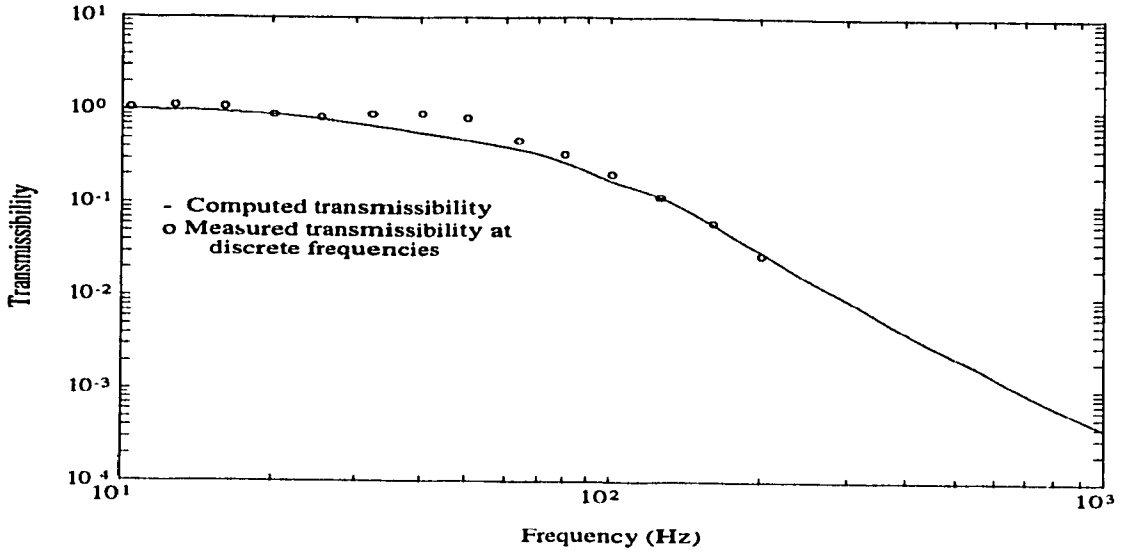

Figure 2.18: Comparison of computed vibration transmissibility at fore-arm (T_2) with the measured data (Model 2)

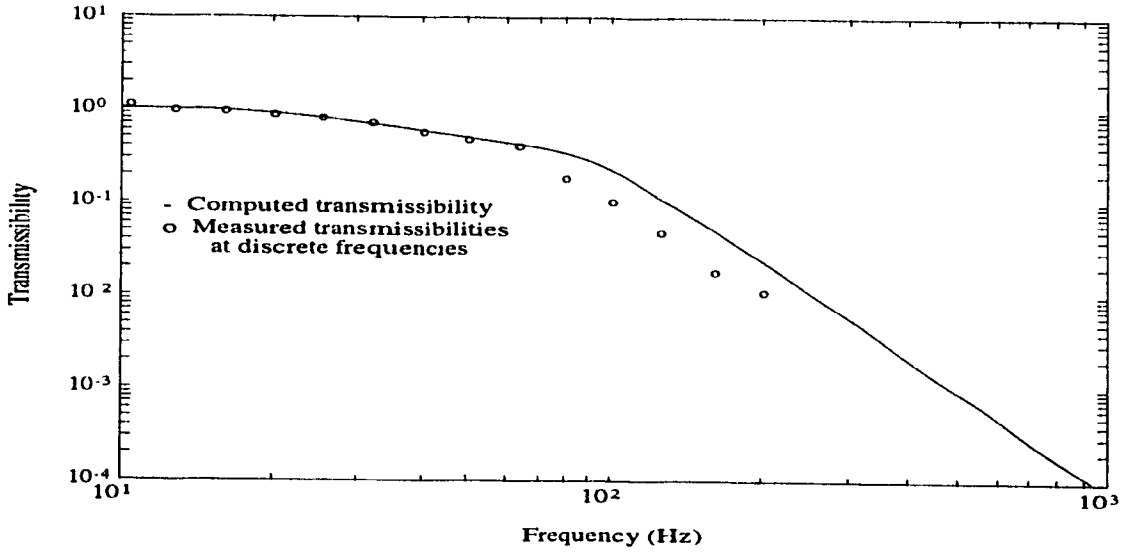

Figure 2.19: Comparison of computed vibration transmissibility at elbow (T_3) with the measured data (Model 2)

range compared to the study conducted by Reynold [31], may be due to the increased grip force (25.0 N) applied in this study.

2.5.1 Effect of Elbow Angle on Transmissibility

It should be observed that the parameters of the models 1 and 2 have been identified for elbow angles of 60 degrees and 90 degrees, respectively. The models 1 and 2 are analyzed for varying values of elbow angles to establish its influence on the vibration transmission. Figures 2.20 to 2.27 illustrate the vibration transmissibility response of models 1 and 2, as a function of elbow angle. The results reveal almost insignificant influence of the elbow angle, in the 60-90 degrees range. Lower elbow angles, the angle between the axis passing through the upper-arm and the horizontal axis, however, yield reduction in hand, fore-arm and elbow transmissibility and an increase in the shoulder transmissibility. These variations in the vibration transmissibility are mostly observed in lower frequency range only ($\leq$ 100 Hz), while the influence of the elbow angle is observed to be insignificant at higher excitation frequencies. Therefore operating the power tools with a stretched hand has the effect of transmitting more vibration to the shoulder, which results in increased whole body vibration compared to the levels encountered with small elbow angles in the lower frequency range ($\leq$ 100 Hz).

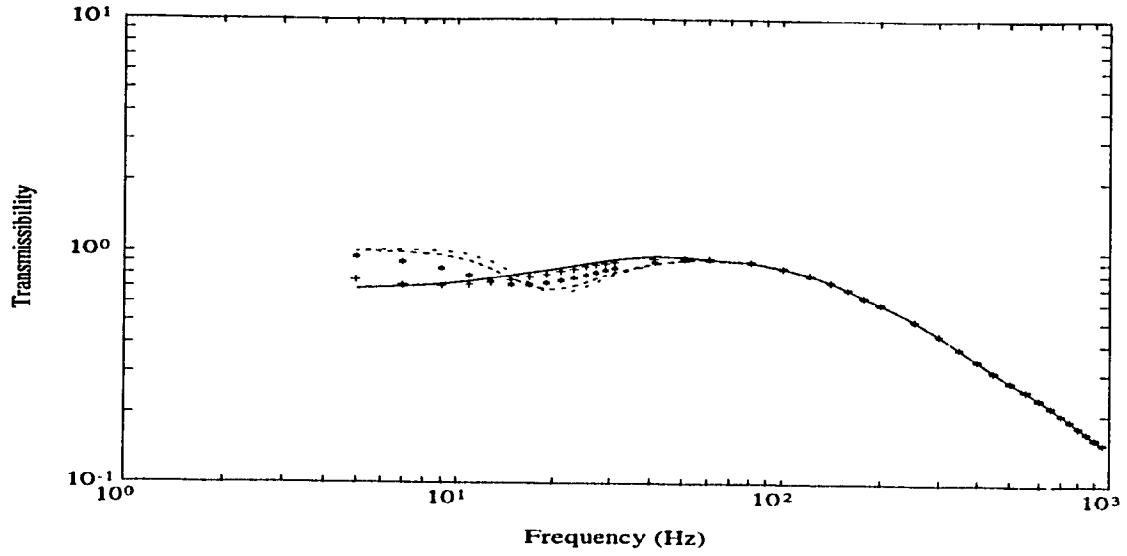

Figure 2.20: Hand transmissibility as a function of frequency at different elbow angles (model 1)
(— 5°; + 20°; * 40°; - - - 60°;— · — · 80°; · · ·90°)

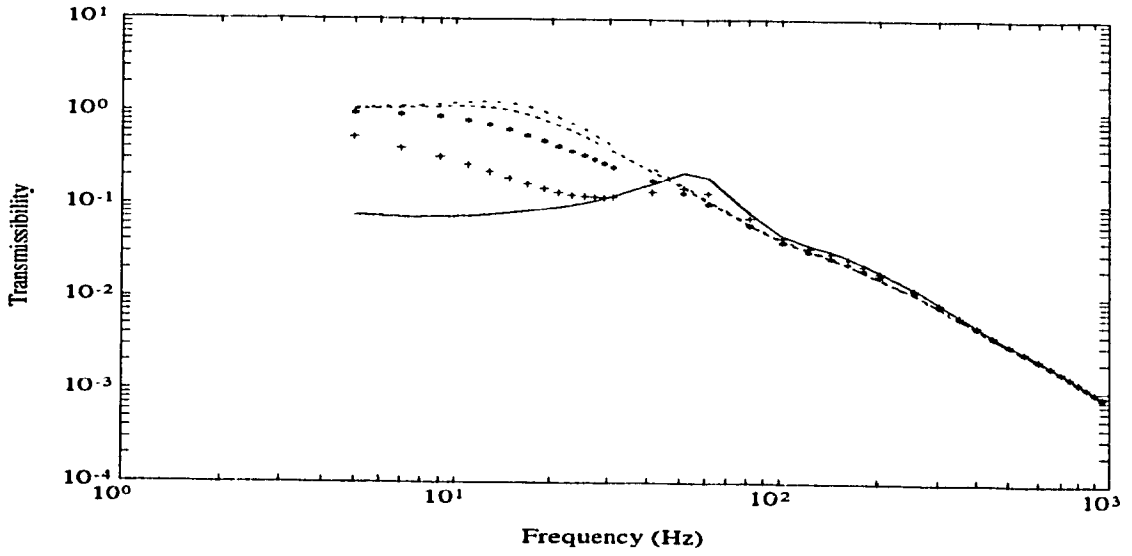

Figure 2.21: Forearm transmissibility as a function of frequency at different elbow angles (model 1)
(— 5°; + 20°; * 40°; - - - 60°;— · — · 80°; · · ·90°)

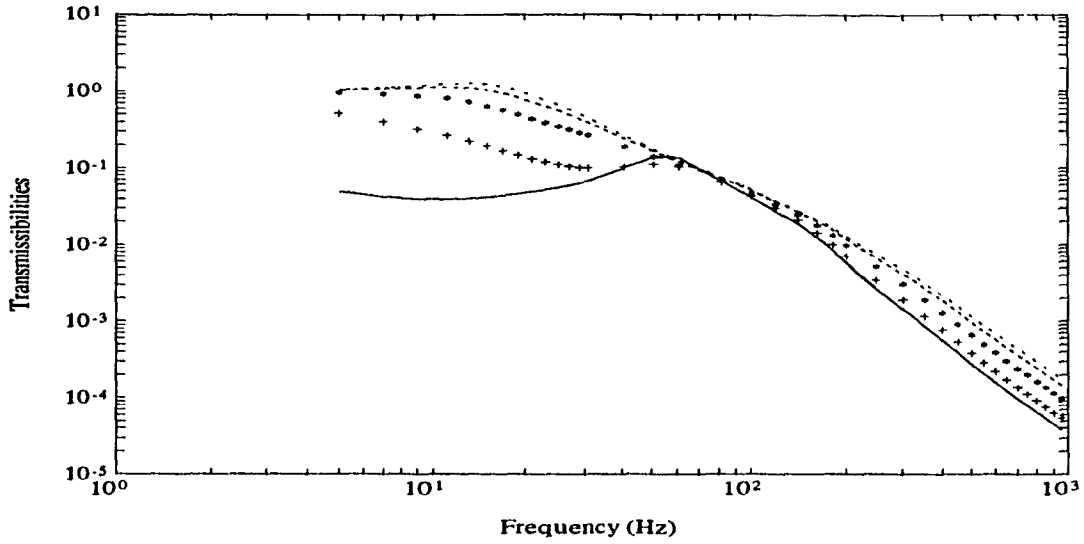

Figure 2.22: Elbow transmissibility as a function of frequency at different elbow angles (model 1)
(— 5°; + 20°; * 40°; - - - 60°;– · — · 80°; · · ·90°)

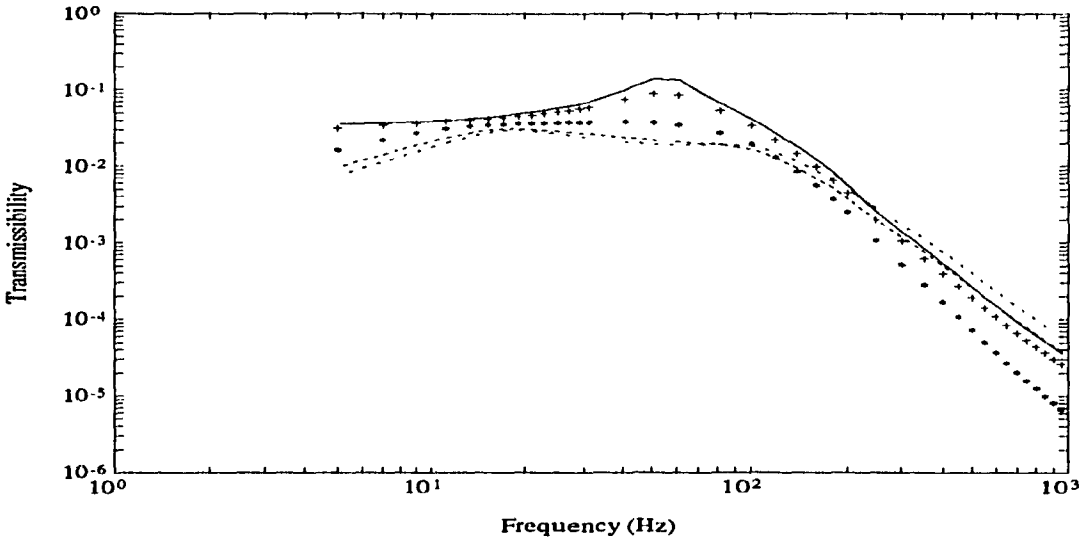

Figure 2.23: Shoulder transmissibility as a function of frequency at different elbow angles (model 1)
(— 5°; + 20°; * 40°; - - - 60°;– · — · 80°; · · ·90°)

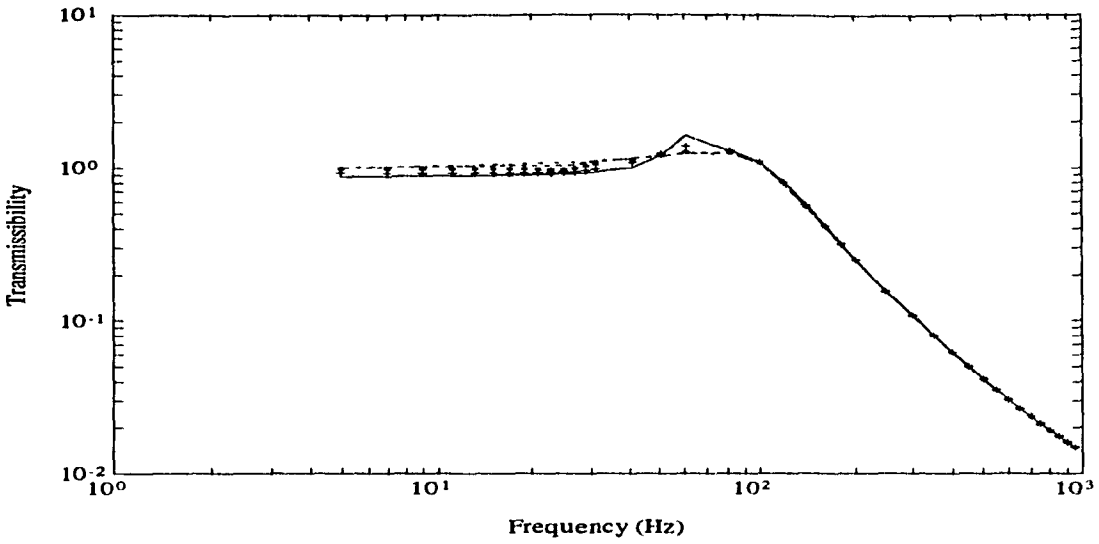

Figure 2.24: Hand transmissibility as a function of frequency at different elbow angles (model 2)
(— 5°; + 20°; * 40°; - - - 60°;– · — · 80°; · · ·90°)

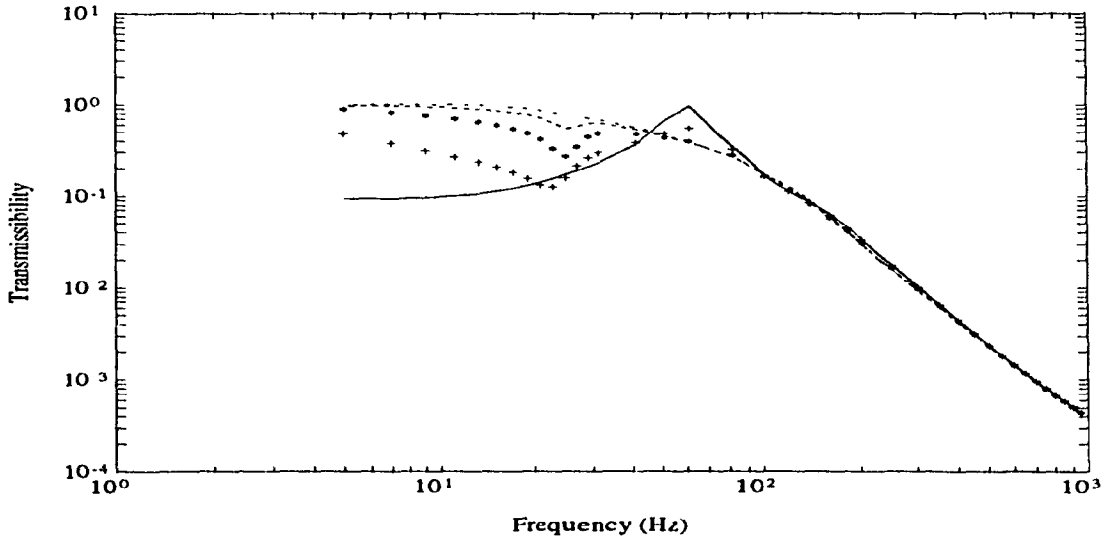

Figure 2.25: Forearm transmissibility as a function of frequency at different elbow angles (model 2)
(— 5°; + 20°; * 40°; - - - 60°;– · — · 80°; · · ·90°)

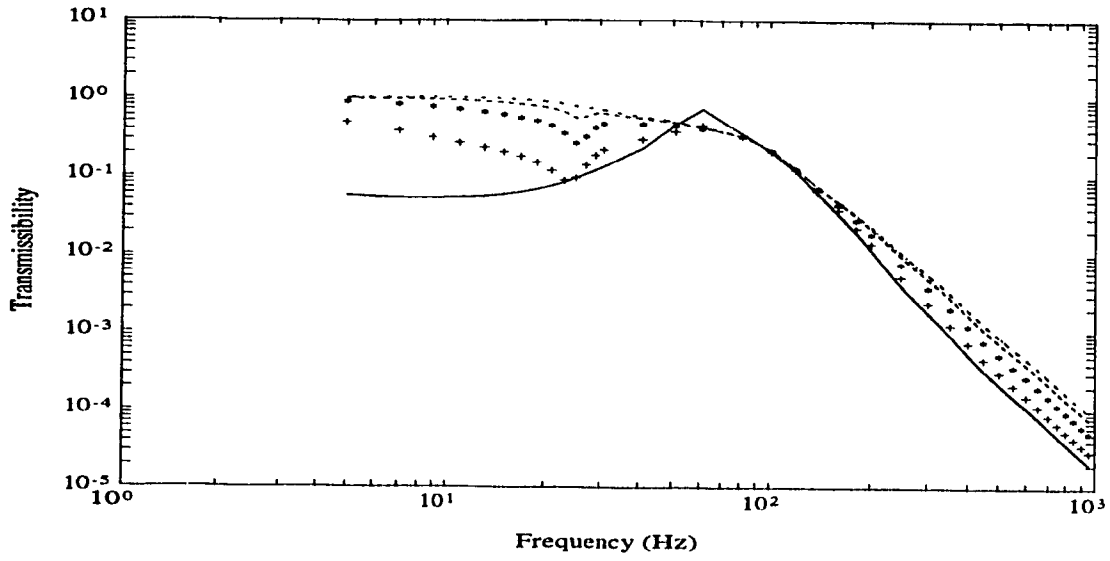

Figure 2.26: Elbow transmissibility as a function of frequency at different elbow angles (model 2)
(— 5°; + 20°; * 40°; - - - 60°;— · — · 80°; · · ·90°)

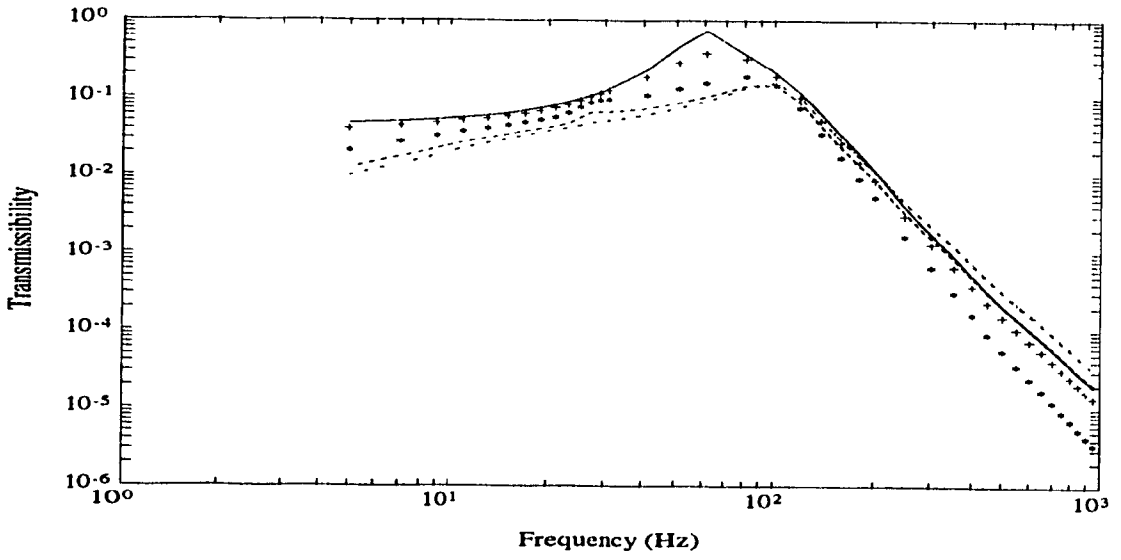

Figure 2.27: Shoulder transmissibility as a function of frequency at different elbow angles (model 2)
(— 5°; + 20°; * 40°; - - - 60°;— · — · 80°; · · ·90°)

2.6 Summary

A bio-mechanical model of the human hand-arm system is developed and the associated assumptions are described. Measurements are carried out to derive the frequency response characteristics of vibration transmitted to various location of the human hand-arm system. The equations of motion are analyzed to determine the frequency response characteristics of vibration transmitted to the hand, fore-arm and upper-arm. A parametric study is performed to establish the influence of model parameters on the analytical transmissibility. The stiffness and damping parameters of the model are identified, by using a non-linear optimization algorithm, and by reducing the errors between the measured and analytical transmissibility characteristics. The model parameters for two different grip forces and grip types are thus derived by considering the corresponding measured data. Finally the effect of elbow angle on the transmission of vibration through the hand-arm system is investigated.

The next chapter will discuss the modal analysis of the hand-arm models for a light finger grip as well as for a high magnitude palm grip force, developed in this Chapter. The natural frequencies and mode shapes of the hand-arm models obtained from the complex eigenvalue analysis will be presented. Further, responses of the hand-arm models for different deterministic excitations are obtained using modal analysis.

Chapter 3

Modal Analysis of HAV Model

The hand-arm model which is developed in the previous chapter based on the experimental measurements carried out on hand-arm system of the live subjects, is analysed in this chapter for its natural frequencies and mode shapes. Further, the responses of the hand-arm model under harmonic excitation is also studied, using modal analysis.

Modal analysis can be conveniently used to obtain the response where a linear model is used to describe the hand-arm system. Since the hand-arm system is a highly damped system, the eigenvalues and eigenvectors are complex [59,62,63,74] and hence a complex modal analysis is performed [59,74]. The eigenvectors obtained from modal analysis provide the deflection pattern of each component of the hand-arm system and the natural frequencies provide the range of frequencies at which responses are significant. Consequently, excitation and response parameters which are critical to operator's health and safety can be identified. Responses of the different components of hand-arm system for a given harmonic input can be derived by modal analysis. It is compared with the responses obtained by numerical method.

3.1 Formulation of the Eigenvalue Analysis of the HAV Model

The equations of motion for the 5DOF hand-arm model can be expressed in the matrix form as follows.

$$[M]\{\ddot{u}\} + [C]\{\dot{u}\} + [K]\{u\} = \{f\} \tag{3.1}$$

where [M], [C] and [K] are $(n \times n)$ mass, damping and stiffness matrices respectively. {u} is a (n $\times$ 1) vector of displacement response quantities, and n is the number of degrees of freedom (DOF).

The Equation (3.1) can be expressed as a system of first order equations,

$$[\mu]\{\dot{\zeta}\} + [\kappa]\{\zeta\} = \{F\} \tag{3.2}$$

where

$$[\mu] = \begin{bmatrix} 0 & M \\ M & C \end{bmatrix}_{2n\times 2n}; \qquad [\kappa] = \begin{bmatrix} -M & 0 \\ 0 & K \end{bmatrix}_{2n\times 2n}; \qquad \zeta = \begin{Bmatrix} \{\dot{z}\} \\ \{z\} \end{Bmatrix}_{2n\times 1};$$

$$F = \begin{Bmatrix} \{f\} \\ \{0\} \end{Bmatrix}_{2n\times 1}$$

In order to obtain the eigenvalues and eigenvectors of the system, the homogeneous form of equation (3.2) is solved initially. Assuming a solution of the form $\zeta = ze^{-\lambda t}$ and with $\{F\} = \{0\}$, the equation (3.2) becomes

$$[[\kappa] - \lambda[\mu]]\{z\} = \{0\} \tag{3.3}$$

The Equation (3.3) can be written as

$$\lambda[I]\{z\} = [k]\{z\} \tag{3.4}$$

From Equation (3.4), the eigenvalues and eigenvectors are solved using IMSL subroutine (GVCRG) [75]. The eigenvalues and eigenvectors are complex numbers or real numbers depending on whether the system is overdamped or underdamped corresponding to each mode.

For an underdamped mode the eigenvalues (λ_i) are of the form $\lambda_i = A_i \pm jB_i$. The imaginary part (B_i) is the damped natural frequency and (A_i) should be positive real number for a stable system, which represents the part of the solution decaying exponentially due to the damping.

For an overdamped mode, $\lambda_i = C_i$ should be positive real numbers, for a stable system.

Undamped natural frequencies and damping factors from the damped analysis can be found out for each mode as follows.

For an underdamped mode

$$\lambda_i = A_i \pm jB_i = \zeta_i\omega_{n_i} \pm j\omega_{d_i} = \zeta_i\omega_{n_i} \pm j\omega_{n_i}\sqrt{1-\zeta_i^2}$$

where

$\omega_{n_i} = \sqrt{A_i^2 + B_i^2}$ = undamped circular natural frequency in rad/sec from damped analysis for each mode

$\omega_{d_i} = B_i$ = damped circular natural frequency in rad/sec

$\zeta_i = \sqrt{1 - (\frac{\omega_{d_i}}{\omega_{n_i}})^2}$ = damping ratio of each mode.

For an overdamped mode

$$\lambda_i = C_i = \zeta_i \omega_{n_i} + \omega_{n_i}\sqrt{\zeta_i^2 - 1}$$

$$\lambda_i^* = C_i^* = \zeta_i \omega_{n_i} - \omega_{n_i}\sqrt{\zeta_i^2 - 1}$$

$\zeta_i = \frac{(C_i + C_i^*)}{\sqrt{(C_i + C_i^*)^2 - (C_i - C_i^*)^2}}$ = damping ratio for the overdamped mode

$\omega_{n_i} = \frac{(C_i + C_i^*)}{2\zeta_i}$ = Undamped circular natural frequency in rad/sec corresponding to the overdamped mode.

3.2 Eigenvalue Analysis of HAV Model

The numerical values of the eigenvalues and eigenvectors of the five-DOF HAV models which are developed in Chapter 2 , with the corresponding undamped and damped natural frequencies and damping factors for each mode calculated from damped analysis are illustrated in appendix E. For the model 1 (based on Reynold's data), one mode is found to be overdamped. The damping ratios obtained by the damped analysis for the both models, reveal that the hand-arm system is heavily damped.

In Table 3.1 and 3.2 the experimental resonance frequencies which are obtained by examining peaks in the experimental transmissibility curves represented in Fig 2.7 and Fig 2.9, as well as the damped natural frequencies and the corresponding dominant deflection modes obtained are given. Since the hand-arm system is a heavily damped system, the peaks occurring at the resonant frequencies are not so prominent, and therefore a range of frequencies is given in Table 3.1 and Table 3.2, where the resonance is suspected to occur by observing a slight peak in the transmissibility curve. The analytical damped natural frequencies are found to be in the range of the observed experimental resonant frequencies. It is to be noted that since the third mode is getting overdamped, for the

case of model one, there is no damped natural frequency for that mode and instead, an undamped natural frequency calculated from the damped analysis is presented.

Table 3.1: Comparison of experimental and analytical resonant frequencies (Model 1)

Resonant frequency (Hz) by examining the peak in the experimental transmissibility curve	Transmissibility curve at which peak is observed	Analytical resonant frequencies (Hz) Damped natural frequencies	Dominant deflection modes (From eigenvectors)
5-20	$\left\{ \begin{matrix} Hand, & Fore-arm, \\ Elbow, & Shoulder \end{matrix} \right\}^{\times}$	12.95	z_3, x_3, z_2, z_1
		15.1	x_4, x_3, z_3, z_2
50-70	$Fore-arm^{\times}$	55.97*	$\left[\begin{matrix} z_1 & & & \\ z_1, & z_3, & z_2, & x_4 \end{matrix} \right]^{+}$
80-150	$\left\{ \begin{matrix} Hand, & Fore-arm, \\ Elbow, & Shoulder \end{matrix} \right\}^{\times}$	85.31	z_3, z_4, x_3, x_4
		96.53	z_4, z_2, x_3, x_4

* Undamped natural frequency from damped analysis
\+ Overdamped modes
× Refer to Figure 2.9

Table 3.2: Comparison of experimental and analytical resonant frequencies (Model 2)

Resonant frequency (Hz) by examining the peak in the experimental transmissibility curve	Transmissibility curve at which peak is observed	Analytical resonant frequencies (Hz) Damped natural frequencies	Dominant deflection modes (From eigenvectors)
10-20	$Fore-arm^{\times}$	11.2062	z_3, z_2
20-30	$Hand^{\times}$	25.798	$\{x_3, x_4\}^*$
50-60	$Hand, Fore-arm, Elbow^{\times}$	81.8075	z_1, z_4, z_2, z_3
80-150	$Hand, Fore-arm, Elbow^{\times}$	82.8014	z_3, z_4, z_2
		104.8411	z_4, z_1, z_2, z_3

$\times$ Refer to Figure 2.7
* Identical values

3.3 Mode Shapes of HAV Model

Natural frequencies and mode shapes are determined from the eigenvalues and eigenvectors of the system matrix. The number of eigenvalues equals the order of the matrix which is equal to the number of degrees of freedom of the system.

The eigenvector associated with any particular eigenvalue represents the amplitudes of the masses when they are vibrating at that natural frequency. The vector is termed

the mode shape vector of the system since its elements represent deformations or displacements of the masses associated with each natural frequency of the system. The eigenvectors provide only relative values of the displacements (generally normalized to a convenient element).

The actual mode shape corresponding to each natural frequency is the representation of the physical system with each element of the system undergoing relative displacements according to the modal vectors for that particular natural frequency. The mode shape provides overall view of the extent of displacement that each element undergoes when the system is excited at its natural frequencies. The deflection pattern of each element observed from the mode shapes, provides the severity of damage imparted to each element, when the system is excited near the natural frequencies.

3.3.1 Formulation of the Mode Shapes from Complex Eigenvectors

Formulation of mode shape data from the complex eigenvectors are described in five stages. The complex eigenvectors obtained from Equation 3.4 is $(2n \times 1)$ vectors, where upper $(n \times 1)$ vectors represent the relative velocity and lower $(n \times 1)$ vectors represent the relative displacements. The lower $(n \times 1)$ vector of displacement is extracted from each mode in order to obtain the mode shapes which is stage 1.

The eigenvectors are complex indicating that each element in the displacement vector has magnitude as well as phase. For convenience, the rotational quantity of the upper arm is converted to the translational motion of the shoulder by the relation

$$\bar{z}_4 = \bar{z}_3 + l sin\gamma\bar{\theta}_3$$

$$\bar{x}_4 = \bar{x}_3 - l cos\gamma\bar{\theta}_3$$

where $\overline{z}_4$ and $\overline{x}_4$ are the complex values of the translation of the shoulder in Z and X direction, respectively. $\overline{z}_3$ and $\overline{x}_3$ are the complex values of the translation of the elbow in Z and X direction and $\overline{\theta}_3$ is complex value of the rotation of the upper-arm about the elbow joint.

Therefore the n×1 complex displacement vector $\{\overline{z}_1, \overline{z}_2, \overline{z}_3, \overline{x}_3, \overline{\theta}_3\}^T$ for each mode is converted into $(n+1) \times 1$ complex displacement vector as $\{\overline{z}_1, \overline{z}_2, \overline{z}_3, \overline{x}_3, \overline{z}_4, \overline{x}_4\}^T$ in stage 2. In stage 3, each displacement vector of the different modes is converted into polar co-ordinates with amplitude and phase angle in degrees. In stage 4 normalization of the displacement quantities for each mode is made with respect to the quantity having maximum amplitude. Since each displacement quantity in a mode, has phase difference with respect to each other, the magnitude of relative displacement of each one with respect to the quantity having maximum amplitude can be found out by considering it as harmonic cosine displacements. This is the fifth (final) stage and mode shape data then can be used for plotting the deflection pattern of each element of the real physical system at each natural frequency.

The various stages adopted can be illustrated symbolically as shown in Table 3.3. The various stages to obtain the mode shape data for the model 1 are given in Appendix F.

3.3.2 Discussion Based on Mode Shapes

The mode shapes illustrated from Figures 3.1 to 3.6, reveal the amount of displacement experienced by the different components of the hand-arm system. The methodology adopted in representing the mode shapes can be explained as follows. The equilibrium position of the hand-arm system is indicated by the solid line connecting the circles at the centre of the hand, fore-arm, elbow and the shoulder position. The two conjugate deflection positions that the hand-arm system can assume in each mode are represented

by the square and triangle marks. The dotted lines connecting the triangles and squares, represent the displaced positions at each mode from the mean position. It is to be noted that the displacement in the hand and the fore-arm occurs only in longitudinal direction, even though it appears that there is a vertical displacement for the fore-arm in the representation of the certain mode shapes. This arises from representing the vertical displacement experienced at the elbow.

Thus the Mode shapes of the developed HAV models provide a qualitative information on the displacement experienced by different components of the hand-arm system under different natural frequencies of the system. Observing the first and second mode shapes of both models, represented in Figure 3.1 and 3.4, it is seen that there is a good amount of stretching and compression occurring at the forearm and upper-arm. The range of damped natural frequencies for both models is in between (10-35) Hz which indicates that operating the tool frequency range will induce a higher damage at fore-arm and upper-arm and hence higher likelihood of injuries and disorders. The third mode (overdamped) for the first model as well as for the second model as illustrated in Figure 3.2 and 3.5, indicated the possibility of more stress in the hand, due to large relative displacements occurring there compared to other components of hand-arm system. The range of frequencies are found to be (50-70) Hz. Operating under these frequency ranges will result in more stress localized at the hand, which is believed to be one of the primary reason for the finger blanching.

By examining the fourth and fifth mode shapes of the first model and the second model, illustrated in Figure 3.3 and 3.6, it is seen, that there is a possibility of higher stress at the shoulder, due to the large relative motion at the shoulder region in longitudinal direction. This results in a higher stress at the upper-arm as seen from the mode shapes. The range of frequencies for both models are from (80-140) Hz. Hence operating the power tools close to these frequency ranges increases the chances of disorders and complexities at the upper part of the hand-arm system.

Table 3.3: Symbolic representation of various stages in forming mode shape data from complex eigenvectors

Stage 1	Stage 2	Stage 3	Stage 4	Stage5
$\begin{Bmatrix} \overline{z}_1 \\ \overline{z}_2 \\ \overline{z}_3 \\ \overline{x}_3 \\ \overline{\theta}_3 \end{Bmatrix}$	$\begin{Bmatrix} \overline{z}_1 \\ \overline{z}_2 \\ \overline{z}_3 \\ \overline{x}_3 \\ \overline{z}_4 \\ \overline{x}_4 \end{Bmatrix}$	$\begin{Bmatrix} z_1\angle\phi_1 \\ z_2\angle\phi_2 \\ z_3\angle\phi_3 \\ x_3\angle\phi_4 \\ z_4\angle\phi_5 \\ x_4\angle\phi_6 \end{Bmatrix}$	$\begin{Bmatrix} \frac{z_1}{z_m}\angle(\phi_1-\phi_m) \\ \frac{z_2}{z_m}\angle(\phi_2-\phi_m) \\ \frac{z_3}{z_m}\angle(\phi_3-\phi_m) \\ \frac{x_3}{z_m}\angle(\phi_4-\phi_m) \\ \frac{z_4}{z_m}\angle(\phi_5-\phi_m) \\ \frac{x_4}{z_m}\angle(\phi_6-\phi_m) \end{Bmatrix}$	$\begin{Bmatrix} \frac{z_1}{z_m}cos(\phi_1-\phi_m) \\ \frac{z_2}{z_m}cos(\phi_2-\phi_m) \\ \frac{z_3}{z_m}cos(\phi_3-\phi_m) \\ \frac{x_3}{z_m}cos(\phi_4-\phi_m) \\ \frac{z_4}{z_m}cos(\phi_5-\phi_m) \\ \frac{x_4}{z_m}cos(\phi_6-\phi_m) \end{Bmatrix} = \begin{Bmatrix} z_{11} \\ z_{22} \\ z_{33} \\ x_{33} \\ z_{44} \\ x_{44} \end{Bmatrix}$

z_m=max($z_1, z_2, z_3, x_3, z_4, x_4$)
ϕ_m=Phase angle corresponding to z_m

3.4 Responses of HAV Model Under Deterministic Excitation

The frequency response of the HAV model under harmonic excitation for different frequencies can be obtained using complex modal analysis. The complex eigenvectors are formed as explained in the section 3.1. The modal matrix $[\phi]$ is formed by concatenating the eigenvectors of the system.

The original co-ordinate $\{\zeta\}$ can be expressed in terms of modal co-ordinates $\{q\}$ using the modal matrix $[\phi]$ as follows

$$\{\zeta\} = [\phi]\{q\} \tag{3.5}$$

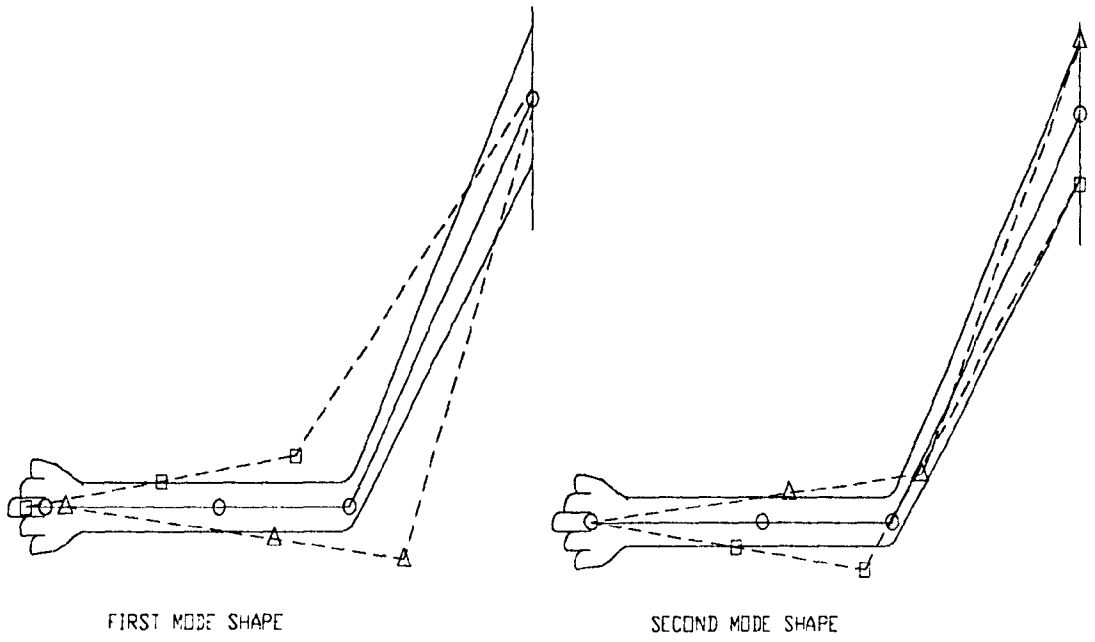

Figure 3.1: First and Second Mode shapes of the HAV model 1

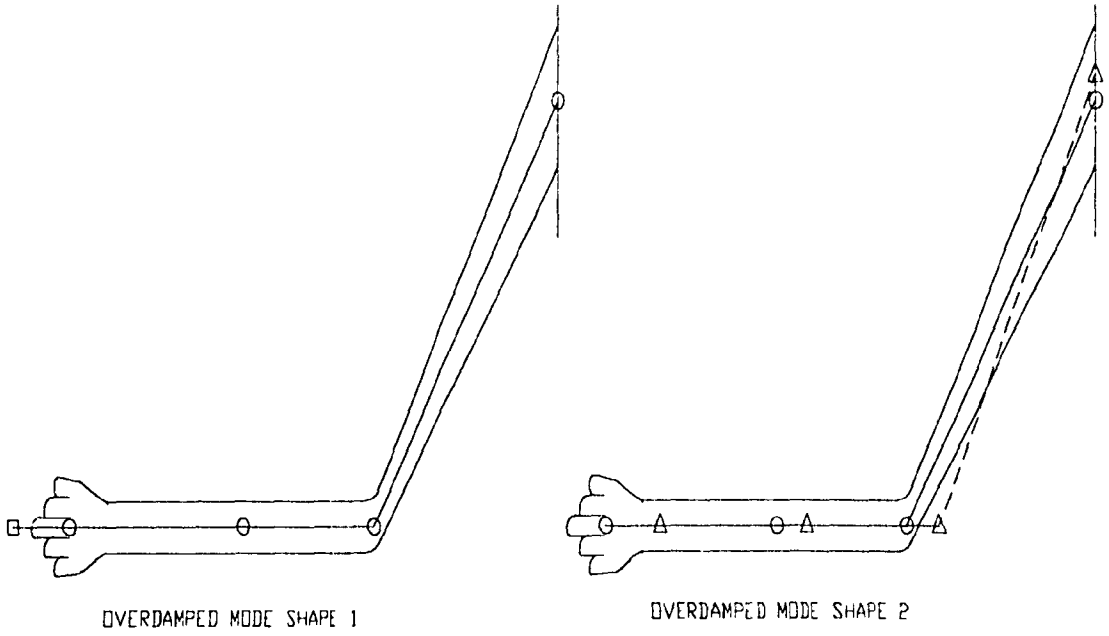

Figure 3.2: Overdamped Mode shapes of the HAV model 1

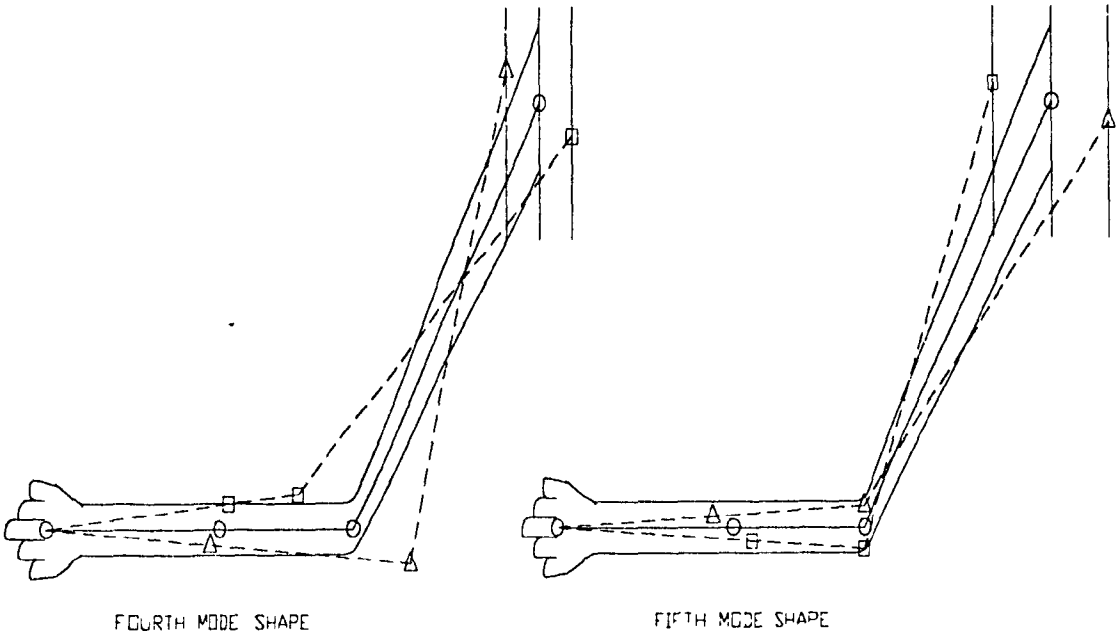

Figure 3.3: Fourth and Fifth Mode shapes of HAV model 1

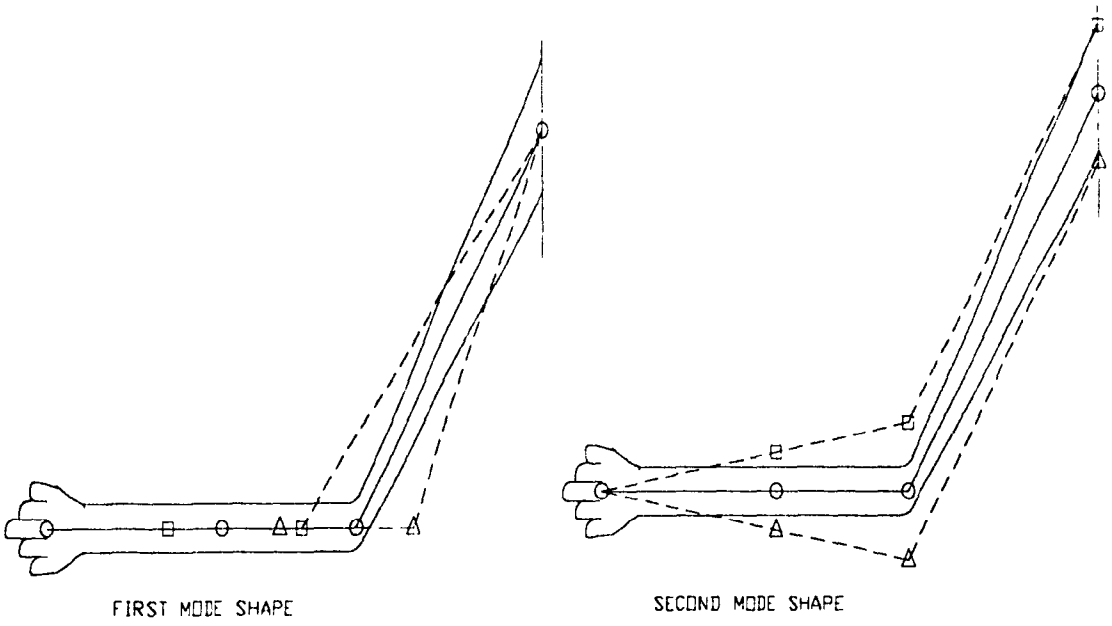

Figure 3.4: First and Second Mode shapes of HAV model 2

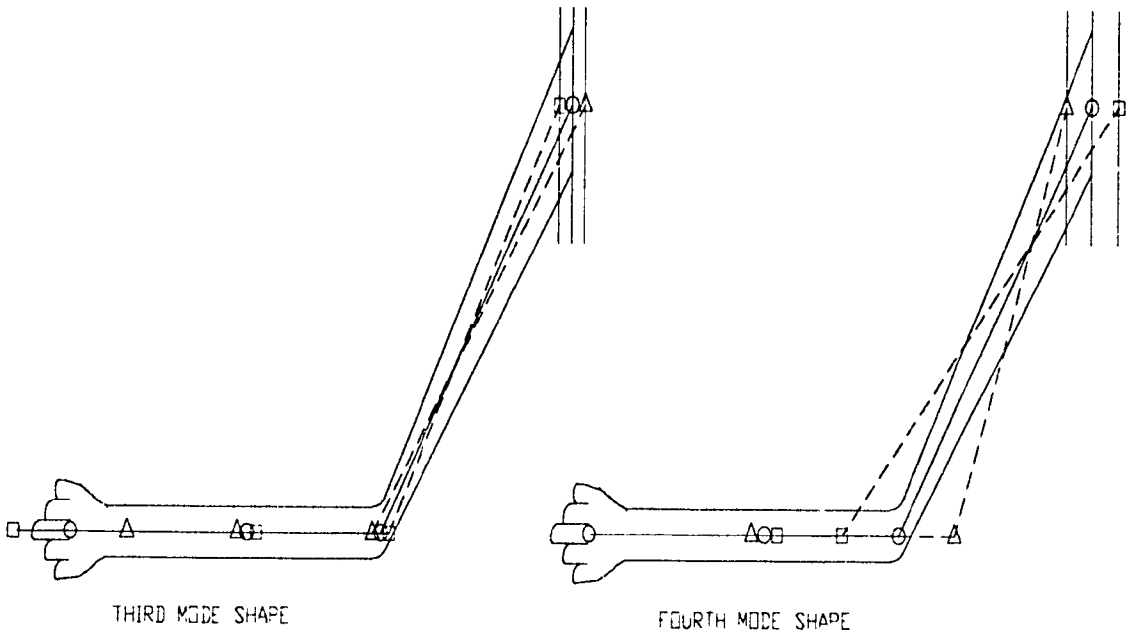

Figure 3.5: Third and Fourth Mode shapes of HAV model 2

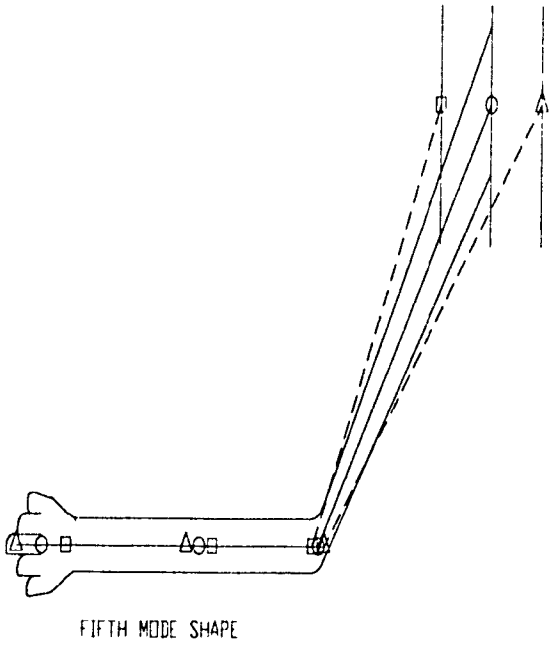

Figure 3.6: Fifth Mode shape of HAV model 2

Substituting equation 3.5 into equation 3.2 and premultiplying the resulting equation by $[\phi]^T$ results in

$$[\phi]^T[\mu][\phi]\{\dot{q}\} + [\phi]^T[\kappa][\phi]\{q\} = [\phi]^T\{F\} \tag{3.6}$$

where $\{F\}_{2n\times 1}$ is the excitation vector.

In view of the orthogonal property of the mode shapes, we have

$[\phi]^T[\mu][\phi] = [M]$

$[\phi]^T[\kappa][\phi] = [K]$

where [M] and [K] are the generalized mass and stiffness matrices, respectively, and are diagonal. Further, $[\phi]^T\{F\} = \{H\}$ is the generalized force vector.

Assuming a sinusoidal harmonic input at the hand (mass m_1), the force vector is of the form, $F = \{\{f\}0,0,0,0,0\}^T_{2n\times 1}$

where $\{f\} = \{f_0 sin\omega t, 0,0,0,0\}^T_{n\times 1}$

The Equation 3.6 is transformed in to 2n uncoupled differential equations.

$$[M]\{\dot{q}\} + [K]\{q\} = \{H(t)\} \tag{3.7}$$

A detailed discussion on the solution of 2n number of uncoupled first order complex differential Equations above, in closed form is explained in Appendix B. The modal responses (q_i) are transformed in original coordinates responses (ζ_i) using the Equation 3.5.

The response under harmonic excitation for the linear equations describing HAV model is also solved by 4^{th} order Runga Kutta method and the responses are compared with those obtained from the modal analysis.

3.4.1 Discussion Based on HAV Response Under Deterministic Excitation

The response of the HAV model under different frequencies of excitation is illustrated from Figure 3.7 to Figure 3.15 for both models. The excitation frequencies are selected to match the damped natural frequencies of the model in order to assess maximum severity due to vibration.

In general for lower excitation frequencies, vibration responses at the hand, fore-arm and elbow are predominant as illustrated in Figures 3.7,3.8,3.11 and 3.12. Hence, for a lower frequency excitation to the hand, a considerable amount of vibration will transmit to the hand, fore-arm and the lower part of the upper-arm. The vibration effect to the shoulder is insignificant when compared with the responses of the hand, fore-arm and elbow. It may be due to the large dissipation of the vibration energy occurring in the upper-arm.

At higher excitation frequencies, the vibration response of the fore-arm, elbow and shoulder are observed to be very low, when compared with that of the hand as illustrated in Figures 3.9,3.10,3.13,3.14 and 3.15. Consequently, it is revealed that at higher excitation frequencies, the vibration is mostly localized to the hand itself, which agrees with the conclusions of the studies reported in [31],[32] and [35].

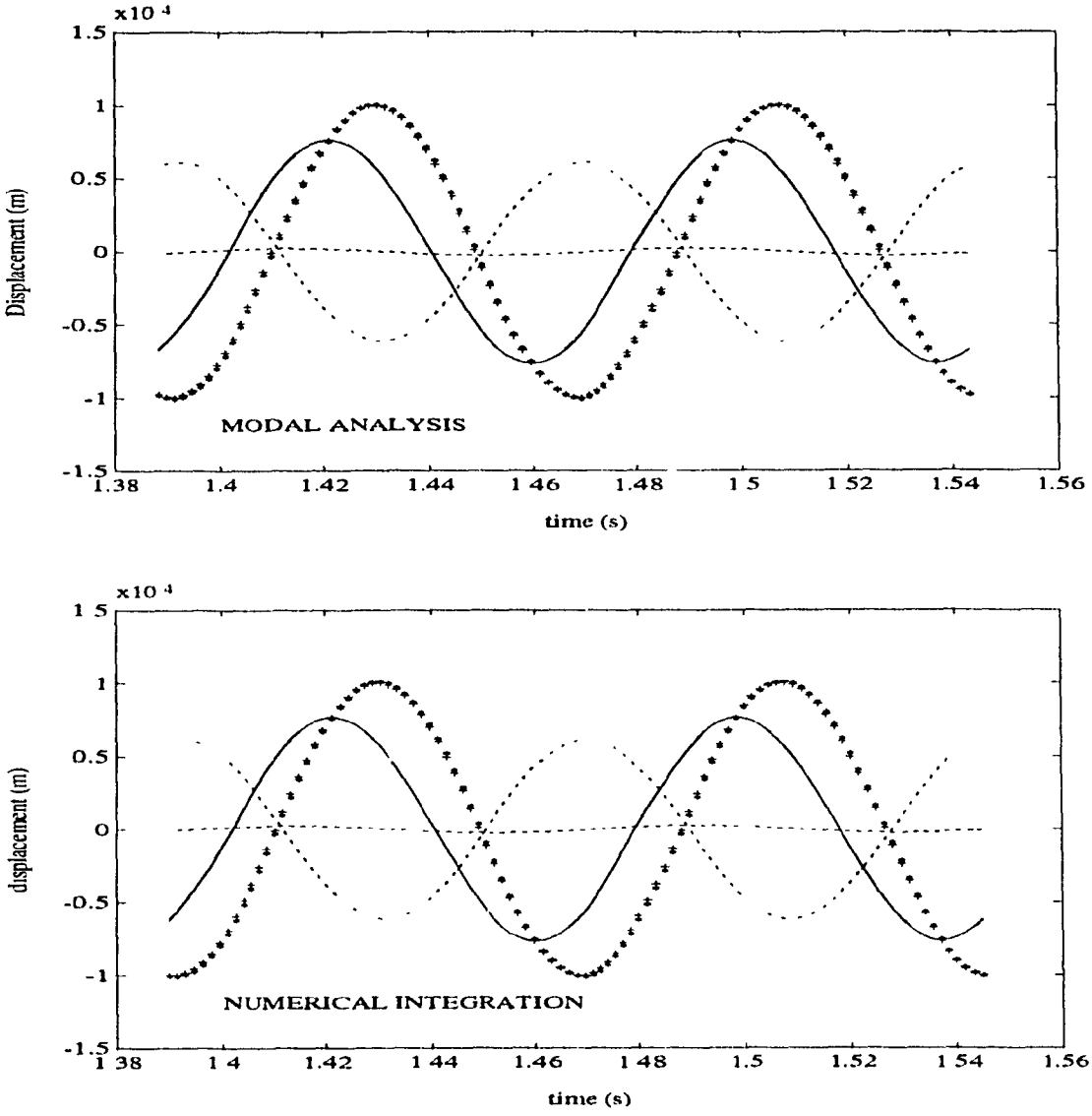

Figure 3.7: Response of HAV model 1 with an excitation amplitude of 5.0 N and frequency of 12.9483 Hz.
(— z_1, + z_2, * z_3, – · – · x_3, - - - z_4, · · · x_4)

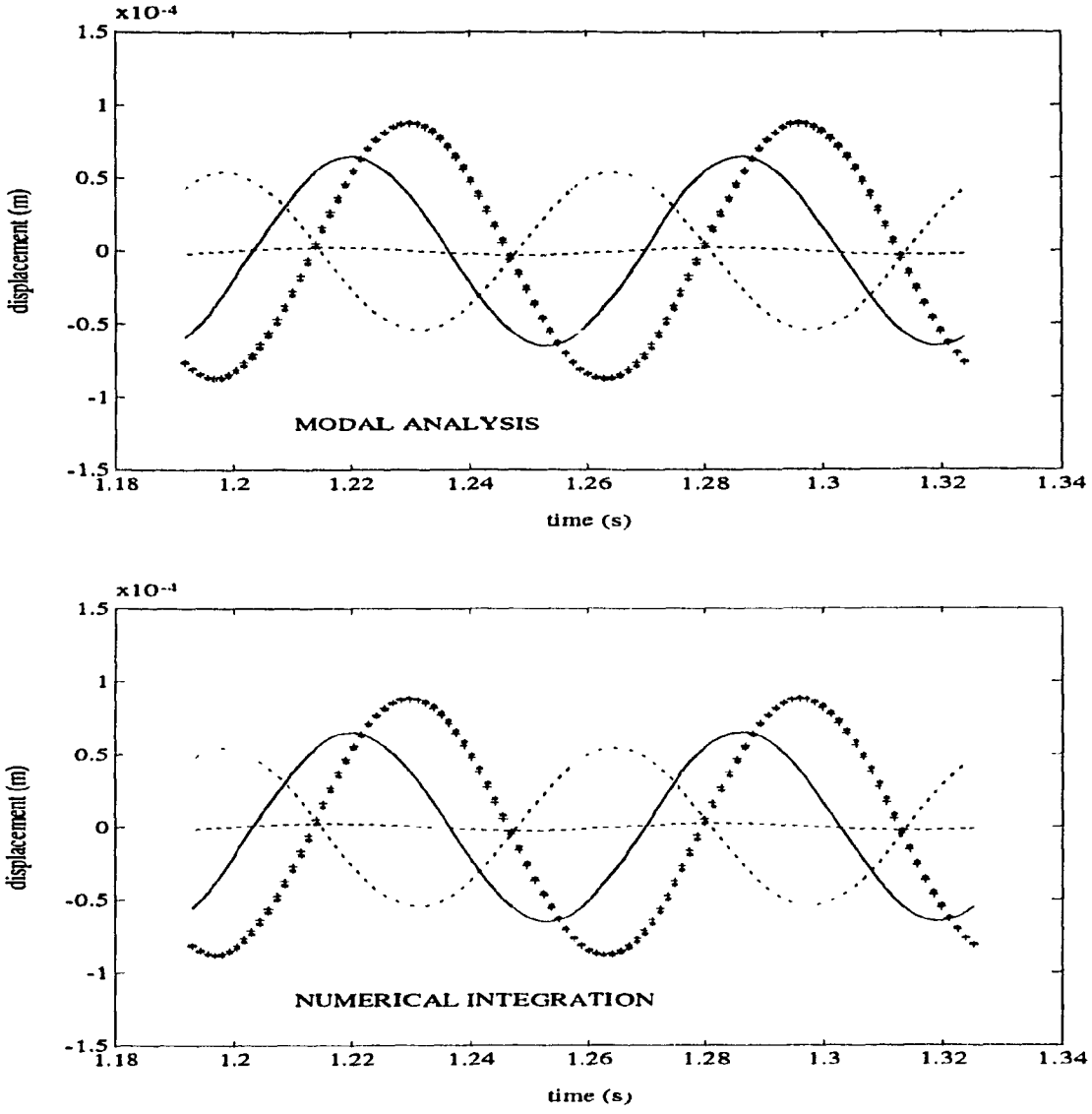

Figure 3.8: Response of HAV model 1 with an excitation amplitude of 5.0 N and frequency of 15.0934 Hz.
(— z_1, + z_2, * z_3, – · – · x_3, - - - z_4, · · · x_4)

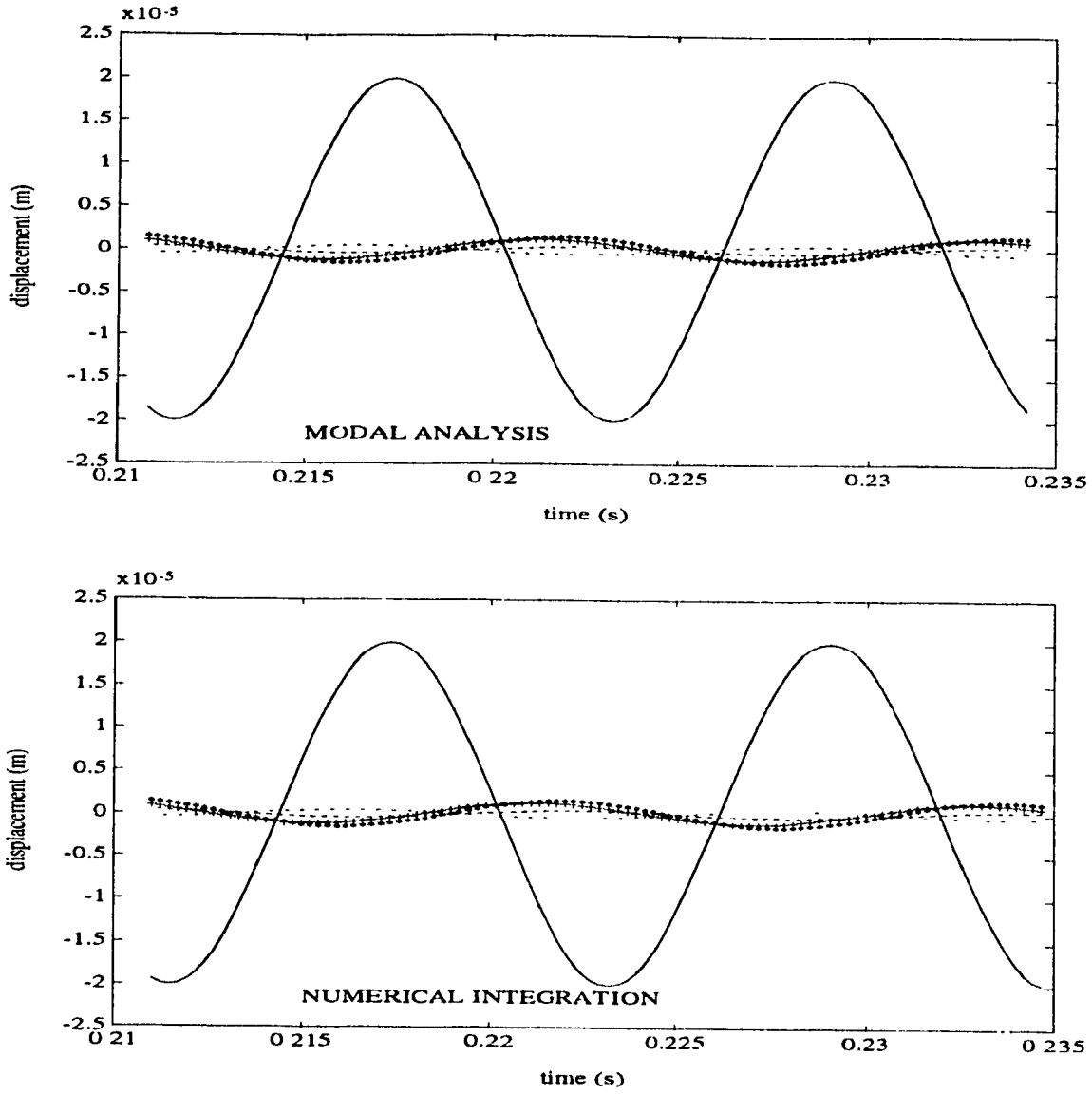

Figure 3.9: Response of HAV model 1 with an excitation amplitude of 5.0 N and frequency of 85.2920 Hz.
(— z_1, + z_2, * z_3, — · — · x_3, - - - z_4, · · · x_4)

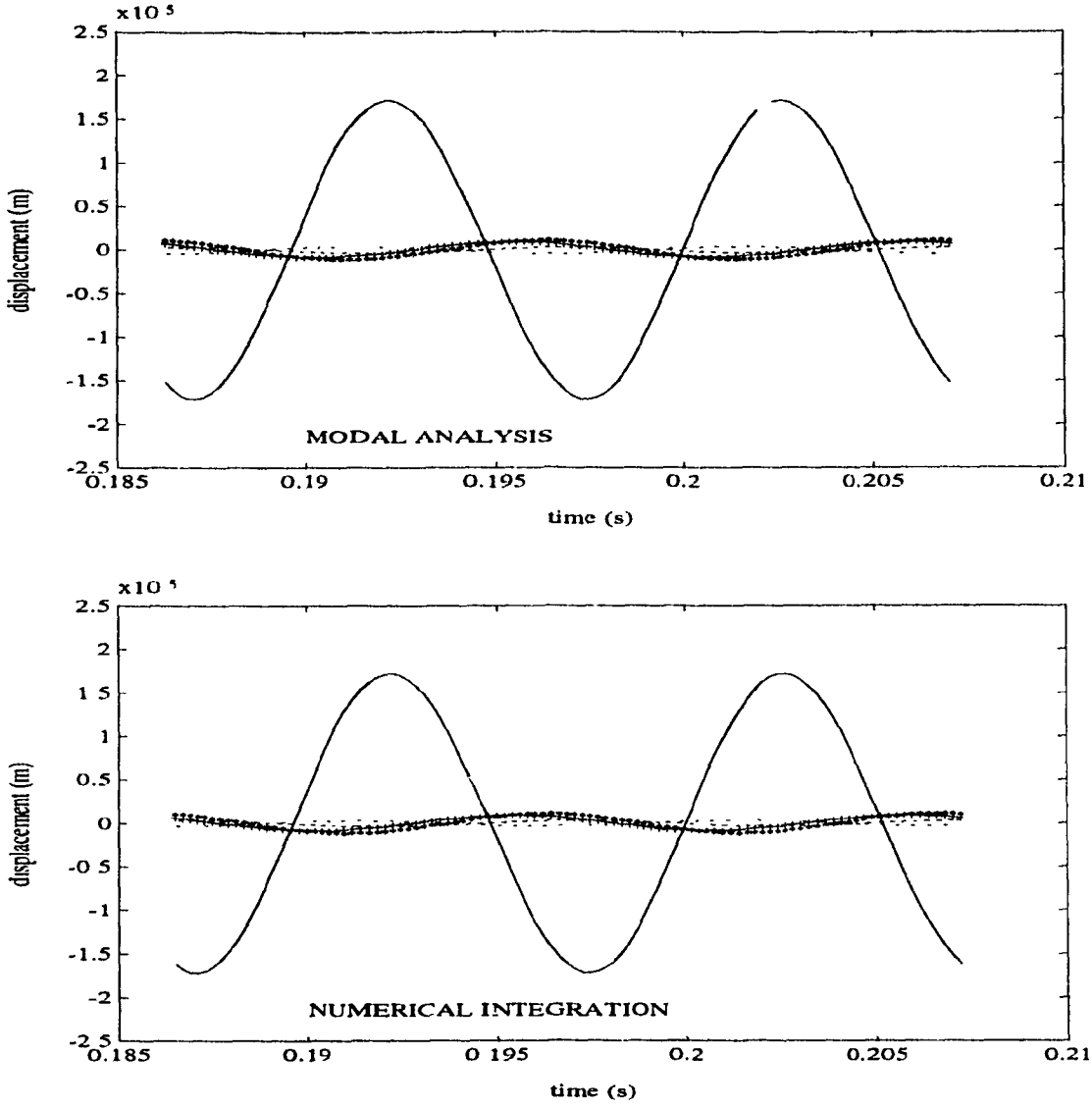

Figure 3.10: Response of HAV model 1 with an excitation amplitude of 5.0 N and frequency of 96.5289 Hz.
(— z_1, + z_2, * z_3, — · — · x_3, - - - z_4, · · · x_4)

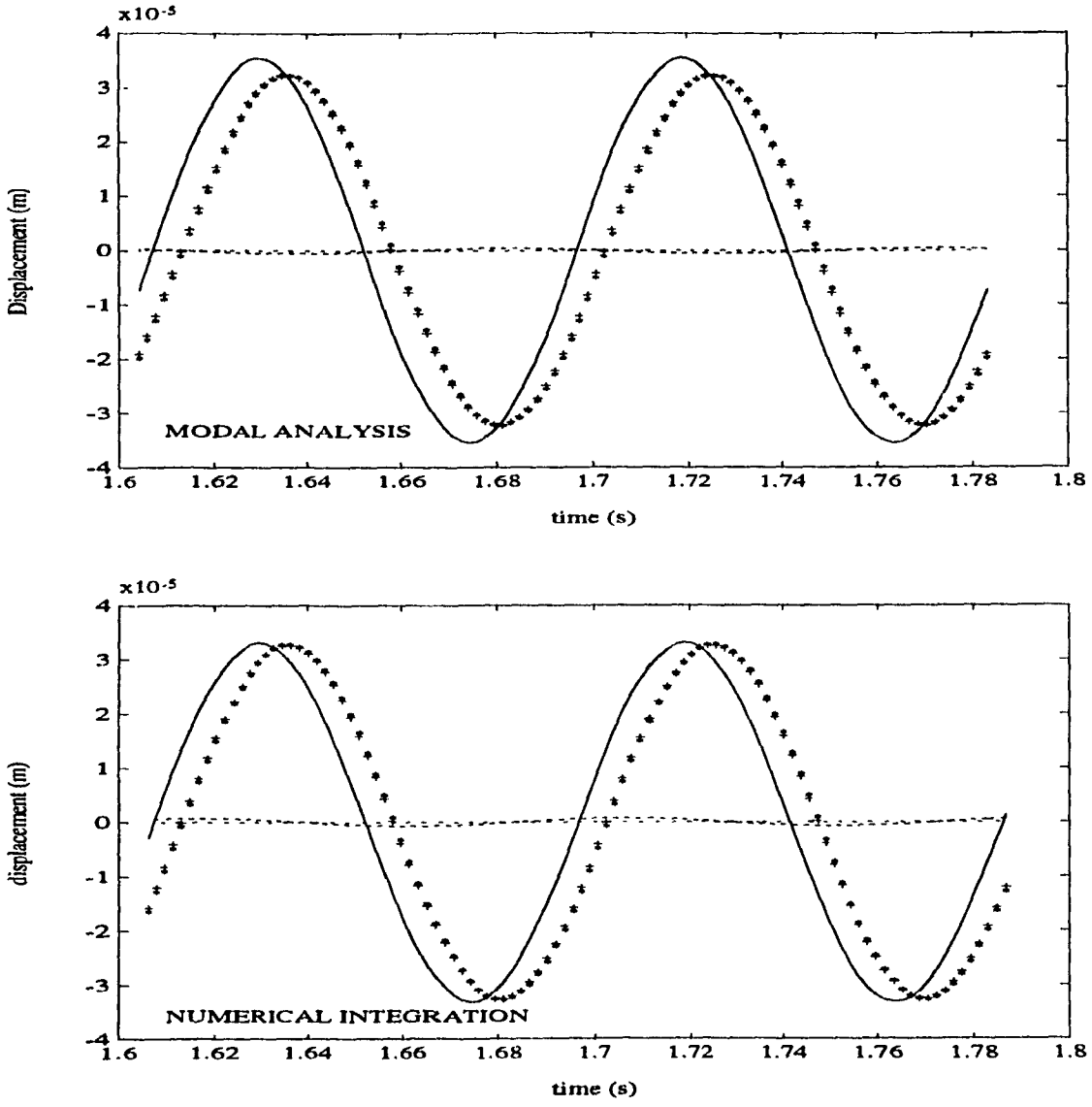

Figure 3.11: Response of HAV model 2 with an excitation amplitude of 5.0 N and frequency of 11.2062 Hz.
(— z_1, + z_2, * z_3, $-\cdot-\cdot x_3$, - - - z_4, $\cdots x_4$)

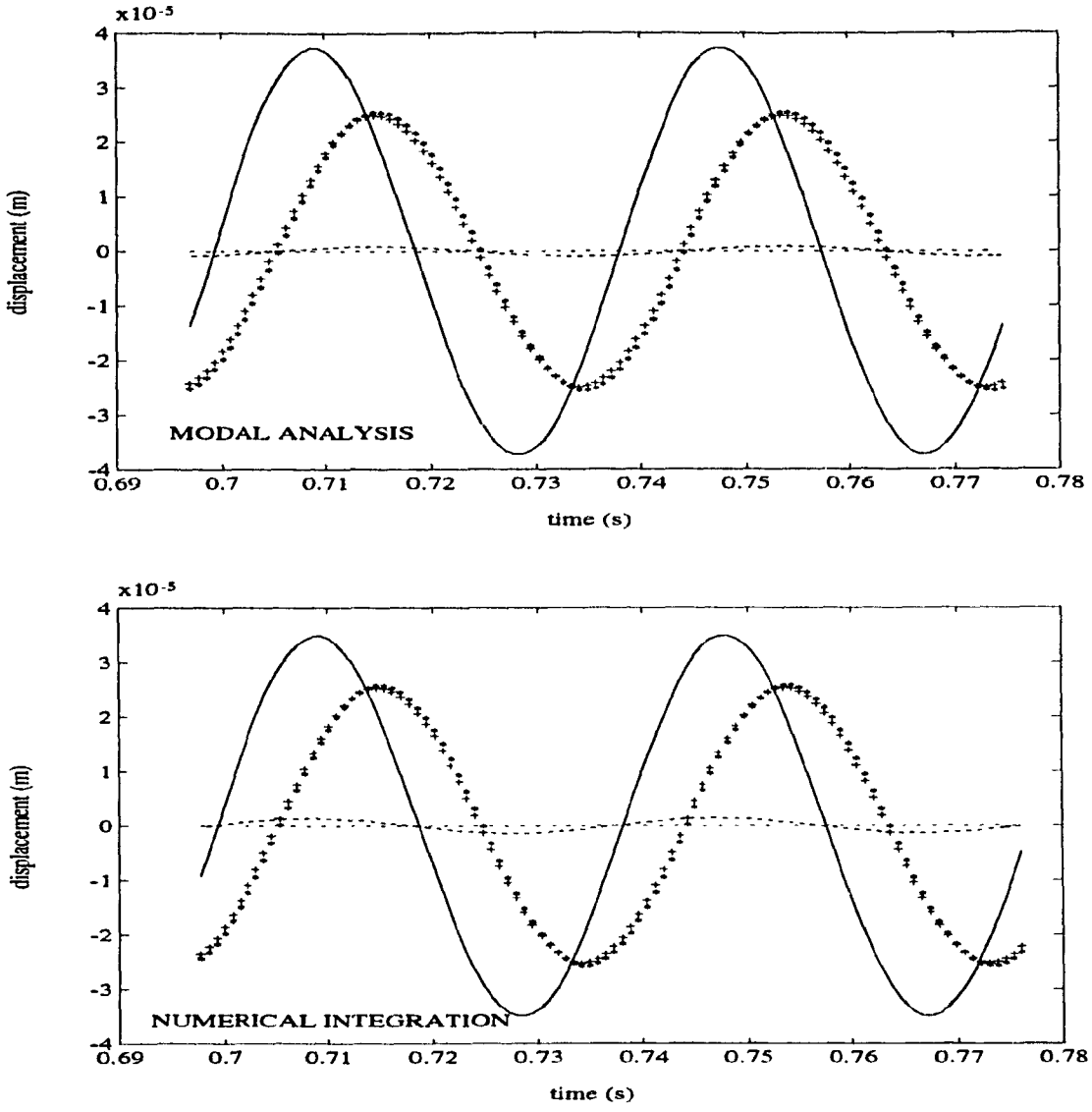

Figure 3.12: Response of HAV model 2 with an excitation amplitude of 5.0 N and frequency of 25.7980 Hz.
(— z_1, + z_2, * z_3, $-\cdot-\cdot x_3$, - - - z_4, $\cdots x_4$)

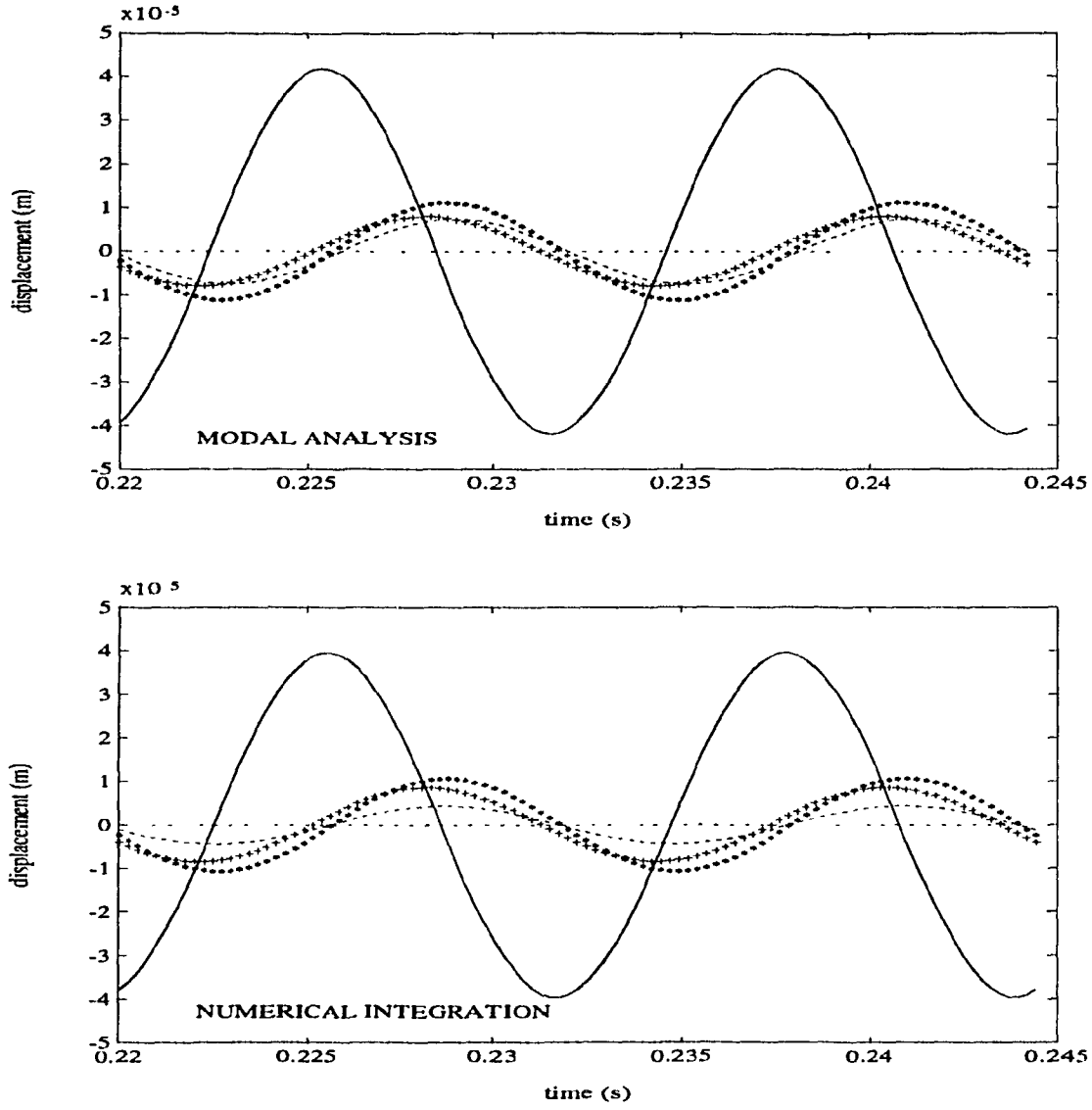

Figure 3.13: Response of HAV model 2 with an excitation amplitude of 5.0 N and frequency of 81.8075 Hz.
(— z_1, + z_2, * z_3, — · — · x_3, - - - z_4, · · · x_4)

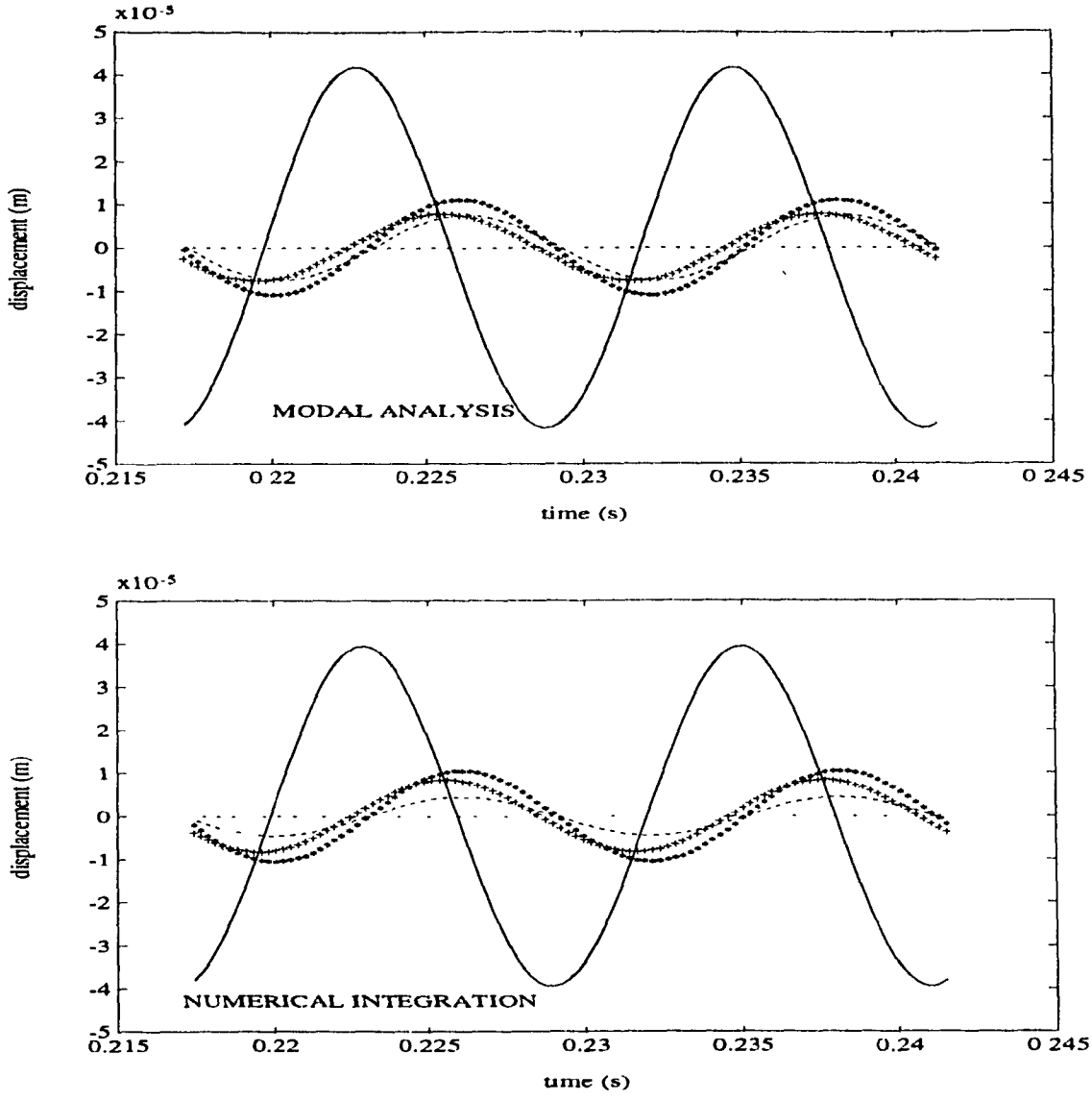

Figure 3.14: Response of HAV model 2 with an excitation amplitude of 5.0 N and frequency of 82.8014 Hz.
(— z_1, + z_2, * z_3, — · — · x_3, - - - z_4, · · · x_4)

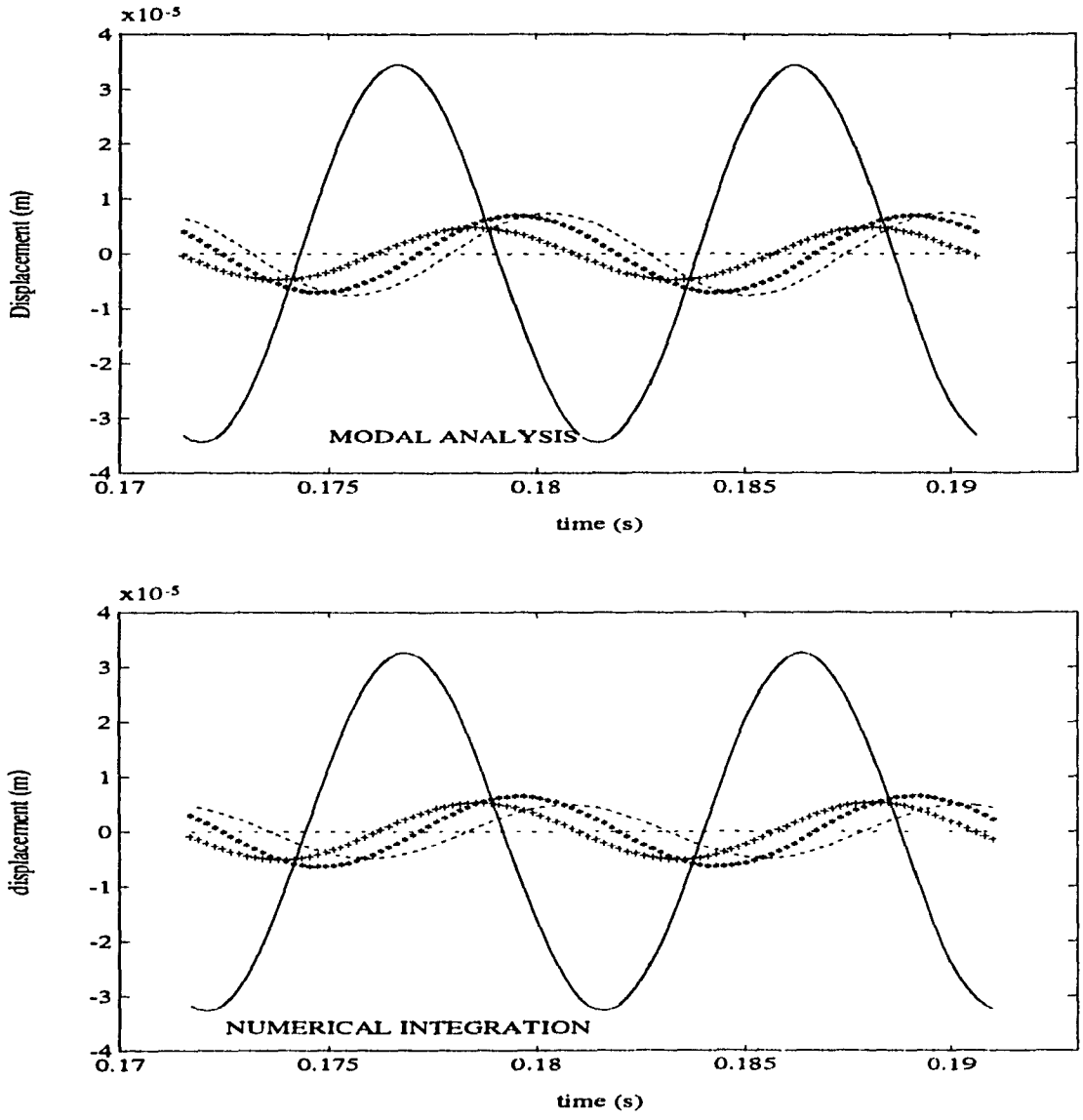

Figure 3.15: Response of HAV model 2 with an excitation amplitude of 5.0 N and frequency of 104.8411 Hz.
(— z_1, + z_2, * z_3, — · — · x_3, - - - z_4, · · · x_4)

3.5 Summary

The complex eigenvalue analysis is performed on the developed hand-arm models and damped natural frequencies are identified where the responses are significant. The mode shape data are formed from the complex eigenvectors and the deflection pattern of the hand-arm system is plotted for each mode. It can be seen from the first and second mode shapes that there is a higher likelihood of causing damage to the fore-arm and the upper-arm at lower resonant frequencies (10-35) Hz. The examination of the third mode shape indicated that the middle resonant frequencies (50-90) Hz are more dangerous to the hand due to the larger relative displacements occurring there compared to other components of hand-arm system. The possibility of higher stress at shoulder region is revealed by examining fourth and fifth mode shapes of higher resonant frequencies (80-140) Hz. Further the response experienced by the different components of the hand-arm system under different frequencies of harmonic excitation is simulated using modal analysis and it is compared with that obtained from the numerical integration. It is observed that at higher frequencies the vibration is mostly localized to the hand itself. Also, the response due to vibration at the shoulder is insignificant.

In the following chapter, the vibration response of the developed model from a field measured stochastic excitation from a power tool is simulated and the harmful effect is discussed based on the dose-response relationship proposed by ISO-5349. Further, a concept of a hand-arm vibration isolator, based on the principle of energy division, is presented. A complete simulation of the response of the hand-arm model after integrating with the isolator model under the same stochastic excitation mentioned above, is performed to assess the effectiveness of the proposed isolator mechanism in containing the harmful vibration transmission to the hand-arm.

Chapter 4

Vibration Response of the Hand-Arm Model and Development of a Vibration Isolator

The characteristics of hand-transmitted vibration are strongly dependant upon the type of power tool and nature of the task performed by the operators. The vibration characteristics of various tools, measured at the handle, have been reported in the literature [55,56,60]. A study of the reported data shows that the handle vibration characteristics of different tools are considerably different. While the rms acceleration of handle vibration of different hand-held power tools varies in the 2.0 g to 205.0 g range [22], the vibrations of most tools are predominantly in the 10-1000 Hz frequency range. The assessment of severity of hand-transmitted vibration thus necessitates appropriate consideration of vibration characteristics of specific tools.

Hand Vibration Exposure guidelines have been proposed to assess the severity as a function of the exposure duration and excitation frequencies [77]. The proposed guidelines further provide an insight to the probability of developing finger blanching or

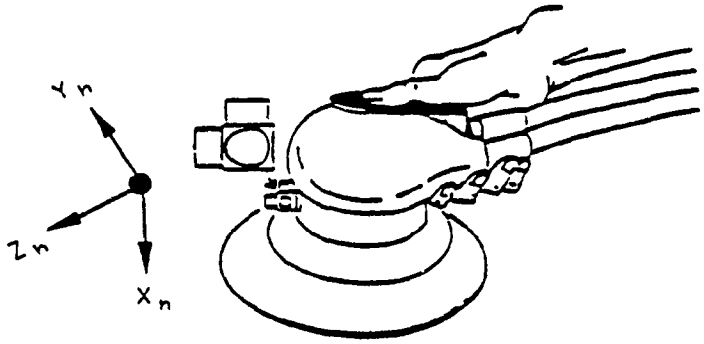

Figure 4.1: A schematic of a palm grip orbital sander [56]

Vibration White Finger associated with exposure to the hand-transmitted vibration [23]. In this section, the response characteristics of the hand-arm vibration model are evaluated for stochastic excitations arising from a palm-grip orbital sander. The methodology to assess the severity of hand-transmitted vibration, in relation to the recommended exposure limits, is described. A vibration isolation mechanism, based upon the concept of energy flow divider, is proposed to reduce the magnitude of hand-transmitted vibration. Parametric optimization is carried out to determine the optimal parameters of the isolator to effectively attenuate the vibration due to an orbital sander. The performance characteristics of the isolator are also evaluated using the proposed exposure limits.

4.1 Handle Vibration of an Orbital Sander

The vibration characteristics of various tools have been measured in order to assess the severity of the exposure [55,60]. Majority of the studies have reported the characteristics of handle vibration in the three orthogonal directions recommended by ISO 5349 [55,56,60], that are conveniently measured by attaching the accelerometers directly to the handle. The characteristics of hand-transmitted vibration, however, have

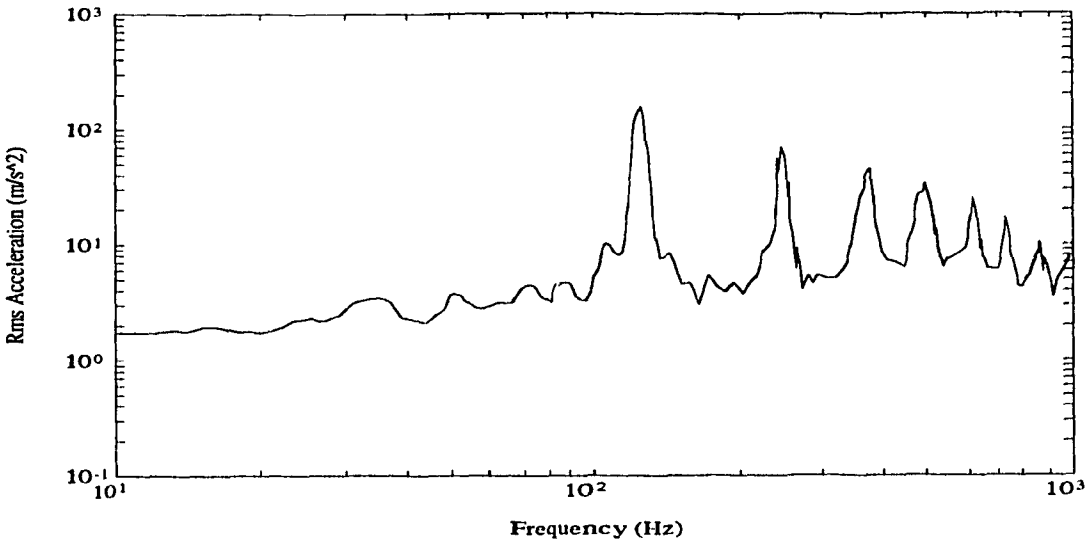

Figure 4.2: Representation of RMS acceleration spectra of handle vibration of palm grip orbital sander

been reported in a few studies only [22]. These measurements are further performed under laboratory test condition due to complexities associated with measurements at the human hand. The field measured vibration of the handle are considered to be the excitation to the hand-arm, assuming negligible interactions due to the operator's hand. Although vibration spectra of many different tools, measured at the handle, have been reported in the literature, the vibration excitation of a palm-grip orbital sander is used to derive the response characteristics of the hand-arm. Figure 4.1 illustrates the schematic of a palm-grip type orbital sander together with the accelerometers arranged along the bio-dynamical coordinate of the hand-arm.

The rms acceleration spectrum of the handle vibration measured along the longitudinal axis, Z_h, is illustrated in Figure 4.2 [56]. The dominant fundamental frequency of the handle vibration is observed near 125 Hz and the corresponding magnitude of rms acceleration is approximately 170 m/s^2. The manufacturer-supplied free running speed of the orbital sander is 8000 rpm, which closely corresponds to the dominant fundamental frequency. The handle vibration spectrum exhibits significant peaks corresponding to

frequencies near 250, 375, 500, 625, 750, 875 and 1000 Hz with respective rms accelerations of about 70, 45, 35, 25, 15, 10 m/s^2. These dominant frequencies are related to higher harmonics of the fundamental operating speed of the orbital sander.

4.2 Response Analysis

The coupled differential equations of motion for five-DOF hand-arm vibration models, described in Chapter 2, can be expressed in the following matrix form :

$$[M]\{\ddot{u}\} + [C]\{\dot{u}\} + [K]\{u\} = \{f\} \tag{4.1}$$

where [M], [C] and [K] are (n × n) mass, damping and stiffness matrices, respectively. n is the number of degrees of freedom and {u} is a (n × 1) vector of displacement response quantities, given by:

$$\{u\} = \{\bar{z}_1, \bar{z}_2, \bar{z}_3, \bar{x}_3, \bar{\theta}_3\}^T$$

'T' designates the transpose and {f} is a (n × 1) forcing vector, given by:

$$\{f\} = \{K_0 z_0 + C_0 \dot{z}_0, 0, 0, 0, 0\}^T$$

Equation (4.1) is solved to determine the complex frequency response function vector, given by:

$$\{h(j\omega)\} = \left[[K] - \omega^2[M] + j\omega[C]\right]^{-1}\{f\} \tag{4.2}$$

where $\{h(j\omega)\}$ is the (n × 1) complex frequency response function vector and ω is the circular frequency in rad/s. The complex frequency response function describes the vibration transmissibility at various co-ordinates of the hand-arm:

$$\{h(j\omega)\} = \left\{\frac{z_1}{z_0}(j\omega), \frac{z_2}{z_0}(j\omega), \frac{z_3}{z_0}(j\omega), \frac{x_3}{z_0}(j\omega), \frac{\theta_3}{z_0}(j\omega)\right\}^T$$

The vertical and longitudinal vibration transmissibility at the shoulder joints is derived using the following transformation:

$$\left\{ \begin{array}{c} \frac{z_4}{z_0}(j\omega) \\ \frac{x_4}{z_0}(j\omega) \end{array} \right\} = [T]\{h(j\omega)\} \tag{4.3}$$

where [T] is [2 × 5] transformation matrix derived from the kinematic constraints, described in Chapter 2. The rms acceleration response of the hand-arm can then be evaluated using the rms acceleration spectrum of the handle vibration:

$$\{S_r(\omega)\} = | h(j\omega) | S_0(\omega) \tag{4.4}$$

where $\{S_r(\omega)\}$ is the (n × 1) vector of rms acceleration response at the generalized coordinates of the five-DOF hand-arm models. $S_0(\omega)$ is the rms acceleration of the handle vibration. The vertical and longitudinal acceleration response at the shoulder joint can be evaluated using Equation (4.3):

$$\{S_p(\omega)\} = | [T]\{h(j\omega)\} | S_0(\omega) \tag{4.5}$$

where $\{S_p(\omega)\}$ is a (2 × 1) vector comprising the vertical and longitudinal rms acceleration response of the shoulder joint. Figure 4.3 illustrates the longitudinal acceleration response of the hand, fore-arm and the elbow together with the excitation. It is observed that response characteristics of the hand (z_1), fore-arm (z_2) and elbow (z_3) follow patterns similar to that of the handle vibration shown in Figure 4.2. The vibration response characteristics of the hand, fore-arm and elbow exhibit dominant peaks near the excitation frequencies of the orbital sander. The corresponding magnitudes of the various peaks, however, are lower than those observed for the handle vibration. While the magnitude of hand vibration closely follows the excitation levels at excitation frequencies upto 200

Hz, the vibration excitations at higher frequencies are observed to be attenuated. The vibration response of the fore-arm and elbow reveal considerable attenuation of vibration at frequencies above 20 Hz. The results clearly reveal that vibrations above 200 Hz remain localized to the hand, which conforms with the observation made from laboratory measurements presented in Chapter 2.

The vibration response characteristics of the hand-arm vibration model 2 are evaluated for excitations upto only 200 Hz, since the model was developed using the measured data in this frequency range. From Figure 4.3 it is apparent that the hand-transmitted vibrations are mostly predominant at frequencies below 200 Hz. Further the weighting factors, proposed in ISO-5349 are well below 0.1 for vibration above 200 Hz. The severity of the hand-transmitted vibration can thus be effectively assessed using the response characteristics in the 10-200 Hz frequency range. Figure 4.3 further reveals that the response characteristics of model 2 are quite similar to those of the model 1 in the 10-200 Hz frequency range. The model 2, however, exhibits slight amplification of hand-transmitted vibration in 20-90 Hz frequency range. The higher levels of transmitted vibration are attributed to the palm-grip and high grip force associated with model 2.

Figure 4.4 illustrates the rotational acceleration response in rad/s^2 of the elbow joint together with the handle acceleration due to orbital sander in m/s^2. The angular acceleration response follows a pattern similar to that of the excitation. The angular acceleration response of model 2, again, is considerably larger than that of model 1. The rms acceleration spectra of longitudinal vibration transmitted to the shoulder joint of both models are presented in Figure 4.5. The figure clearly reveals considerable attenuation of vibration transmitted to the shoulder. Figures 4.4 and 4.5 also reveal that the magnitudes of angular acceleration response of the upper-arm and the longitudinal acceleration response of the shoulder of model 2 are relatively higher than those of the model 1, due to higher grip force considered for model 2.

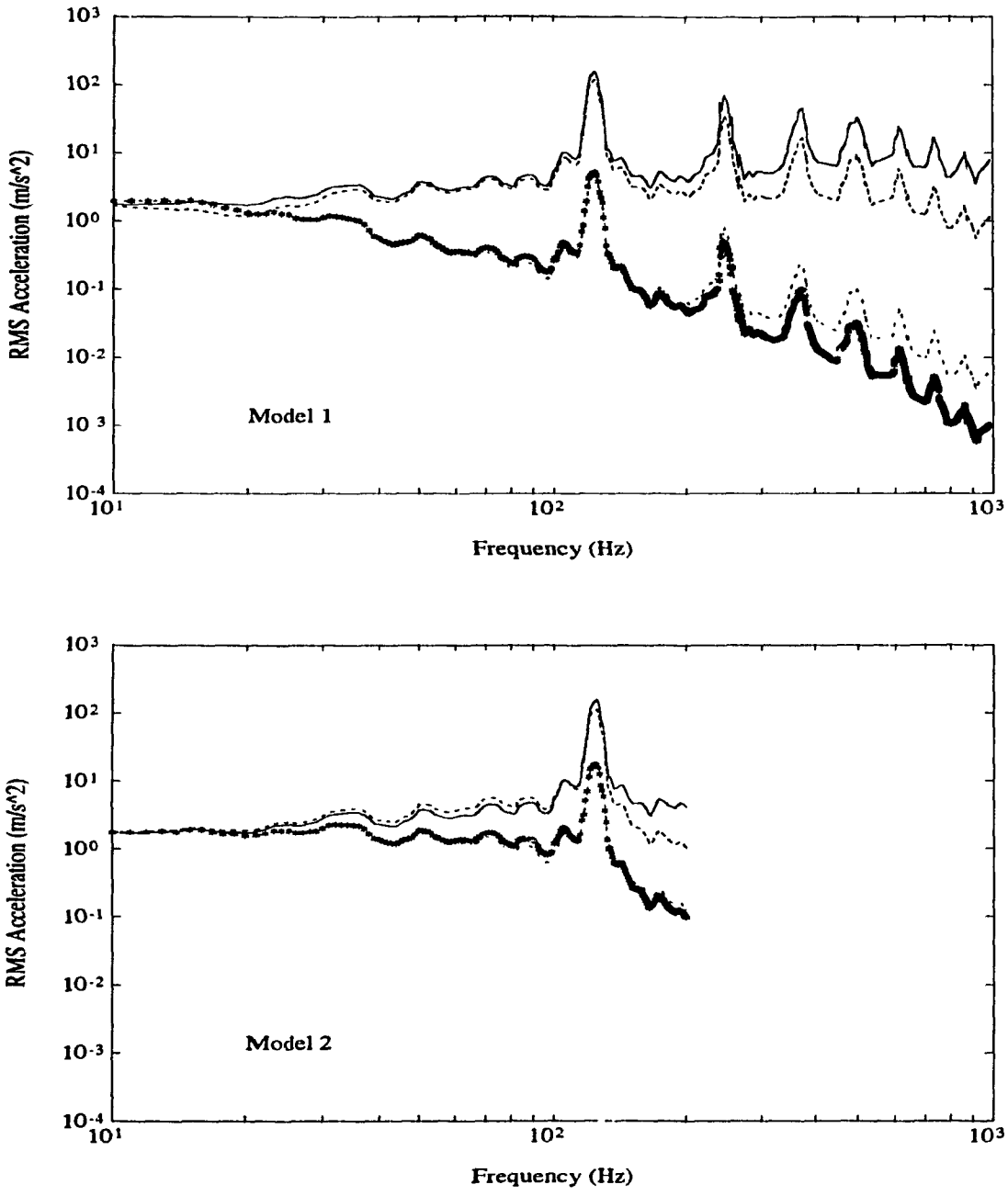

Figure 4.3: RMS acceleration spectra of handle vibration due to orbital sander and corresponding longitudinal acceleration responses in m/s^2 of the hand, fore-arm and elbow
(z_0 —, z_1- - -,z_2 — · — ·—, z_3 ***)

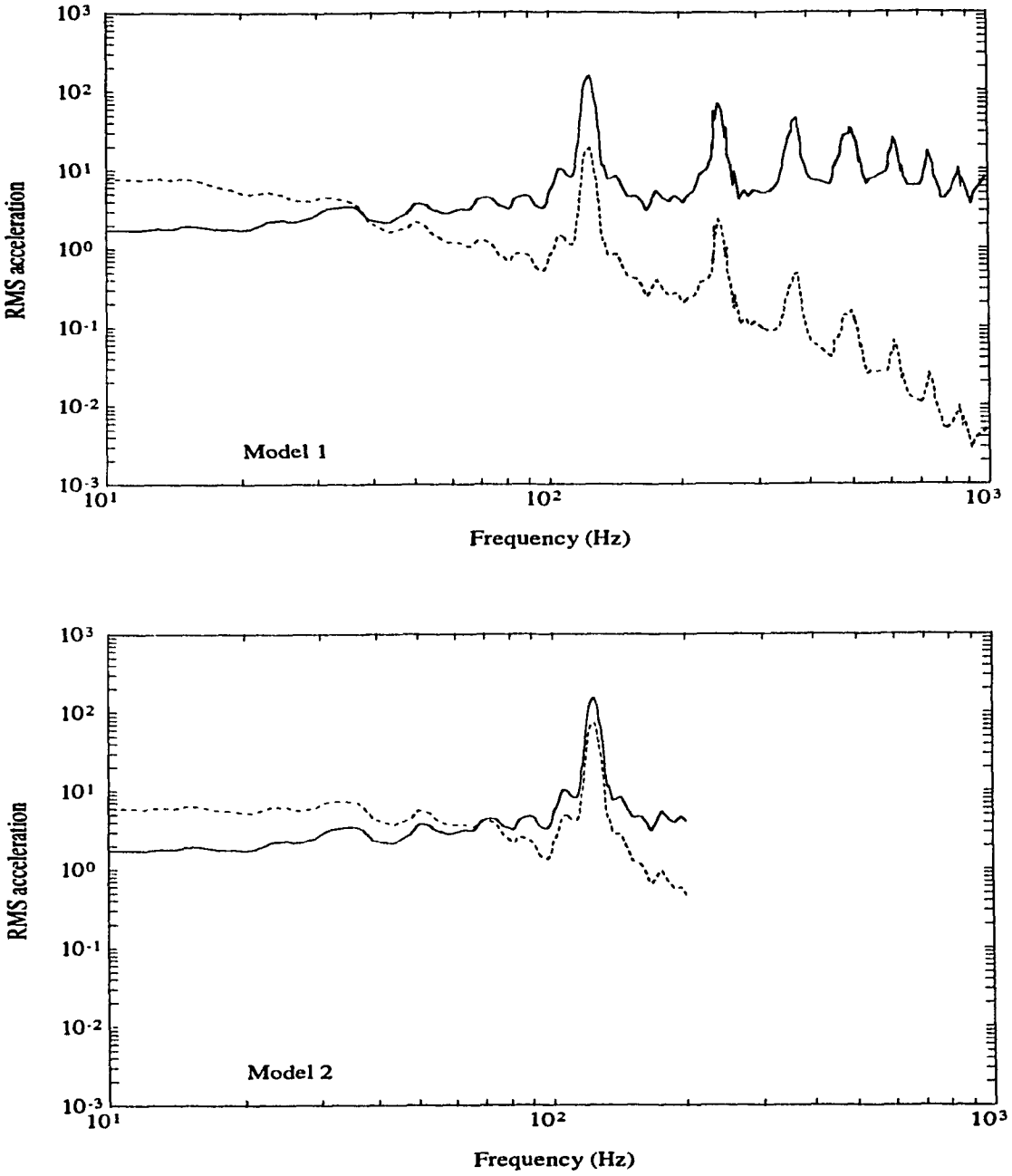

Figure 4.4: RMS acceleration spectra due to orbital sander in m/s^2 and the corresponding rotational acceleration response in rad/s^2 of the upper-arm about the elbow joint (z_0 —, θ_3 - - -)

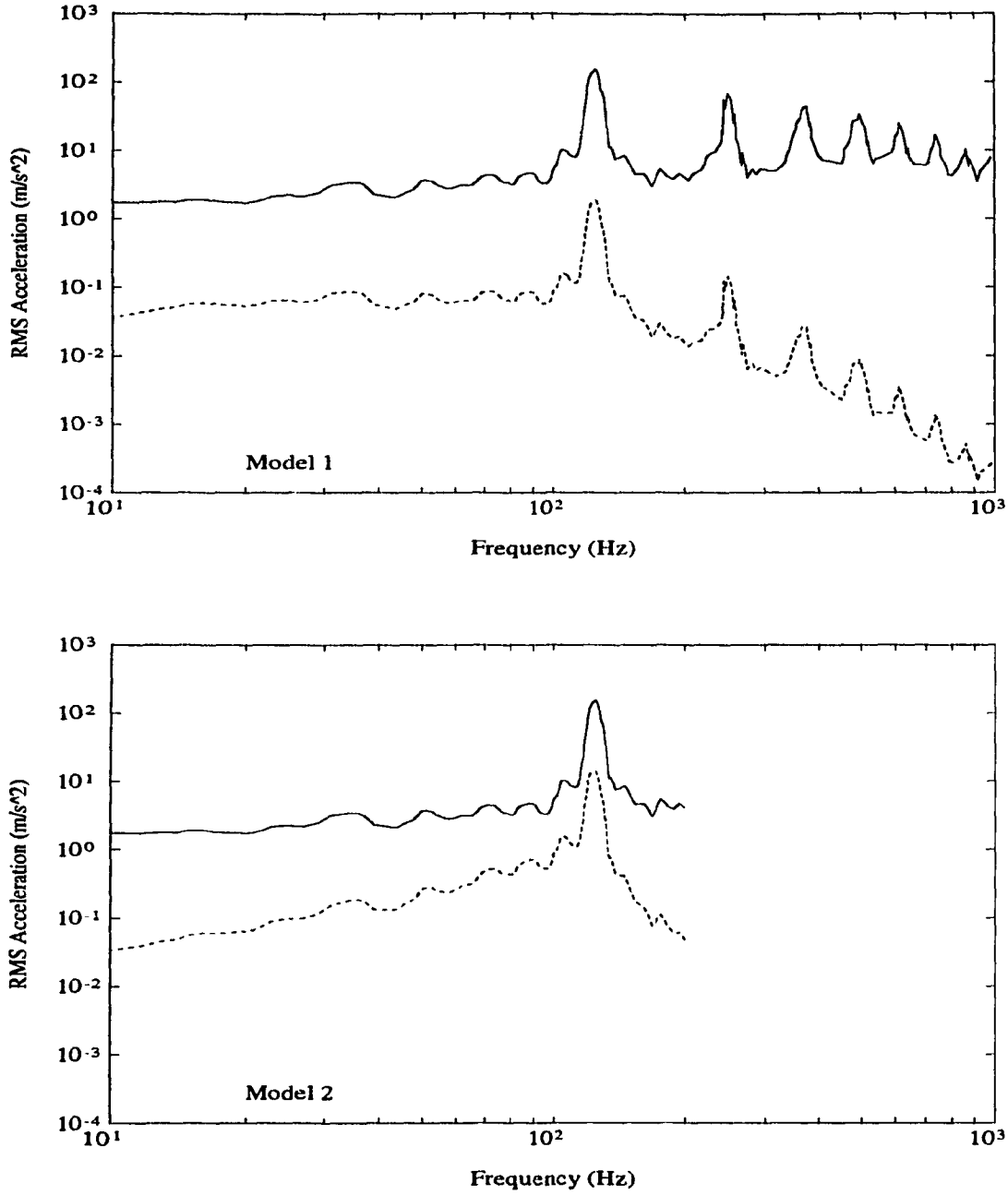

Figure 4.5: RMS acceleration spectra of handle vibration due to orbital sander and corresponding longitudinal acceleration response in m/s^2 of the shoulder
(z_0 —, z_4 - - -)

4.3 Assessment of Severity of Hand-Transmitted Vibration

The vibrations transmitted to the hand-arm are assessed using the ISO proposed exposure limits to determine the severity of the exposure. Figure 4.6 illustrates the recommended exposure limits of rms acceleration in the 10-1000 Hz frequency range [77]. The exposure limits are also listed in Table 4.1. The proposed exposure limits represent the rms acceleration levels in m/s^2 corresponding to third octave-band center frequencies, that are considered safe for a daily exposure duration of 4-8 hours [23]. In order to assess the vibration transmitted from the orbital sander, the rms acceleration response characteristics are first expressed in third-octave frequency bands. Figure 4.7 illustrates a comparison of the acceleration response of the hand-arm models and the proposed exposure limits expressed in third-octave band frequency. The hand transmitted acceleration levels lower than the recommended limits are considered to be within the limits of safe exposure to vibration. The hand-transmitted acceleration levels exceeding the recommended limits at any centre frequency are considered to be unsafe in view of the associated health and safety risks.

An examination of Figure 4.7 reveals that the hand-transmitted vibration under light finger-grip (model 1) exceeds the recommended limits in the 100-160 Hz frequency bands. The hand-transmitted vibration under high palm-grip (model 2), however, exceeds the limits in the entire frequency range up to 160 Hz. The vibrations transmitted in the 100-160 Hz frequency range are observed to be most severe.

4.3.1 Assessment of RISK of Acquiring Vibration Induced White Finger

The most severe symptoms of prolonged exposure to hand-transmitted vibration

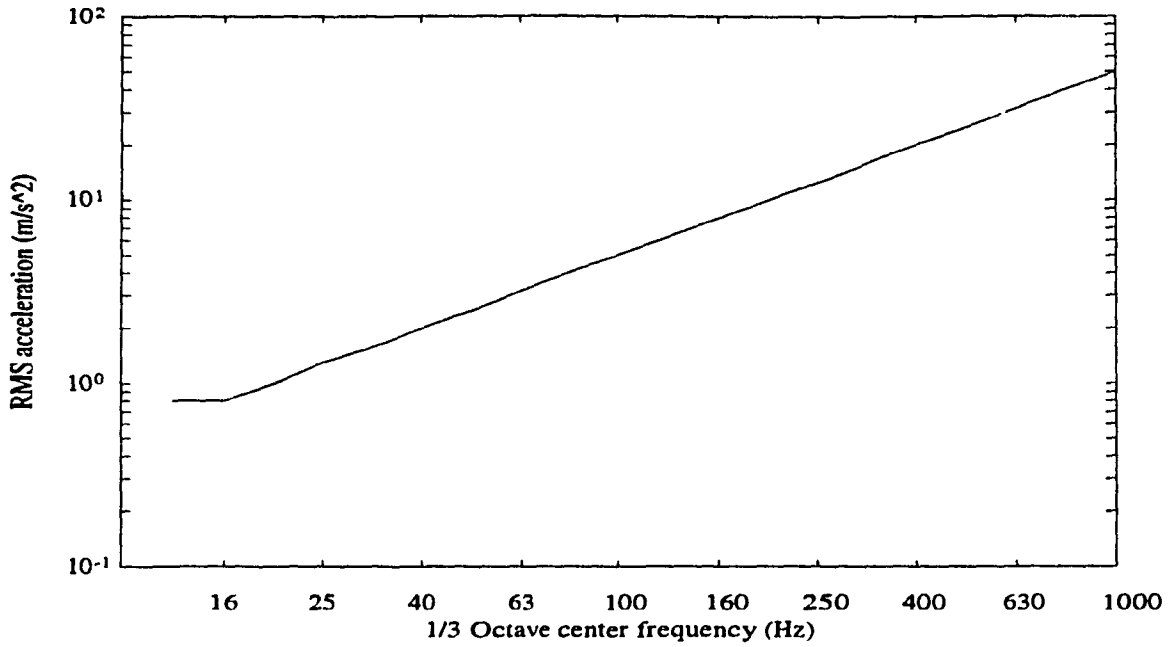

Figure 4.6: Vibration Exposure Guidelines for hand ISO(1978) [77]

is known to be finger blanching or vibration induced white finger. The dose-response relationship, presented in Figure 4.8, is frequently employed to assess the degree of risk of acquiring the Vibration Induced White Finger [23]. The dose-effect relationship has been established from the results of approximately 40 studies of populations of workers who have been exposed to hand-transmitted vibration in their occupations for periods up to 25 years. Each study involved workers who, all year round, normally work all day with only one type of power tool or on an industrial process whereby vibration was transmitted to the hand. Factors of primary importance in determining the risk of VWF include intensity, frequency and duration of exposure to vibration. The vibration level, frequency and the cumulative exposure period are thus considered to determine the dose. These factors are then combined to produce a uniform dose measurement procedure, so as to form the dose-effect relationship based upon the epidemiologic data derived from several reports that contained information on the vibration level produced by the tools used as frequency-weighted acceleration, daily tool use (hours/day), and the latency

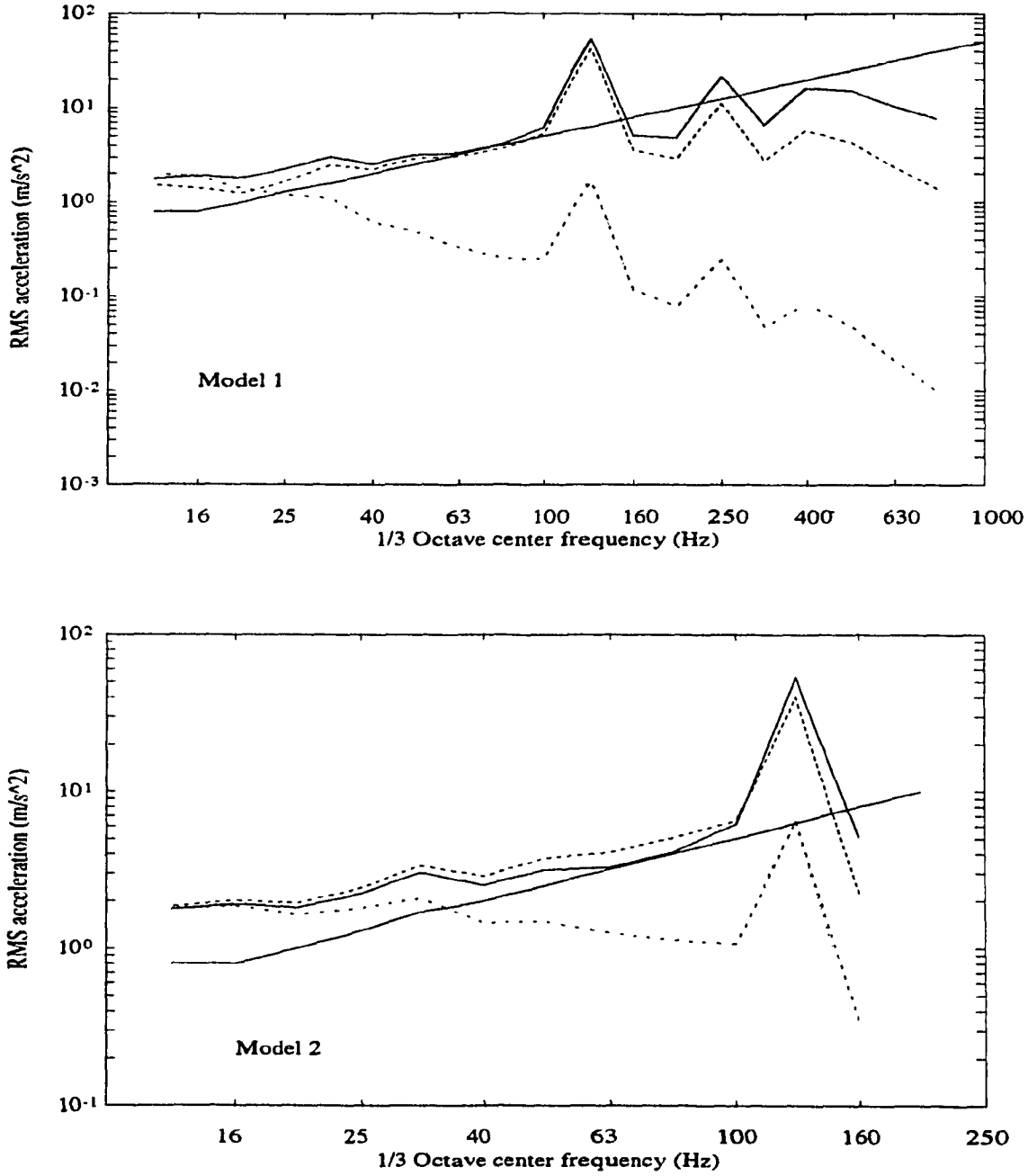

Figure 4.7: RMS spectra of handle vibration and corresponding response of hand-arm model for a palm grip orbital sander
(z_0 —, z_1 - - -,z_2 — · — ·—, z_3 · ··)

period (years of tool use) preceding the first appearance of vascular symptoms. By deriving the overall weighted acceleration at the hand, subjected to the handle excitation from the power tool, the exposure time that may be required for developing VWF among a probable percentage of population can be extrapolated from the dose-response relationship.

The dose-response relationship yields the probability associated with acquiring the VWF based upon the years of exposure and level of weighted hand-transmitted vibration. Figure 4.9 illustrates the weighting filter characteristics and the weighting factors corresponding to various third-octave center frequencies which are listed in Table 4.1. The overall weighted hand-transmitted acceleration is then obtained from:

$$a_{h,w} = \sqrt{\sum_{j=1}^{m} (k_j a_{h,j})^2} \tag{4.6}$$

where $a_{h,w}$ is the overall weighted rms acceleration, k_j is the weighting factor corresponding to the j^{th} 1/3 octave frequency band, $a_{h,j}$ is the rms acceleration corresponding to j^{th} 1/3-octave band and m is the number of 1/3 octave bands used.

The dose-response relationship is derived based on the overall weighted acceleration measured at the handle. Since the hand-arm and hand-arm-isolator models yield the acceleration response of the hand-mass, the dose-response relationship cannot be applied to assess the effectiveness of the isolator. An examination of the response characteristics of the hand-arm model illustrated in Figure 4.3, however, reveals that the hand-response closely follows the handle excitation with only little attenuation upto 200 Hz. Further the weighting factor, k_j, beyond the frequency of 200 Hz approaches values well below 0.1. The contribution due to higher frequency acceleration response may thus be considered relatively small. The overall weighted hand acceleration response may thus be used in conjunction with the dose-response relationship to assess the effectiveness of the isolator

in terms of the latent period. It must be emphasized, however, the dose-response relationships have been proposed for use with the acceleration levels measured at the handle alone. In this study, the dose-relationship is used in conjunction with the hand-mass acceleration, to obtain a preliminary relative assessment of the isolator.

Equations (4.4) and (4.6) are solved to determine the overall weighted hand-transmitted acceleration. The overall weighted acceleration is then assessed using the dose-response relationship to derive the number of years of exposure that may lead to a risk of acquiring the VWF. Table 4.2 illustrates the overall weighted hand acceleration, the probable percentage of population that may acquire VWF and number of years of exposure leading to the symptoms. The overall weighted hand acceleration of models 1 and 2 are quite similar, 6.336 and 6.84 m/s^2, respectively. A comparison of the overall weighted acceleration with the dose-response relationship yields the number of years of exposure and probable percentage of population that can acquire VWF symptoms, as shown in Table 4.2. As an example, the response characteristics of both models reveal that 50% of the population of workers exposed to vibration due to an orbital-sander are at a risk of acquiring VWF with 12-13 years of exposure. While the two models yield similar number of years of exposure associated with different percentages of population that may acquire VWF symptoms, the years of exposure for model 2 are relatively less than those for model 1. The higher risk associated with the response characteristics of model 2 is associated with higher levels of transmitted vibration due to high magnitude palm grip.

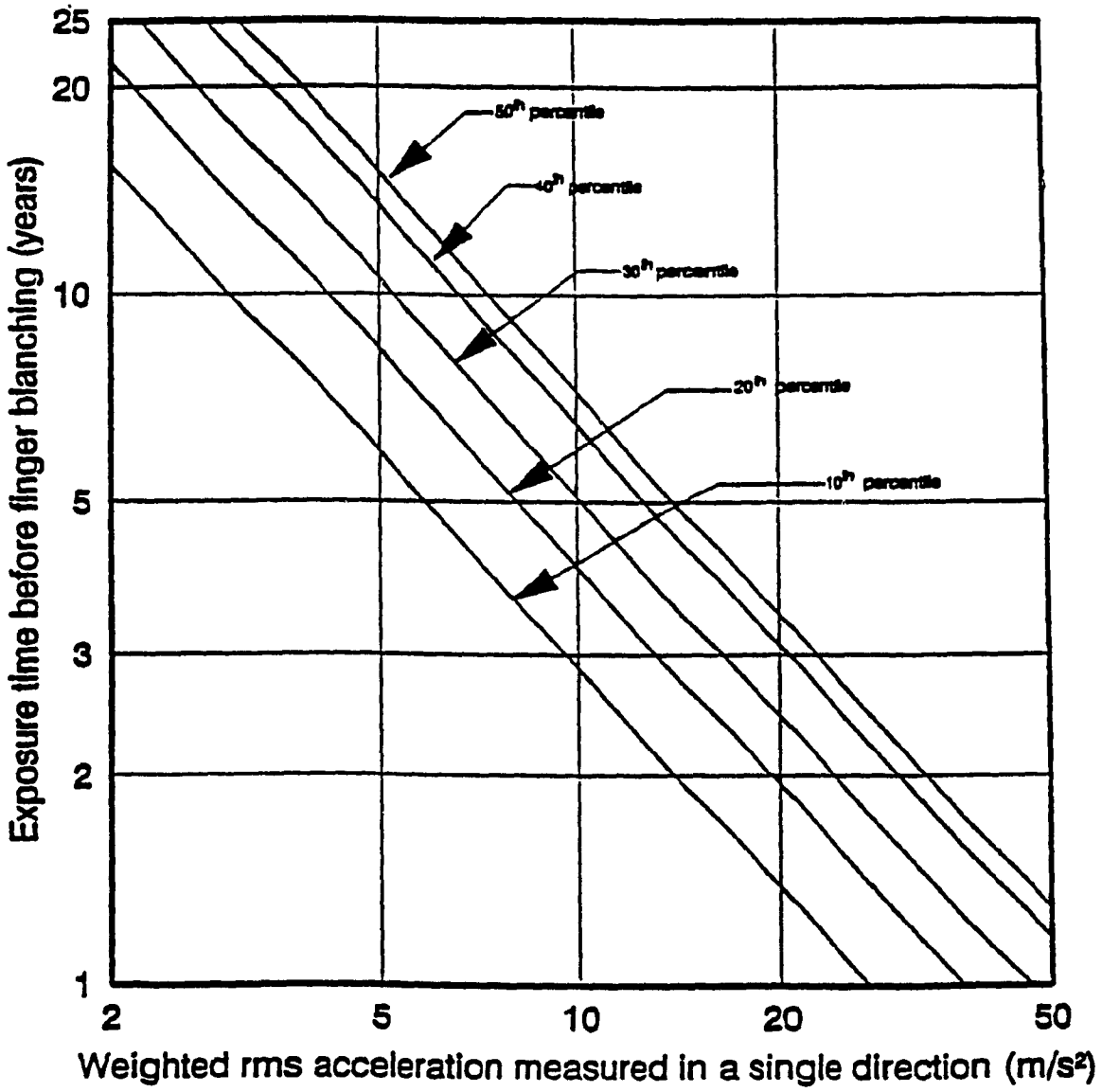

Figure 4.8: Dose-response relationship of hand vibration and prevalence of VWF as proposed by ISO [23]

Table 4.1: Weighting factor for 1/3 octave band frequencies and exposure limit values for vibration acceleration in the 1/3 octave band as proposed by ISO [77]

Third octave band center Frequency (Hz)	Weighting factor (k_j)	RMS acceleration exposure limit values in m/s^2
10.0	1.0	0.8
12.5	1.0	0.8
16.0	1.0	0.8
20.0	0.8	1.0
25.0	0.63	1.3
31.5	0.5	1.6
40.0	0.4	2.0
50.0	0.3	2.5
63.0	0.25	3.2
80.0	0.2	4.0
100.0	0.16	5.0
125.0	0.125	6.3
160.0	0.1	8.0
200.0	0.08	10.0
250.0	0.063	12.5
315.0	0.05	16.0
400.0	0.04	20.0
500.0	0.03	25.0
630.0	0.025	31.5
800.0	0.02	40.0
1000.0	0.016	50.0

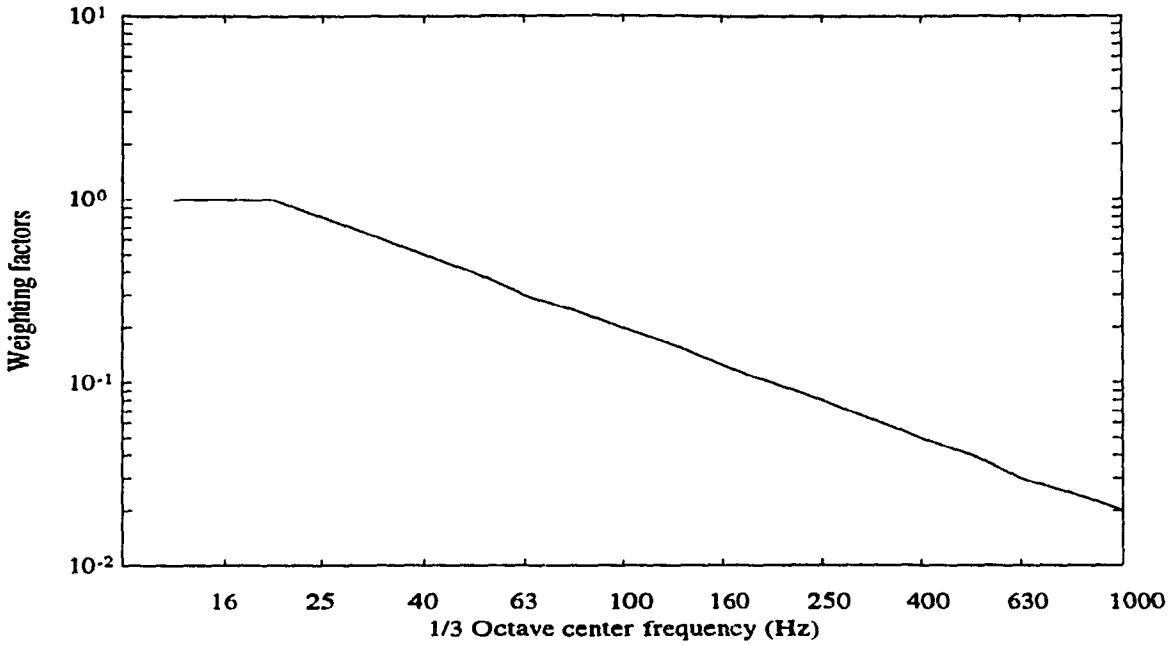

Figure 4.9: Weighting factors for different third octave bands as proposed by ISO [23]

Table 4.2: Weighted hand acceleration and corresponding degree of risk of acquiring VWF

Tool and Model		Overall Weighted acceleration at the hand	Probable percentage of population that may acquire VWF				
			10%	20%	30%	40%	50%
			Years of exposure prior to VWF symptoms				
Palm grip orbital sander	Model 1	6.3359	4.9	7.24	8.96	11.38	13.1
	Model 2	6.8373	4.62	6.72	8.45	10.34	12.06

4.4 Control of Hand-Transmitted Vibration

High levels of hand-transmitted vibration and severe health and safety risks associated with the prolonged exposure have prompted numerous studies to design effective tools and vibration isolators. The effectiveness of various anti-vibration hand gloves in reducing the vibration intensity at the hand have been thoroughly investigated [48,54]. Theses studies have concluded that the gloves do not attenuate the handle vibration. In certain cases, the gloves tend to amplify the handle vibration transmitted to the hand and lead to loss of dexterity. Consequently attention has been directed in developing the vibration isolation mechanisms either at the handle bars [29] or at the hand-handle interface [30].

The general methods employed to attenuate the vibration are:

1. Implementing vibration isolators, in the form of elastomers or springs between the engine and the handles.
2. Dynamic balancing of the rotating components of the power tools.
3. Using vibration absorbing materials on the power tool handles or antivibration gloves.

The effectiveness of the vibration isolators using the first method, integrated within the tools, has been demonstrated for some tools. The method, however, involves extensive redesign for tools where the handle is designed to be a part of the motor. A need to develop hand or handle vibration isolators has thus been strongly emphasized in the literature [50,76].

4.4.1 Concept of a Hand Vibration Isolator

The analytical and experimental results presented in this dissertation reveal that majority of the high frequency vibration remain limited to the hand. Relieving the high intensity of vibration from the hand can significantly enhance the operator safety by reducing the risks associated with occurrence of VWF among the operators. A concept of a coupled hand-arm vibration isolator, referred to as the energy flow divider, is thus proposed. The energy flow divider comprises two rigid links coupled through a parallel combination of energy restoring and dissipative elements. The flow divider, when attached between the hand and the elbow joint, permits the flow of the portion of vibration energy through the links. Figure 4.10 illustrates the schematic of the proposed vibration isolator. The flow divider thus offers potentials to reduce the vibration of the hand. While the energy directed through the divider links is partially dissipated within the isolator, a part of the vibration energy is directly injected to the elbow joint. The vibration levels at the elbow joint may thus be expected to increase. Although an increase in the vibration at the other parts of the arm is not desirable, a compromise may be achieved by tuning the flow divider parameters to attain an optimum exchange of vibration energy between the hand and the other parts of the arm.

4.4.2 Development of the Hand-Arm-Flow Divider Model

The coupled hand-arm and the isolator system is modeled as an in-plane six-degrees-of-freedom (DOF) dynamical system, subjected to longitudinal (Z_h) handle vibration. Figure 4.11 illustrates the in-plane lumped parameter model of the human hand-arm with the proposed flow divider mechanism. Physically the flow divider mechanism may comprise rigid linkages with a visco-elastic material possessing the necessary elastic and energy dissipating properties, which connects hand to the elbow. The flow divider, shown in Figure 4.10 is modeled as a lumped mass (M^*) with identical visco-elastic

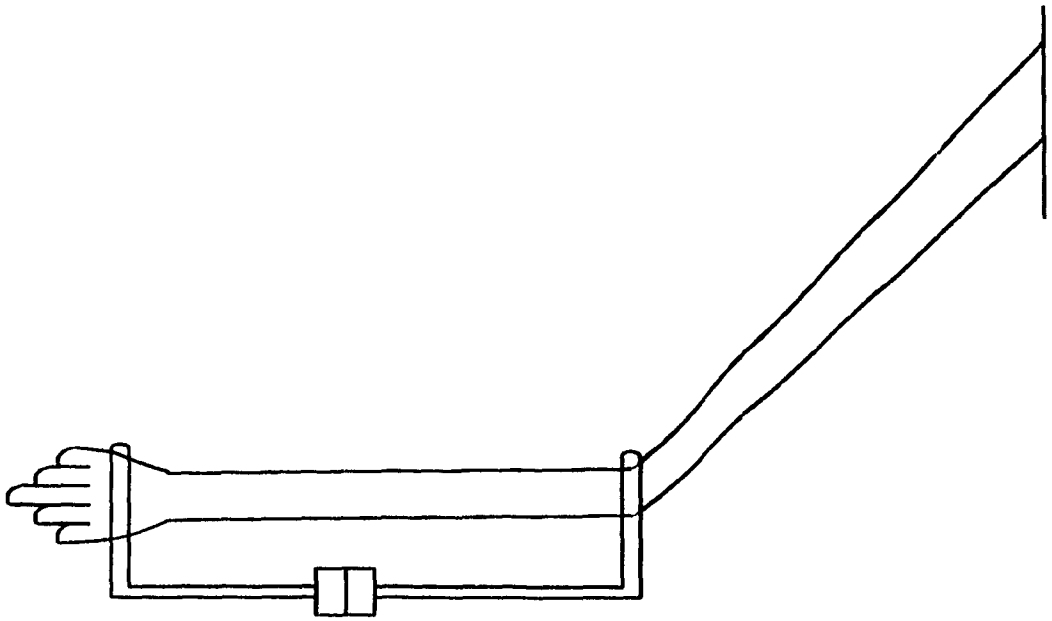

Figure 4.10: Physical representation of hand arm system with the flow divider

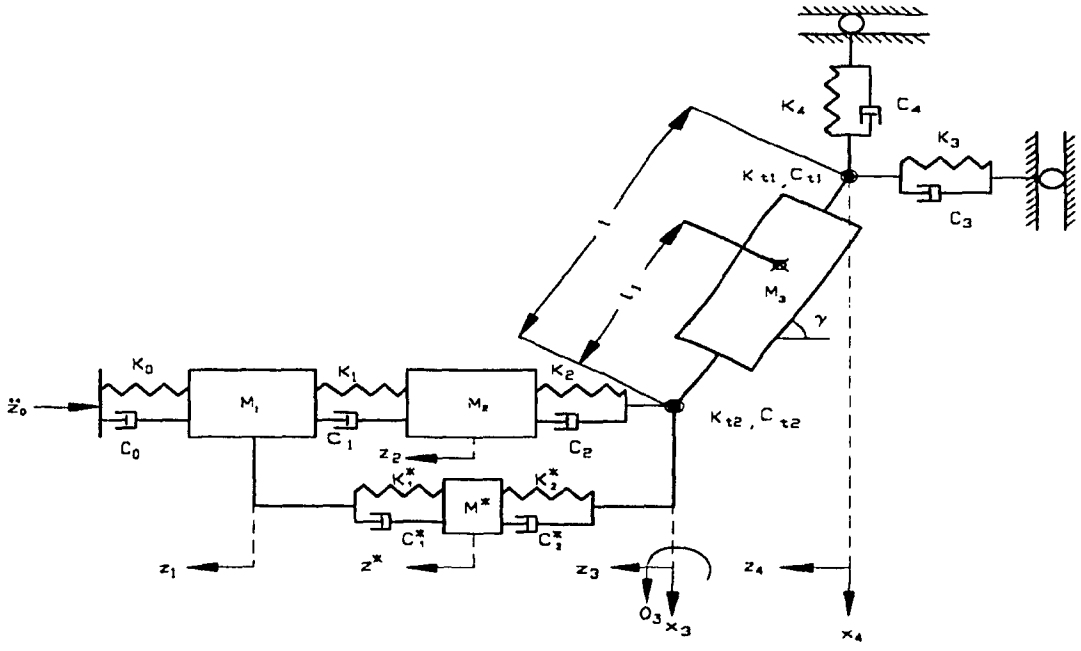

Figure 4.11: Hand arm vibration model with the flow divider

properties coupling the links attached to hand and the elbow. The differential equations of motion for the model, derived subject to the assumptions discussed in Chapter 2, can be summarized as follows:

$$M_1\ddot{z}_1 + C_0\dot{z}_1 + C_1(\dot{z}_1 - \dot{z}_2) + C_1^*(\dot{z}_1 - \dot{z}^*)$$
$$K_0 z_1 + K_1(z_1 - z_2) + K_1^*(z_1 - z^*) = C_0\dot{z}_0 + K_0 z_0 \tag{4.7}$$

$$M_2\ddot{z}_2 + C_1(\dot{z}_2 - \dot{z}_1) + C_2(\dot{z}_2 - \dot{z}_3) + K_1(z_2 - z_1) + K_2(z_2 - z_3) = 0 \tag{4.8}$$

$$M_3\ddot{z}_3 \quad + M_3 l_{31} sin\gamma\ddot{\theta}_3 + C_2(\dot{z}_3 - \dot{z}_2) + C_3[\dot{z}_3 + l\dot{\theta}_3 sin\gamma]$$
$$K_2(z_3 \quad - z_2) + K_3[z_3 + l\theta_3 sin\gamma] + C_2^*(\dot{z}_3 - \dot{z}^*) + K_2^*(z_3 - z^*) = 0 \tag{4.9}$$

$$M_3\ddot{x}_3 - M_3 l_{31} cos\gamma\ddot{\theta}_3 + C_4[\dot{x}_3 - l\dot{\theta}_3 cos\gamma] + K_4[x_3 - l\theta_3 cos\gamma] = 0 \tag{4.10}$$

$$(J_c + M_3 l_{31}^2)\ddot{\theta}_3 + M_3 l_{31} sin\gamma\ddot{z}_3 - M_3 l_{31} cos\gamma\ddot{x}_3 + C_3 l sin\gamma\dot{z}_3$$
$$-C_4 l cos\gamma\dot{x}_3 + \left[\left(C_3 sin^2(\gamma) + C_4 cos^2\gamma\right) l^2 + C_{t_1} + C_{t_2}\right]\dot{\theta}_3$$
$$+K_3 l sin\gamma z_3 - K_4 l cos\gamma x_3$$
$$+ \left[\left(K_3 sin^2\gamma + K_4 cos^2\gamma\right) l^2 + K_{t_1} + K_{t_2}\right]\theta_3 = 0 \tag{4.11}$$

$$M^*\ddot{z}^* + C_1^*(\dot{z}^* - \dot{z}_1) + C_2^*(\dot{z}^* - \dot{z}_3) + K_1^*(z^* - z_1) + K_2^*(z^* - z_3) = 0 \tag{4.12}$$

where $K_1^* = K_2^* = K^*/2$ and $C_1^* = C_2^* = C^*/2$

4.4.3 Tuning of the Energy Flow Divider

The effectiveness of the proposed isolator, based upon the concept of energy flow divider, is related to its mass, stiffness and damping parameters. Since the isolator, is

attached to the operator's hand and arm, its mass must be constrained to a reasonable value. The tuning of the flow divider parameters thus involves the selection of its stiffness and damping values such that the hand vibration can be effectively attenuated with minimal increase in the elbow vibration.

Equations (4.7) to (4.12) are solved to determine the rms longitudinal acceleration responses of the hand and the elbow for handle vibration presented in Figure 4.2. The overall weighted accelerations of the hand mass and the elbow joint are evaluated using the weighting factors described in Table 4.1. In order to select optimal isolator parameters, an optimization function is formulated to minimize the weighted sum of weighted hand and elbow acceleration response:

$$F(\overline{X}) = Minimize\,[\alpha_1 W_1 + \alpha_3 W_3] \tag{4.13}$$

where $\{\overline{X}\}$ is the vector of design variables M^*, K^* and C^*. W_1 and W_3 are the overall weighted accelerations transmitted to the hand mass and elbow joint, respectively, derived using Equation (4.6). α_1 and α_3 are the respective weighting factors such that $\alpha_1+\alpha_3 = 1$. $F(\overline{X})$ is the objective function to be minimized . The objective function is minimized using the sequential search optimization algorithm [75], subject to following equality and inequality constraints.

$$M^* = 0.5kg$$

$$K^* > 0.$$

$$C^* > 0.$$

The optimal parameters of the proposed isolator are strongly related to the weighting factors (α_1) and (α_3). A unit value of $\alpha_1(\alpha_3 = 0)$ minimizes the overall weighted acceleration of the hand, while the weighted acceleration of the elbow joint remains unconstrained. Alternatively, a unit value of $\alpha_3(\alpha_1 = 0)$ will yield minimum weighted acceleration of

elbow joint. Adequate values of α_1 and α_3 thus need to be selected to achieve minimal weighted acceleration of both the hand and the elbow joint. The optimization is performed for different values of α_1 and α_3, and the results are analyzed to identify the appropriate values such that the weighted acceleration of hand is minimized with the minimal increase in the elbow acceleration. Each optimization search is performed for 10 different starting values of the design vector, in order to approach the global optimum. For a selected set of weighting factors, majority of the searches converged to similar design parameters. The optimization search is then repeated for different values of the weighting factors. Figure 4.12 illustrates the weighted accelerations of the hand, fore-arm and elbow as a function of the weighting factors. While the hand acceleration decreases with increase on α_1, the fore-arm and elbow acceleration increase with increase in α_1. The response characteristics of model 2 reveal that fore-arm and elbow accelerations are quite similar for $\alpha_1 \leq 0.9$. The fore-arm acceleration response of model 1, however, is considerably larger than that of the elbow, as shown in Figure 4.12. A compromise among the hand, fore-arm and elbow acceleration may be achieved by selecting the weighting factors corresponding to the intersection of the weighted acceleration response characteristics. Since the acceleration response of the elbow is lower than that of the fore-arm for all values of α_1 the corresponding intersection of the hand and fore-arm acceleration response may be selected. The weighting factors and the corresponding optimal parameters are summarized in Table 4.3. The results presented in Table 4.3 reveal that a lightly damped and high natural frequency coupler is well suited to reduce the hand vibration under light finger grip. High magnitude palm grip, however, necessitates a relatively soft flow divider with higher energy dissipating capacity.

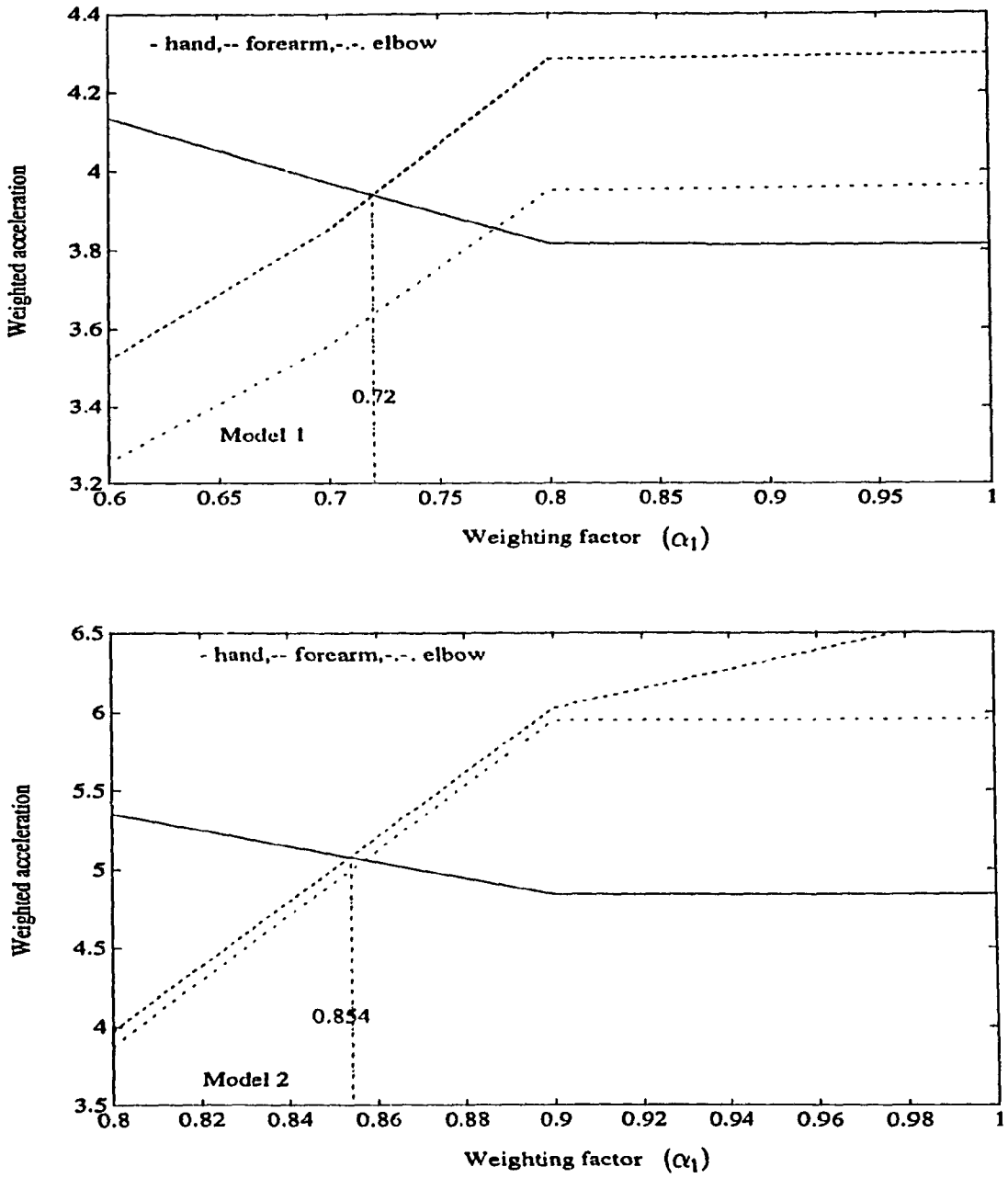

Figure 4.12: Effect of weighting factor (palm grip orbital sander)

Table 4.3: Comparison of the weighted acceleration of HAV models with and without flow divider

Name of the tool		Optimum weighting factor		Optimum flow divider parameters		Overall Weighted acceleration		
		α_1	α_3	$K^* \times 10^5$ N/m	$C^* \times 10^2$ N-sec/m	Hand	Forearm	Elbow
Palm grip orbital sander	Model 1	0.72	0.28	100.0	0.001	6.3359+	3.1157+	3.1534+
						3 81756X	4.2783X	3.9474X
	Model 2	0.854	0.146	0.001	9.3825	6.8373+	3.4909+	3 5275+
						5.3447X	4.0147X	3 9096X

+ without flow divider X with flow divider

4.4.4 Discussion of the Effectiveness of the Flow Divider Mechanism

The hand-arm vibration models coupled with optimal energy flow divider mechanism are solved to yield the overall weighted acceleration of the hand and the elbow joint. The overall weighted acceleration of the hand is compared to that obtained without the energy flow divider to determine the effectiveness of the proposed energy flow divider. The hand-transmitted vibration, with and without the energy flow divider, are further assessed using the dose-response relationship. Figure 4.13 illustrates the rms acceleration response of the model 1 with and without energy flow divider, together with the handle excitation. A comparison of the vibration response with the ISO proposed exposure limits reveals that the hand-transmitted vibration response, without flow divider, exceeds the exposure limits in the 10-160 Hz frequency range. With the energy flow divider, the hand-transmitted vibration exceed the proposed limits only in the 10-40 Hz frequency range with vibration at 125 Hz slightly above the exposure limit. While the addition of flow divider reduces the hand-transmitted vibration in almost the entire frequency

range, the magnitude of vibration transmitted to the fore-arm and the elbow increases considerably. The flow divider tends to increase the hand-transmitted vibration at low frequencies (below 25 Hz). The hand-transmitted vibration response of the model 1 with the energy flow divider, however, is observed to be within the proposed exposure limits at frequencies above 40 Hz. The vibrations transmitted to the fore-arm and elbow, increase considerably in the entire frequency range. Although the exposure limits for the vibration transmitted to the fore-arm and elbow have not yet been established, the vibration levels are similar to those transmitted to the hand and within the proposed limits for the hand vibration.

Figure 4.14 illustrates the rms acceleration response characteristics of the hand-arm model 2 with and without the flow divider mechanism. A comparison of the hand-transmitted vibration response, without the flow divider, with the ISO proposed limits reveals that the vibration levels exceed the limits in the entire 10-160 Hz frequency range. While the flow divider effectively reduces the magnitude of hand-transmitted vibration, the vibration levels exceed the proposed limits in the 10-63 Hz and 100-150 Hz frequency bands. A comparison of Figures 4.13 and 4.14 shows that the flow divider is relatively less effective with model 2, which is attributed to increased grip force and the palm grip used in model 2. The corresponding increase in the vibration levels transmitted to fore-arm and the elbow, however, is relatively less than that observed for model 1.

The effectiveness of the proposed energy flow divider is further investigated by assessing the overall weighted acceleration response with respect to the dose-response relationship. The overall weighted acceleration of the hand, fore-arm and the elbow of the two models with and without the flow divider are compared in Table 4.3. For light finger grip, the energy flow divider tends to reduce the overall weighted hand acceleration by nearly 40%. The overall weighted acceleration of the fore-arm and the elbow joint, however, increase by approximately 36% and 25%, respectively. For high magnitude palm-grip, the overall weighted acceleration of the hand decreases by nearly 22%, when

the proposed energy flow divider is introduced. The corresponding increases in the fore-arm and elbow accelerations are approximately 13% and 10%, respectively.

Table 4.4 illustrates the effectiveness of the energy flow divider in terms of the degree of risk of acquiring the VWF. The overall weighted hand acceleration is assessed with respect to the dose-response relationship to derive the probable percentage of population that may acquire VWF and the corresponding number of years of exposure. High levels of weighted vibration transmitted to the hand yield a high prevalence of VWF in a relatively short period. The interacting relationship between the prevalence of VWF, weighted acceleration and the latent period is described in the ISO-5349 [23] and illustrated in Figure 1.4 and Table 1.3. The effectiveness of the proposed energy flow divider thus can be demonstrated through examination of the latent period. The results, summarized in Table 4.4, clearly illustrate that the latent period is increased considerably with the use of flow divider. For light finger grip (model 1), 10% of population exposed to orbital sander handle vibration for an average of 4 hours or more per day, is likely to develop VWF in 4.9 years. With the use of the flow divider, however, the period required for developing the VWF to same percentage of population increases to 8.96 years. The use of the flow divider with high magnitude palm-grip (model 2) also yields an increase in the latent period, although the flow divider is relatively less effective. The latent period for 10% of the population of workers likely to acquire VWF, increases from 4.62 years to 5.86 years, when the flow divider is introduced. The reduced effectiveness is due to the increased hand vibration caused by increased grip force and coupling of the hand with the vibrating handle due to palm grip.

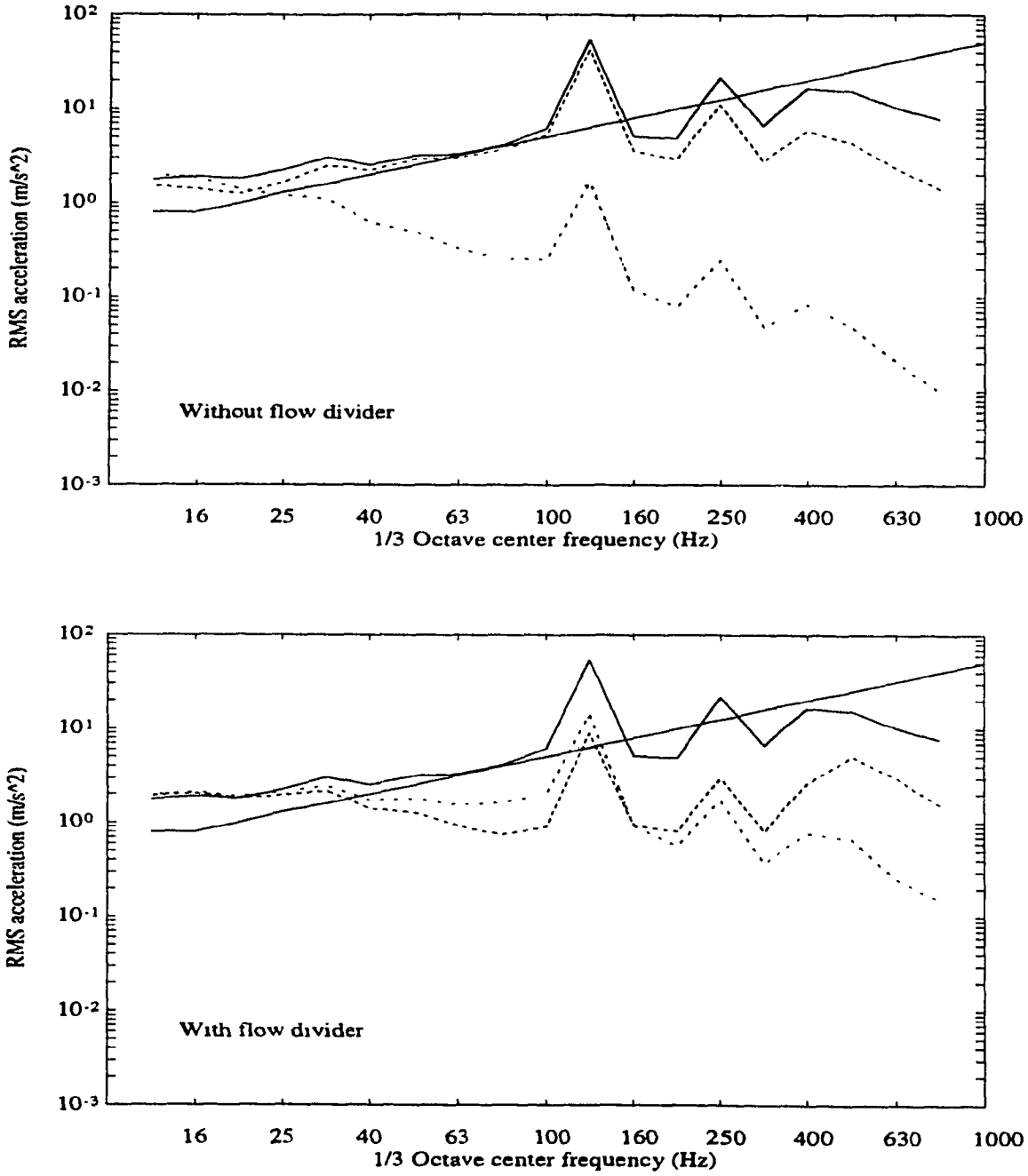

Figure 4.13: Comparison of RMS spectra in 1/3 octave band of handle vibration of palm grip orbital sander and its corresponding response of hand-arm model(1) without and with flow divider

(z_0 —, z_1- - -,z_2 — · — ·—, z_3 · ··)

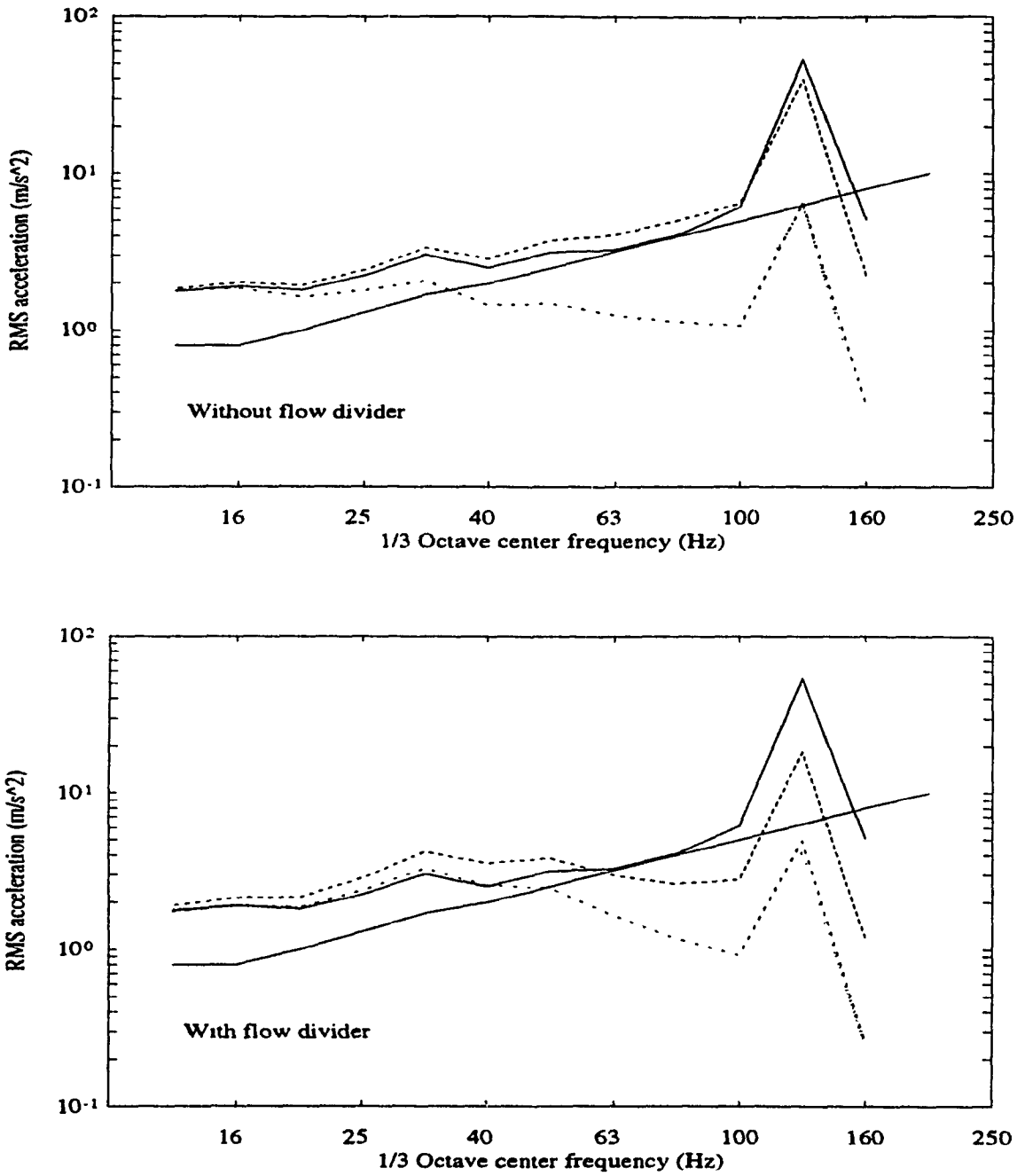

Figure 4.14: Comparison of RMS spectra in 1/3 octave band of handle vibration of palm grip orbital sander and its corresponding response of hand-arm model(2) without and with flow divider

(z_0 —, z_1- - -,z_2 — · — ·—, z_3 · ··)

Table 4.4: Degree of risk of acquiring VWF with and without flow divider

Tool and Model		Without flow divider					With flow divider				
		Probable Percentage of population that may acquire VWF					Probable Percentage of population that may acquire VWF				
		10%	20%	30%	40%	50%	10%	20%	30%	40%	50%
		Years of exposure Prior to VWF symptoms					Years of exposure Prior to VWF symptoms				
Palm grip orbital sander	Model 1	4.9	7.24	8.96	11.38	13.1	8.96	13.1	16.20	20.0	22.5
	Model 2	4.62	6.72	8.45	10.34	12.06	5.86	8.45	10.0	13.45	15.17

4.5 Summary

The vibration response characteristics of the hand-arm models, subjected to field measured stochastic excitations from a palm grip orbital sander, are evaluated. The vibration transmitted to the hand is observed to follow the excitations very closely up to 200 Hz, and considerable vibration attenuation is observed at higher frequencies. Vibration transmitted to the fore-arm and the elbow, is attenuated significantly beyond 20 Hz. The localization of transmitted vibration to the hand at higher excitation frequencies is thus illustrated. Further the vibration transmitted to the shoulder was observed to be insignificant. The hand-transmitted vibration is assessed using the ISO proposed vibration exposure limits and it is concluded that the hand-transmitted vibration exceeds the ISO proposed limits. An assessment using the proposed dose-response relationship revealed that 10% of the population of workers exposed to vibration due to an orbital sander in their occupation is likely to acquire VWF in 4-5 years. The latent period for the 50%

population of workers are likely to acquire VWF in 12-13 years range. A vibration isolator, based upon the concept of energy flow division is proposed and analyzed. The response characteristics of the coupled isolator-hand-arm model are evaluated using the exposure limits and the dose-response relationship. The results clearly illustrated that the proposed isolator can reduce the levels of hand-transmitted vibration considerably. The vibration transmitted to the fore-arm and elbow, however, may increase. The major highlights and conclusions of this investigation are summarized in the following Chapter.

Chapter 5

Conclusions and Recommendations for the Future Work

5.1 Major Highlights of the Investigation

The primary objective of this dissertation research was to contribute to the attainment of a safer operating environment for operators of hand-held power tools through systematic studies on: (i) enhancement of an understanding of the tool vibration transmitted to the human hand-arm; (ii) development and analysis of the hand-arm vibration models; and (iii) analysis of vibration isolation concepts.

The major highlights of this investigation are summarized as follows:

1) The human hand-arm subject to handle vibration in the longitudinal direction is characterized by a five-DOF in-plane bio-mechanical model. Parameters of the proposed model are identified by reducing the error between the measured and analytical transmissibility characteristics using an optimization algorithm.

2) Laboratory tests are performed to establish the vibration transmissibility characteristics of the human hand-arm system for 25 N palm grip force and discrete sinusoidal excitations. The measured data are analyzed to derive the vibration transmitted to the hand, fore-arm and the elbow.

3) Parameters of two hand-arm vibration models are identified using the measured data for light finger grip (8.9 N) and high magnitude palm grip (25 N). The validity of the analytical models is demonstrated by comparing the analytical results with the measured data.

4) The influence of elbow angle, grip type and grip force on the transmission of vibration to the human hand-arm system is investigated.

5) A complex modal analysis is performed to enhance an understanding of the vibration patterns of the human hand-arm. A methodology of deriving the mode shapes from the complex eigenvectors is described and corresponding mode shapes of the hand-arm vibration models are formulated.

6) The hand-arm vibration models subject to stochastic vibration excitations from an orbital sander are analyzed.

7) A hand vibration isolator, based upon the concept of energy flow division, is proposed. The coupled hand-arm-isolator is analytically modeled and represented by a six-DOF in-plane dynamical system.

8) A constrained optimization problem is formulated to tune the isolator parameters, such that the magnitude of hand-transmitted vibration is minimized with minimal increase in the vibration transmitted to the fore-arm and the elbow. The vibration isolator parameters are identified for light finger-type and high level palm grip.

9) The effectiveness of the vibration isolator is demonstrated by comparing the vibration response characteristics of the coupled hand-arm-isolator model to those of

the hand-arm model.

10) A methodology to assess the occupational health and safety risks due to the hand-transmitted vibration is described. The dose-response relation is employed to determine the number of years of exposure prior to risk of acquiring the VWF.

5.2 Conclusions

Following conclusions are drawn from the analytical and experimental studies performed in this dissertation research:

- The vibration transmissibility characteristics measured in the laboratory, revealed that less than 20% of impinged vibration is transmitted to the fore-arm and the elbow above 100 Hz, irrespective of the grip-type and grip-force. Amplification of vibration transmitted to the hand, under palm grip, can be observed in the 20-90 Hz excitation frequency range.

- The optimization technique of reducing the error between the measured and analytical vibration transmissibility can be conveniently used to identify the parameters of the hand-arm vibration models. It is concluded that the proposed models accurately describe the vibration transmitted to hand, fore-arm, elbow and shoulder under light finger grip and high magnitude palm-grip.

- The measured vibration data revealed that the human hand-arm can be characterized by a heavily damped dynamical system. The various resonances of the hand-arm system were identified in the 5-20 Hz, 50-70 Hz and 80-150 Hz frequency ranges. The damped resonant frequencies of the proposed models, identified from the complex eigenvalue analysis, were observed to lie close to the above frequency ranges.

- The comparison of the damping parameters representing the upper-arm with that of the fore-arm and hand of the developed models, indicated the high energy dissipating nature of the upper-arm. This explains for very little transmission of vibration to the shoulder, as demonstrated by the experimental and analytical response of the hand-arm subject to deterministic and field measured stochastic excitations.

- The complex eigenvalue analysis of the developed model indicated that the hand-arm system is highly damped system, with presence of some overdamped modes. Further the deflection mode shapes indicated that lower resonances are more harmful to the fore-arm and upper-arm, while the deflection of the hand mass corresponding to middle resonances were considerably large. The shoulder deflection were observed to be large near the high frequency resonances.

- The vibration transmitted to the hand-arm is strongly influenced by the grip type and grip force. The magnitude of hand-transmitted vibration under high palm grip force is considerably larger than that transmitted under light finger grip. An increase in the grip force tends to increase the vibration transmitted to the hand-arm system.

- The elbow angle (angle between the horizontal axis passing through the fore-arm and the axis passing through the upper-arm) has no pronounced effect on the transmission of vibration. Nevertheless as the arm is stretched (low elbow angles), it is observed that there is a reduction of longitudinal vibration transmitted to the hand, fore-arm and elbow and an increase in the transmitted vibration to the shoulder in the lower frequency range (< 100 Hz).

- The visco-elastic parameters and response characteristics, both revealed that the hand acts as a low pass filter to the rest of the hand-arm system with most of the vibration energy localized to the hand itself at higher excitation frequencies.

- The magnitude of hand-transmitted vibration under stochastic excitations from the power tool (orbital sander) is considered and is found to exceed the ISO proposed exposure limits. The vibration transmitted under high palm grip were observed to be considerably more severe than under light finger grip.

- The isolator mass should be limited to a convenient value such that it won't interfere with the operator's task. The visco-elastic parameters of the isolator need to be tuned for the handle vibration of specific tools.

- While the effectiveness of the proposed isolator in reducing the hand-transmitted vibration is clearly demonstrated, the corresponding levels of vibration transmitted to the fore-arm and elbow joint are observed to increase.

- The proposed energy flow divider mechanism is effective in attenuating the levels of hand transmitted vibration under light finger grip. The energy flow divider tends to reduce the overall weighted acceleration of hand transmitted vibration by nearly 40%, with corresponding increase in the overall weighted acceleration at the fore-arm and elbow around 36% and 25%, respectively.

- For light finger grip it is revealed from the dose-response relationship that 10% of the population of workers exposed to vibration due to an orbital sander in their occupation are likely to acquire VWF in 4-5 years. Also it is assessed that 50% of the population of workers are likely to develop VWF in 13-14 years. With introduction of the flow divider the latent period for 10% of the population is increased by 83% and for 50% of the population to 71.75%.

- For high palm-grip force, the proposed isolator resulted in reduction in the hand-transmitted vibration by approximately by 22% with corresponding increase in the fore-arm and elbow vibration of approximately 13% and 10% respectively.

- Also a similar assessment using the dose-response relationship that 10% of the population exposed to orbital vibration are likely to acquire VWF in 4-5 years and

50% of the population of workers are likely to develop VWF in 12-13 years. Again the use of flow divider increases the latent period by 27% and 26% respectively.

- From the tuning of parameters of the flow divider mechanism it is revealed that lightly damped and high natural frequency coupler is suited to reduce hand vibration for light finger grip. The soft flow divider with high energy dissipating capacity is found to be suitable for the high magnitude palm grip. In general the proposed vibration isolator is found to be more effective for a light finger grip than a high palm grip. This may be due to increased coupling of the hand with the vibrating handle because of the high grip force and more area of contact due to the palm grip.

5.3 Recommendations for Future Work

The validity of the models proposed in this study is demonstrated for longitudinal tool vibration in the vicinity of selected grip force and type of grips. Further the validation under more realistic palm grip is performed through laboratory measurements on a single subject only. Since the hand-transmitted vibration is dependant upon many subject and tool-related parameters, further studies involving a wider range of subjects and tools are extremely important. Apart from the longitudinal tool vibration, the magnitude of vertical vibration (X_h) transmitted to the hand-arm is known to be significant in certain tools. An extension of the analytical model, proposed in this study is thus essential to assess the severity of coupled longitudinal and vertical vibration. The model can further serve as an important tool to explore different vibration isolation concepts. The longitudinal-vertical dynamic model of the hand-arm necessitates the inclusion of additional rotational DOF due to wrist, elbow and shoulder joints.

Accurate measurement of vibration transmitted to different locations of the hand-

arm necessitates development of effective sensors and attachment techniques. Non-contacting laser based sensors may be explored to measure vibration transmitted to the elbow and shoulder joints.

The effectiveness of the vibration isolator demonstrated in this analytical study needs to be substantiated through laboratory experiments. A laboratory prototype must be fabricated with different possible attachment techniques and tests be performed under varied range of operating conditions.

Concepts of passive or active vibration isolation mechanisms, integrated within the hand-held power tools, must be explored to reduce the magnitude of handle vibration. Such tool vibration isolators are considered extremely desirable since they do not interfere with the operator's task. The operating speed of the hand-held power tools must be selected such that it does not correspond with the predominant resonant frequencies of the hand-arm system.

Bibliography

[1] Loriga G., *Pneumatic Tools: Occupation and Health*, Ball. Inspect. Lorboro, 2, 35-37, 1911.

[2] Hamilton A., *A study of Spastic Anemia in the Hands of Stonecutters: An effect of the Air Hammer on the Hands of Stonecutters*, Industrial Accidents and Hygiene Series, Bulletin 236, No.19, U.S.D.O.L, Bureau of Labor Statistics, 53-66, 1918.

[3] Rothstein T., *Report of the physical findings in eight stonecutters from the limestone region of Indiana*, Industrial Accidents and Hygiene series, Bulletin 236, U.S.D.O.L, Bureau of Labor Statistics, 67-96, 1918.

[4] Leake J.P., *Health hazards from the use of the air hammer in cutting Indianna limestone*, Industrial Accidents and Hygiene series, Bulletin 236, U.S.D.O.L, Bureau of Labor statistics, 100-113, 1918.

[5] Taylor, W., and Pelmear, P.L., (eds) *Vibration white finger in industry*, Academic press, London, 1975.

[6] Cannon, L.J., Berknaeki E.J and Walter S.D., *Personal and Occupational Factors Associated with Carpal Tunnel Syndrome*, Journal of Occupational Medicine 23:255-258, (1981).

[7] Rothfleisch, S., and Sherman, D., *Carpal Tunnel Syndrome, Biomedical Aspects of Occupational Occurrence and Implications Regarding Surgical Management*, Orthop. Rev 7:107-109, (1978).

[8] Pyykkö, I., *Vibration Syndrome a Review*, Vibration and work proceedings of the Finnish-Soviet-Scand. Symposium, 1-24, 1975.

[9] Pyykkö, I., *Clinical aspects of the hand arm vibration syndrome*, Sca. J. Work Envi. & Health, 12(4),439-47, 1986.

[10] Taylor, W. and Brammer, A.J., *Vibration effects on the hand and arm in industry: An introduction and review*, Vibration Effects on the Hand and Arm in Industry, Edited by A.J. Brammer and W. Taylor., John Wiley and Sons, Newyork, 1-12, 1982.

[11] Teleky L., *Pneumatic tools*, Occ.Health, 1, 1-12, 1938.

[12] Banister, P.A., and Smith F.W., *Vibration induced white fingers and manipulative dexterity*, Brit. Journal of indust. Medi. 29, 264-67, 1972.

[13] Farkkila M., *et al.*, *Vibration induced decrease in muscle force in lumberjacks*, Eur. J. App. Physio, 43,1-9, 1980.

[14] Iwata, H., *Effects of Rock Drills on operators, Part 3. Joint and Muscle pain and Deformity of Bone and Joint*, Industrial Health 6: 47-58, 1968.

[15] Kumlin, T. *et al.*, *Radiological changes in carpal and metacarpal bones and phalanges caused by chain saw vibration*, Brit. Journal of Indus. Medic., 30,71-73,1973.

[16] Bovenzi, M., *et al.*, *Epidemiological survey of shipyard workers exposed to Hand Arm Vibration*, Int. Arch. Occup. Envi. Health, 46, 251-256, 1980.

[17] Klimkov-Deutschova E., *Neurologische aspekte der vib. krankheit*, Arch. Gewerbepath. Gewerbehyg. 22, 297-305, 1966.

[18] Griffin, M.J., *Vibration injuries of the hand and arm; Their occurrence and the evaluation of standards and limits*, Health and Safety Executive, Research Paper No. 9, London, England, 1980.

[19] Habu, K., *Electromyographic studies of the upper extremities under static and vibration loading*, Z Arb. Wiss, 36, 185-188, 1984.

[20] Wasserman, D., *et al.*, *Industrial Vibration - An overview*, Journal of American society of Safety Engineers, 19, 38-43, 1974.

[21] Brammer A. J., *Exposure of the hand to vibration in industry*, NRC, Canada, NRCC No. 22844, 1984.

[22] Gurram, R., *A study of Vibration Response Characteristics of the Human Hand Arm System*, Ph.D dissertation, Concordia University, 1993.

[23] ISO 5349 Mechanical vibration - Guidelines for the measurement and the assessment of human exposure to hand transmitted vibration.

[24] Brammer, A.J., and Taylor, W., *Vibration effects on the hand and arm in industry: An introduction and review*, John Wiley & Sons, NewYork, 1982.

[25] Griffin, M. J., *Some problems associated with the formulation of human response to vibration*, In : W.Taylor, ed. The vibration syndrome, Academic press, London, 1974.

[26] Reynolds, D.D., *Hand -arm vibration: A review of three year's research*, Proceedings of the International Hand-Arm Vibration Conference, Cincinnati, Ohio, U.S.A, 99-129,1977.

[27] Taylor, W., and Pealmear, P.L., *Vibration White Finger in Industry*, A report comprising edited versions of papers submitted to the Department of Health and Social Security, 1973.

[28] Suggs, C.W., Hanks, J.M., and Roberson, G.T., *Vibration of power tool Handles*, In Brammer AJ and Taylor W, eds., Vibration effects on the Hand and Arm in industry, New York, Wiley, 245-251, 1982.

[29] Miwa T., *Vibration - Isolation systems for Hand - Held vibrating tools*, In Brammer AJ. and Taylor W, eds., Vibration effects on the Hand and Arm in industry, New York, Wiley, 303-310, 1982.

[30] Suggs C.W., and Hanks J.M., *Resilient Hand grips*, In A.J. Brammer and W. Taylor eds., Vibration effects on the Hand and Arm in Industry, New York, Wiley, 333-337, 1982.

[31] Reynolds, D.D., and Angevine, E.N., *Hand Arm Vibration, part II : Vibration Transmission characteristics of the hand and arm*, Journal of sound and vibration, 51(2), 255-265, 1977.

[32] Pyykö I., Farkkila, M., Toivanen, J., Korhonen, O., and Hyvarinen, J., *Transmission of vibration in the hand - arm system with special reference to change in compression force and acceleration*, Scandinavian Journal of work, Environment and Health, 2,87-95, 1976.

[33] Aatola, S., *Transmission of vibration to the wrist and compression of frequency response and comparison of frequency estimators*, Journal of Sound and Vibration, 131(3), 497-507, 1989.

[34] Hartung, E., Dupuis, H., and Scheffer, M., *Acute effects of vibration depending on different coupling forces of the hand*, International Conference of Hand-Arm vibration, 437-449, 1992.

[35] Abrams, C.F Jr., and Suggs C.W , *Chain saw vibration, Isolation and Transmission through the Human Arm*, Transactions of the ASAE, 423-425, 1969.

[36] Abrams C.F., *A study of the transmission of high frequency vibration in the human arm.* Masters thesis. North Carolina University, Raleigh, 1968.

[37] Griffin, M.J., Macfarlane, C.R., and Norman, C.D., *The transmission of vibration to the hand and the influence of gloves*, A.J. Brammer and W. Taylor eds., Vibration Effects on the Hand and Arm in Industry, John Wiley & Sons, Newyork, 103-116, 1982.

[38] Abrams, C.F., *Modeling the vibrational characteristics of the human hand by driving point mechanical impedance method*, Ph.D thesis, North Carolina State University, Raleigh, 1971.

[39] Reynolds, D.D., *Three and Four degree of freedom models of vibration response of the human hand* in Brammer and Taylor ed. Vibration effects on the hand arm in industry, 117-132, 1982.

[40] Reynolds, D.D., and Charles Jokel., *Hand-Arm Vibration–An Engineering approach*, American Industrial Hygiene Association Journal, 613- 622, 1974.

[41] Mishoe, J.W., and Suggs, C.W., *Hand arm vibrational part II: Vibrational responses of the human hand*, Journal of Sound and Vibration 53(4), pp. 545-558, 1977.

[42] Wood, L.A., Suggs, C.W., Distributed parameter dynamic model of the human forearm. Proceedings of the international occupational hand arm vibration conference, Cincinnati, Ohio, U.S.A, pp 142-145, 1977.

[43] Meltzer G. et. al., Ein mathematisches schwingungsmodel fur das menschliche hand arm system. Maschinenbautechnik 29,2 Seite 54-58, 1980.

[44] Fritz, M., Simulation of the Hand arm vibration by means of a Bio-mechanical model, *International series on Bio-mechanics*, Edited by Gert de Groot et al., Free University press, Amsterdam volume 7-a, 456-460, 1987.

[45] Politschuk, A.P., and Oblivin, V.N., *Methods of reducing the efforts of noise and vibration on power saw operators*, Proceedings of International occupational Hand - Arm Vibration Conference, Cincinnati, Ohio, U.S.A, 230-232, 1977.

[46] Suggs, C.W., and Abrams Jr. C.F., *Vibration Isolation of Power tool operators*, Proceedings of the Human Factors Society, 27^{th} Annual meeting, 1983.

[47] Miwa, T., Yonekawa, Y., Nara A., Kanada, K., and Baba, K., *Vibration isolation gloves for portable vibrating tools part 4: Vibration Isolation gloves*, Industrial Health (Japan), 17, 141-152, 1979.

[48] Macfarlane CR., *The vibrational response of gloves and the human hand and arm*, United Kingdom Informal Group Meeting on Human Response to Vibration, Royal Aircraft establishment, Farnborough, 1979.

[49] Suggs, C.W., Abrams, C.F. Jr., and Cundiff, J.S., *Attenuation of high frequency vibration in chain saws*, Journal of Sound and Vibration, 2(6), 1968.

[50] Miwa, T., *Design of vibration isolators for hand - held vibrating tools*, Third international Symposium of Hand - Arm Vibration, Ottawa, 4, 1981.

[51] Macfarlane CR., *Antivibration gloves and the dynamic response of the human hand-arm*, United Kingdom Informal Group Meeting on Human Response to Vibration. Univ. College, Swansea, 1980.

[52] INRS., cahierde Notes Documentaires, ND 409 -110-83, 47-52,1983.

[53] Clarke, J.B., and Dalby, W., *Noise vibration control*, 16, 146-149, 1985.

[54] Rens G., Dubrulle P., and Malchaire J., *Efficiency of Conventional Gloves against vibration*, Ann.Occp.Hyg., Vol 31, No.2, 249-254, 1987.

[55] Reynolds, D.D ., and Wilson F.L, *Mechanical test stand for measuring the vibration of chain saw handles during cutting operations*, Vibration effects on the hand and arm in industry edited by A.J Brammer, W., and Taylor., 1982.

[56] Radwin, Robert G., Armstrong, Thomas J., and Vanbergeijk, Ernst., *Vibration Exposure for selected power hand tools used in Automobile Assembly*, American Industrial Hygiene Association Journal, 51(9): 510-518 (1990).

[57] Francis S.T ., Ivan E.M ., and Rolland T.H ., *Mechanical vibrations, Theory and applications*, Allyn and Bacon Inc., 1978.

[58] Gurram, R., Rakheja, S., Gouw, G.J., *Parameter Identification of Hand-Arm Vibration (HAV) Models Using Non-linear optimization techniques*, Sixth International Conference on Hand-Arm Vibration, 713-726, 1992.

[59] Newland D.E., *Mechanical vibration Analysis and Computation*, New York, Wiley, 1989.

[60] Radwin, Robert G., Armstrong, Thomas J., *Assessment of Hand vibration exposure on an Assembly line*, American Industrial Hygiene Association Journal 46(4):211-219(1985).

[61] Thomson, T. W., *Theory of vibration with applications*, Prentice hall, Englewood Cliffs, N.J., 1988.

[62] Vernon, James D., *Linear vibration and control system theory, with computer applications*, Wiley, New York, 1967.

[63] Vernon, James D., *Linear vibration theory generalized properties and numerical method*, Wiley, New York, 1967.

[64] Boileau, P.-E., Boutin, J., and Drouin, P., *Experimental validation of a wrist measurement method using Laser Interferometry*, Proceedings of 6^{th} international conference on hand - arm vibration, Bonn, Germany, 519-527, 1992.

[65] Inman, Daniel J., *Vibration with control measurement and stability*, Prentice-Hall, Inc., Englewood Cliffs, New Jersey, 1989.

[66] Williams, M., and Lissner R.H., *Bio-mechanics of Human Motion*, W.B. Saunders Company, 1962.

[67] Dempster W., *Space requirements of the seated operator*, WADC Technical report, 55:159, 1955.

[68] Page, R.L., *The physics of Human Movement*, A. Wheaton and Company Limited, 1978.

[69] Ghista, Dhanjoo N., *Human Body Dynamics: impact,occupational, and athletic aspects*, Clarendon press, Oxford, 1982.

[70] McConnell, Kenneth G., *Notes on Vibration Frequency Analysis*, A society for experimental stress analysis, Education committee project, spring annual meeting, 1989.

[71] Crandall, H.S., *Random Vibration*, Volume 2, M.I.T Press, 1963.

[72] Del Pedro, Michel., and Pahud Pierre., *Vibration Mechanics*, Klawer Academic Publishers, 1993.

[73] Hatter, D.J., *Matrix Computer Methods of Vibration Analysis*, John Wiley & Sons, New York, 1973.

[74] Foss, K.A., *Co-ordinates which uncouple the Equations of Motion of Damped Linear Dynamic systems*, Journal of Applied Mechanics, 361-364, 1958.

[75] IMSL 1988: IMSL is a trade mark of IMSL, Inc., Texas, USA.

[76] Rodgers, L.A., Eglin, D., and Hart, W.F.D., *Rock-Drill Vibration and White Fingers in Miners*, In A.J. Brammer and W. Taylor eds., Vibration effects on the Hand and Arm in industry, New York, Wiley, 317-323, 1982.

[77] Guide for the measurement and the evaluation of human exposure to vibration transmitted to the hand. International Standard Organization Draft Proposal No. 5349, ISO TC 108/SC4/WG3, (1978).

Appendix A

Terminology

Artery	Tubes conveying blood from the heart
Acroparesthia	Numbness, tingling and other abnormal sensations of one or more of the extremities
Anatomic	Similar to the bodily structure
Blanching	Finger look white and pale
Carpal tunnel syndrome	Phenomena which results in sensory loss over the median nerve distribution in the fingers
Caulkers	Group of workers who are engaged in filling or closing of seams or joint in marine vessels
Cyanotic	A dark bluish or purplish coloration of the skin deficient oxygenation of the blood
Cysts	Abnormal sac containing gas, fluid or semisolid material
Dexterity	Skill in handling the things
Epidemiology	The study of the prevalence and spread of disease in community
Episodic	Sporadic; occurring irregularly; incidental
Ischemic	Local anemia (a condition due to the insufficient

	oxygenation of the blood) due to mechanical obstruction (mainly arterial narrowing) to the blood supply
Insomnia	Condition leading to sleeplessness
Necrosis	Death of piece of bone or tissue
Numbness	Deprived of feeling or power of motion
Percussive	Forcible striking of one body against another
Phalanges	Bone between two joints of the fingers
Spasm	Sudden involuntary muscular contraction
Tingling	Slight pricking or stinging sensation
Traumatic	Causing trauma (Unpleasant)
Ulna	Bone of the forearm on the side opposite to the thumb
Vacuoles	Tiny cavity in organ or cell containing air or fluid
Vascular	Containing vessels for conveying blood

Appendix B

Mass, Stiffness and Damping Matrix of 5dof Hand-Arm Model

B.1 Mass Matrix

$$\begin{bmatrix} M_1 & 0 & 0 & 0 & 0 \\ 0 & M_2 & 0 & 0 & 0 \\ 0 & 0 & M_3 & 0 & M_3 l_1 \sin\gamma \\ 0 & 0 & 0 & M_3 & -M_3 l_1 \cos\gamma \\ 0 & 0 & M_3 l_1 \sin\gamma & -M_3 l_1 \cos\gamma & J_c + M_3 l_1^2 \end{bmatrix}$$

B.2 Stiffness Matrix

$$\begin{bmatrix} K_0 + K_1 & -K_1 & 0 & 0 & \\ -K_1 & K_1 + K_2 & -K_2 & 0 & \\ 0 & -K_2 & K_2 + K_3 & 0 & K_3 l \sin\gamma \\ 0 & 0 & 0 & K_4 & -K_4 l \cos\gamma \\ 0 & 0 & K_3 l \sin\gamma & -K_4 l \cos\gamma & (K_3 \sin^2\gamma + K_4 \cos^2\gamma) l^2 + K_{t_1} + K_{t_2} \end{bmatrix}$$

B.3 Damping Matrix

$$\begin{bmatrix} C_0 + C_1 & -C_1 & 0 & 0 & 0 \\ -C_1 & C_1 + C_2 & -C_2 & 0 & 0 \\ 0 & -C_2 & C_2 + C_3 & 0 & C_3 l \sin\gamma \\ 0 & 0 & 0 & C_4 & -C_4 l \cos\gamma \\ 0 & 0 & C_3 l \sin\gamma & -C_4 l \cos\gamma & (C_3 \sin^2\gamma + C_4 \cos^2\gamma) l^2 + C_{t_1} + C_{t_2} \end{bmatrix}$$

Appendix C

Mass, Stiffness and Damping Matrix of 6dof Hand-Arm-Isolator Model

C.1 Mass Matrix

$$\begin{bmatrix} M_1 & 0 & 0 & 0 & 0 & 0 \\ 0 & M_2 & 0 & 0 & 0 & 0 \\ 0 & 0 & M_3 & 0 & M_3 l\sin\gamma & \\ 0 & 0 & 0 & M_3 & -M_3 l\cos\gamma & 0 \\ 0 & 0 & M_3 l\sin\gamma & -M_3 l\cos\gamma & J_c + M_3 l^2 & 0 \\ 0 & 0 & 0 & 0 & 0 & M^* \end{bmatrix}$$

C.2 Stiffness Matrix

$$\begin{bmatrix} K_0 + K_1 + K_1^* & -K_1 & 0 & 0 & 0 & -K_1^* \\ -K_1 & K_1 + K_2 & -K_2 & 0 & 0 & 0 \\ 0 & -K_2 & K_2 + K_3 + K_2^* & 0 & K_3 l\sin\gamma & -K_2^* \\ 0 & 0 & 0 & K_4 & -K_4 l\cos\gamma & 0 \\ 0 & 0 & K_3 l\sin\gamma & -K_4 l\cos\gamma & (K_3\sin^2\gamma + K_4\cos^2\gamma)l^2 + K_{t_1} + K_{t_2} & 0 \\ -K_1^* & 0 & -K_2^* & 0 & 0 & K_1^* + K_2^* \end{bmatrix}$$

C.3 Damping Matrix

$$\begin{bmatrix} C_0 + C_1 + C_1^* & -C_1 & 0 & 0 & 0 & -C_1^* \\ -C_1 & C_1 + C_2 & -C_2 & 0 & 0 & 0 \\ 0 & -C_2 & C_2 + C_3 + C_2^* & 0 & C_3 l \sin\gamma & -C_2^* \\ 0 & 0 & 0 & C_4 & -C_4 l \cos\gamma & 0 \\ 0 & 0 & C_3 l \sin\gamma & -C_4 l \cos\gamma & (C_3 \sin^2\gamma + C_4 \cos^2\gamma) l^2 + C_{t_1} + C_{t_2} & 0 \\ -C_1^* & 0 & -C_2^* & 0 & 0 & C_1^* + C_2^* \end{bmatrix}$$

Appendix D

Closed Form Solution of the Uncoupled First Order Complex Differential Equation

The uncoupled first order complex differential equation is

$$M_i\dot{q}_i + K_i q_i = H_{i0}sin(\omega t)$$

where H_{i0} is complex in nature.

Homogeneous part of the equation is

$$M_i\dot{q}_i + K_i q_i = 0$$

The solution is

$$q_i = Be^{-\lambda_i t}$$

$$where \qquad \lambda_i = \frac{K_i}{M_i}$$

Forced response

Since the excitation is sinusoidal

$$M_i\ddot{q}_i + K_i q_i = H_{i0} sin(\omega t)$$

$$M_i\ddot{q}_i + K_i q_i = \frac{H_{i0}}{2i}[e^{i\omega t} - e^{-i\omega t}]$$

Total response is the sum of the individual responses,

$$q_i = q_{i01}e^{i\omega t} + q_{i02}e^{-i\omega t}$$

In order to obtain the first term of the response, assume

$q_{i1} = q_{i01}e^{i\omega t}$

Substituting in the differential equation,

$$iM_i\omega q_{i01}e^{i\omega t} + K_i q_{i01}e^{i\omega t} = \frac{H_{i0}}{2i}e^{i\omega t}$$

$$q_{i01} = \frac{H_{i0}}{2i}\left[\frac{1}{K_i + iM_i\omega}\right]$$

Similarly for the second term of the response

$$q_{i02} = \frac{H_{i0}}{2i}\left[\frac{1}{K_i - iM_i\omega}\right]$$

Hence,

$$q_i = \frac{H_{i0}}{2i}\left[\frac{e^{i\omega t}}{K_i + iM_i\omega} + \frac{e^{-i\omega t}}{K_i - iM_i\omega}\right]$$

$$= \frac{-iH_{i0}}{2}\left[\frac{(K_i - iM_i\omega)e^{i\omega t} - (K_i + iM_i\omega)e^{-i\omega t}}{K_i^2 + M_i^2\omega^2}\right]$$

$$= \frac{-iH_{i0}}{2(K_i^2 + M_i^2\omega^2)} [(K_i - M_i\omega)(cos\omega t + isin\omega t) - (K_i + M_i\omega)(cos\omega t - isin\omega t)]$$

After simplification the final expression is as follows

$$= \frac{H_{i0}}{K_i^2 + M_i^2\omega^2} [K_i sin\omega t - M_i\omega cos\omega t]$$

The complete response is $q_i = q_i(Homogeneous) + q_i(Forced)$

$$q_i = Be^{-\lambda_i t} + \frac{H_{i0}}{K_i^2 + M_i^2\omega^2} [K_i sin\omega t - M_i\omega cos\omega t]$$

For the system starting from rest

$$q_i = \begin{Bmatrix} V_i \\ X_i \end{Bmatrix} = \begin{Bmatrix} 0 \\ 0 \end{Bmatrix}$$

Therefore $B = \frac{H_{i0}}{K_i^2 + M_i^2\omega^2} M_i\omega$

The total solution is

$$q_i = \frac{H_{i0}}{K_i^2 + M_i^2\omega^2} \left[M_i\omega(e^{-\lambda_i t} - cos\omega t) + K_i sin\omega t\right]$$

Appendix E

Eigenvalues and Eigenvectors of Hand-Arm Vibration Models

MODEL 1

EIGENVALUES AND EIGENVECTORS -DAMPED SYSTEM

0.5639008E+02 -0.8135683E+02 (MODE 1)

-0.089406	0.048495
-0.248026	-0.009382
-0.253809	-0.007077
0.187749	0.008561
1.000000	0.000000
0.000922	0.000480
0.001347	0.002109
0.001399	0.002137
-0.001007	-0.001600
-0.005743	-0.008240

0.5638998E+02 0.8135707E+02

-0.089406	-0.048495
-0.248026	0.009382
-0.253809	0.007077
0.187749	-0.008561
1.000000	0.000000
0.000922	-0.000480
0.001347	-0.002109
0.001399	-0.002137
-0.001007	0.001600
-0.005743	0.008240

0.1548614E+03 -0.9483437E+02 (MODE 2)

-0.067083	0.110010
-0.212581	-0.034316
-0.230570	-0.023711
-0.264571	-0.147250
1.000000	0.000000
0.000632	-0.000329
0.000900	0.000774

```
   0.001013     0.000769
   0.000819     0.001455
  -0.004687    -0.002841


0.1548614E+03  0.9483437E+02

  -0.067083    -0.110010
  -0.212581     0.034316
  -0.230570     0.023711
  -0.264571     0.147250
   1.000000     0.000000
   0.000632     0.000329
   0.000900    -0.000774
   0.001013    -0.000769
   0.000819    -0.001455
  -0.004687     0.002841


0.9502402E+03 -0.5359056E+03    (MODE 4)

  -0.003764    -0.001092
   0.027027    -0.023320
  -0.160116     0.010637
   0.075758    -0.009100
   1.000000     0.000000
   0.000003     0.000003
  -0.000032     0.000006
   0.000133     0.000064
  -0.000065    -0.000027
  -0.000798    -0.000450


0.9502404E+03  0.5359060E+03

  -0.003764     0.001092
   0.027027     0.023320
  -0.160116    -0.010637
   0.075758     0.009100
   1.000000     0.000000
   0.000003    -0.000003
  -0.000032    -0.000006
   0.000133    -0.000064
  -0.000065     0.000027
```

```
  -0.000798      0.000450


0.3391313E+03  0.6065091E+03     (MODE 5)

  -0.008828     -0.009560
  -0.076369      0.077444
  -0.000804     -0.043961
   0.081980      0.024208
   1.000000      0.000000
   0.000018     -0.000005
  -0.000044     -0.000150
   0.000056      0.000030
  -0.000088      0.000086
  -0.000702      0.001256


0.3391308E+03 -0.6065106E+03

  -0.008828      0.009560
  -0.076369     -0.077444
  -0.000804      0.043961
   0.081980     -0.024208
   1.000000      0.000000
   0.000018      0.000005
  -0.000044      0.000150
   0.000056     -0.000030
  -0.000088     -0.000086
  -0.000702     -0.001256


0.8106963E+03  0.0000000E+00     (OVERDAMPED MODE 3)

   1.000000      0.000000
  -0.010691      0.000000
  -0.005233      0.000000
   0.002075      0.000000
   0.031535      0.000000
  -0.001233      0.000000
   0.000013      0.000000
   0.000006      0.000000
  -0.000003      0.000000
  -0.000039      0.000000
```

0.1525654E+03 0.0000000E+00

-0.415341	0.000000
-0.229635	0.000000
-0.238287	0.000000
0.002589	0.000000
1.000000	0.000000
0.002727	0.000000
0.001504	0.000000
0.001554	0.000000
-0.000012	0.000000
-0.006508	0.000000

FREQUENCIES IN Hz AND DAMPING RATIOS

UNDAMPED NATURAL FREQUENCY	15.7546	(MODE 1)
DAMPED NATURAL FREQUENCY	12.9483	
DAMPING RATIO	0.569661	
UNDAMPED NATURAL FREQUENCY	28.9012	(MODE 2)
DAMPED NATURAL FREQUENCY	15.0934	
DAMPING RATIO	0.852799	
NATURAL FREQUENCY	173.6286	(MODE 4)
DAMPED NATURAL FREQUENCY	85.2920	
DAMPING RATIO	0.871028	
NATURAL FREQUENCY	110.5942	(MODE 5)
DAMPED NATURAL FREQUENCY	96.5289	
DAMPING RATIO	0.488040	
NATURAL FREQUENCY	55.9728	(OVERDAMPED MODE)
DAMPED NATURAL FREQUENCY	0.0000	
DAMPING RATIO	1.369485	

MODEL 2

EIGENVALUES AND EIGENVECTORS -DAMPED SYSTEM

0.1034802E+03 0.7041057E+02 (MODE 1)

-0.000096	0.026951
-0.292743	0.012851
-0.297429	0.009385
0.000000	0.000000
1.000000	0.000000
-0.000082	-0.000197
0.001884	-0.001403
0.001946	-0.001420
0.000000	0.000000
-0.006935	0.004713

0.1034803E+03 -0.7041061E+02

-0.000096	-0.026951
-0.292743	-0.012851
-0.297429	-0.009385
0.000000	0.000000
1.000000	0.000000
-0.000082	0.000197
0.001884	0.001403
0.001946	0.001420
0.000000	0.000000
-0.006935	-0.004713

0.1315766E+02 0.1620938E+03 (MODE 2)

-0.000001	0.000001
0.000000	0.000000
0.000000	0.000000
1.000000	0.000000
0.000001	0.000000
0.000000	0.000000
0.000000	0.000000

```
   0.000000      0.000000
  -0.000497      0.006129
   0.000000      0.000000


0.1315730E+02 -0.1620938E+03

  -0.000001     -0.000001
   0.000000      0.000000
   0.000000      0.000000
   1.000000      0.000000
   0.000001      0.000000
   0.000000      0.000000
   0.000000      0.000000
   0.000000      0.000000
  -0.000497     -0.006129
   0.000000      0.000000


0.2695249E+03  0.5140115E+03   (MODE 3)

   1.000000      0.000000
  -0.142004      0.210729
  -0.139518      0.276829
   0.000000      0.000000
   1.030750     -0.499676
  -0.000777      0.001471
  -0.000199     -0.000403
  -0.000311     -0.000442
   0.000000      0.000000
  -0.000189      0.002316


0.2695250E+03 -0.5140116E+03

   1.000000      0.000000
  -0.142004     -0.210729
  -0.139518     -0.276829
   0.000000      0.000000
   1.030750      0.499676
  -0.000777     -0.001471
  -0.000199      0.000403
  -0.000311      0.000442
   0.000000      0.000000
```

```
  -0.000189    -0.002316


0.1188026E+04 -0.5202563E+03   (MODE 4)

  -0.017811    -0.003619
   0.044827    -0.007057
  -0.204014    -0.000682
   0.000000     0.000000
   1.000000     0.000000
   0.000011     0.000008
  -0.000034    -0.000009
   0.000144     0.000064
   0.000000     0.000000
  -0.000706    -0.000309


0.1188026E+04  0.5202563E+03

  -0.017811     0.003619
   0.044827     0.007057
  -0.204014     0.000682
   0.000000     0.000000
   1.000000     0.000000
   0.000011    -0.000008
  -0.000034     0.000009
   0.000144    -0.000064
   0.000000     0.000000
  -0.000706     0.000309


0.1617493E+03 -0.6587361E+03  (MODE 5)

  -0.158827     0.049498
  -0.087458    -0.024180
   0.039354    -0.019599
   0.000000     0.000000
   1.000000     0.000000
   0.000124     0.000210
  -0.000005     0.000133
  -0.000042    -0.000048
   0.000000     0.000000
  -0.000335    -0.001439
```

0.1617493E+03	0.6587362E+03
-0.158827	-0.049498
-0.087458	0.024180
0.039354	0.019599
0.000000	0.000000
1.000000	0.000000
0.000124	-0.000210
-0.000005	-0.000133
-0.000042	0.000048
0.000000	0.000000
-0.000335	0.001439

FREQUENCIES IN Hz AND DAMPING RATIOS

NATURAL FREQUENCY	19.9203	(MODE 1)
DAMPED NATURAL FREQUENCY	11.2062	
DAMPING RATIO	0.826763	
NATURAL FREQUENCY	25.8829	(MODE 2)
DAMPED NATURAL FREQUENCY	25.7980	
DAMPING RATIO	0.080907	
NATURAL FREQUENCY	92.3718	(MODE 3)
DAMPED NATURAL FREQUENCY	81.8075	
DAMPING RATIO	0.464387	
NATURAL FREQUENCY	206.4156	(MODE 4)
DAMPED NATURAL FREQUENCY	82.8014	
DAMPING RATIO	0.916017	
NATURAL FREQUENCY	107.9554	(MODE 5)
DAMPED NATURAL FREQUENCY	104.8411	
DAMPING RATIO	0.238462	

Appendix F

Various Stages in Forming Mode Shape Data from Complex Eigenvectors (Model 1)

MODEL 1
STAGE ONE

0.5639008E+02 -0.8135683E+02 (MODE 1)

0.000922	0.000480
0.001347	0.002109
0.001399	0.002137
-0.001007	-0.001600
-0.005743	-0.008240

0.5638998E+02 0.8135707E+02

0.000922	-0.000480
0.001347	-0.002109
0.001399	-0.002137
-0.001007	0.001600
-0.005743	0.008240

0.1548614E+03 -0.9483437E+02 (MODE 2)

0.000632	-0.000329
0.000900	0.000774
0.001013	0.000769
0.000819	0.001455
-0.004687	-0.002841

0.1548614E+03 0.9483437E+02

0.000632	0.000329
0.000900	-0.000774
0.001013	-0.000769
0.000819	-0.001455
-0.004687	0.002841

0.9502402E+03 -0.5359056E+03 (MODE 4)

0.000003	0.000003
-0.000032	0.000006
0.000133	0.000064
-0.000065	-0.000027
-0.000798	-0.000450

0.9502404E+03 0.5359060E+03

0.000003	-0.000003
-0.000032	-0.000006
0.000133	-0.000064
-0.000065	0.000027
-0.000798	0.000450

0.3391313E+03 0.6065091E+03 (MODE 5)

0.000018	-0.000005
-0.000044	-0.000150
0.000056	0.000030
-0.000088	0.000086
-0.000702	0.001256

0.3391308E+03 -0.6065106E+03

0.000018	0.000005
-0.000044	0.000150
0.000056	-0.000030
-0.000088	-0.000086
-0.000702	-0.001256

0.8106963E+03 0.0000000E+00 (OVERDAMPED MODE 3)

-0.001233	0.000000
0.000013	0.000000
0.000006	0.000000
-0.000003	0.000000
-0.000039	0.000000

0.1525654E+03 0.0000000E+00

0.002727	0.000000
0.001504	0.000000
0.001554	0.000000
-0.000012	0.000000
-0.006508	0.000000

MODEL1
STAGE 2

```
0.5639008E+02 -0.8135683E+02      (MODE  1)

   0.000922      0.000480
   0.001347      0.002109
   0.001399      0.002137
  -0.001007     -0.001600
  -0.000083      0.000011
  -0.000151     -0.000373


0.5638998E+02  0.8135707E+02

   0.000922     -0.000480
   0.001347     -0.002109
   0.001399     -0.002137
  -0.001007      0.001600
  -0.000083     -0.000011
  -0.000151      0.000373


0.1548614E+03 -0.9483437E+02       (MODE 2)

   0.000632     -0.000329
   0.000900      0.000774
   0.001013      0.000769
   0.000819      0.001455
  -0.000196      0.000036
   0.001518      0.001878


0.1548614E+03  0.9483437E+02

   0.000632      0.000329
   0.000900     -0.000774
   0.001013     -0.000769
   0.000819     -0.001455
  -0.000196     -0.000036
   0.001518     -0.001878
```

0.9502402E+03 -0.5359056E+03 (MODE 4)

0.000003	0.000003
-0.000032	0.000006
0.000133	0.000064
-0.000065	-0.000027
-0.000073	-0.000053
0.000054	0.000040

0.9502404E+03 0.5359060E+03

0.000003	-0.000003
-0.000032	-0.000006
0.000133	-0.000064
-0.000065	0.000027
-0.000073	0.000053
0.000054	-0.000040

0.3391313E+03 0.6065091E+03 (MODE 5)

0.000018	-0.000005
-0.000044	-0.000150
0.000056	0.000030
-0.000088	0.000086
-0.000125	0.000354
0.000017	-0.000101

0.3391308E+03 -0.6065106E+03

0.000018	0.000005
-0.000044	0.000150
0.000056	-0.000030
-0.000088	-0.000086
-0.000125	-0.000354
0.000017	0.000101

0.8106963E+03 0.0000000E+00 (OVERDAMPED MODE 3)

-0.001233	0.000000
0.000013	0.000000
0.000006	0.000000
-0.000003	0.000000
-0.000004	0.000000
0.000003	0.000000

0.1525654E+03 0.0000000E+00

0.002727	0.000000
0.001504	0.000000
0.001554	0.000000
-0.000012	0.000000
-0.000125	0.000000
0.000957	0.000000

MODEL 1
STAGE 3

0.5639008E+02 -0.8135683E+02 (MODE 1)

0.001039	27.499355
0.002503	57.437462
0.002555	56.783073
0.001891	237.820633
0.000083	172.665863
0.000402	247.893768

0.5638998E+02 0.8135707E+02

0.001039	332.500641
0.002503	302.562531
0.002555	303.216919
0.001891	122.179375
0.000083	187.334137
0.000402	112.106232

0.1548614E+03 -0.9483437E+02 (MODE 2)

0.000712	332.477997
0.001187	40.687382
0.001272	37.205894
0.001670	60.606007
0.000200	169.624771
0.002415	51.055046

0.1548614E+03 0.9483437E+02

0.000712	27.521990
0.001187	319.312622
0.001272	322.794098
0.001670	299.393982
0.000200	190.375229
0.002415	308.944946

```
0.9502402E+03 -0.5359056E+03    (MODE 4)

   0.000004    45.681080
   0.000033   168.630600
   0.000147    25.632557
   0.000070   202.587906
   0.000090   215.628571
   0.000068    36.506542


0.9502404E+03  0.5359060E+03

   0.000004   314.318909
   0.000033   191.369400
   0.000147   334.367432
   0.000070   157.412094
   0.000090   144.371429
   0.000068   323.493469


0.3391313E+03  0.6065091E+03    (MODE 5)

   0.000018   344.604340
   0.000157   253.814011
   0.000063    28.172602
   0.000123   135.641830
   0.000376   109.510391
   0.000103   279.346619


0.3391308E+03 -0.6065106E+03

   0.000018    15.395662
   0.000157   106.185989
   0.000063   331.827393
   0.000123   224.358170
   0.000376   250.489609
   0.000103    80.653397
```

```
0.8106963E+03  0.0000000E+00   (OVERDAMPED MODE 3)

   0.001233   180.000000
   0.000013     0.000000
   0.000006     0.000000
   0.000003   180.000000
   0.000004   180.000000
   0.000003     0.000000


0.1525654E+03  0.0000000E+00

   0.002727     0.000000
   0.001504     0.000000
   0.001554     0.000000
   0.000012   180.000000
   0.000125   180.000000
   0.000957     0.000000
```

MODEL 1
STAGE 4

0.5639008E+02 -0.8135683E+02 (MODE 1)

0.406803	-29.283718
0.979753	0.654388
1.000000	0.000000
0.740224	181.037567
0.032620	115.882790
0.157483	191.110703

0.5638998E+02 0.8135707E+02

0.406803	29.283722
0.979753	-0.654388
1.000000	0.000000
0.740224	-181.037552
0.032620	-115.882782
0.157483	-191.110687

0.1548614E+03 -0.9483437E+02 (MODE 2)

0.294962	281.422943
0.491717	-10.367664
0.526836	-13.849152
0.691432	9.550961
0.082670	118.569725
1.000000	0.000000

0.1548614E+03 0.9483437E+02

0.294962	-281.422943
0.491717	10.367676
0.526836	13.849152
0.691432	-9.550964
0.082670	-118.569717
1.000000	0.000000

```
0.9502402E+03 -0.5359056E+03    (MODE 4)

   0.025218     20.048523
   0.222567    142.998047
   1.000000      0.000000
   0.475382    176.955353
   0.614183    189.996017
   0.460117     10.873985


0.9502404E+03  0.5359060E+03

   0.025218    -20.048523
   0.222567   -142.998032
   1.000000      0.000000
   0.475382   -176.955338
   0.614183   -189.996002
   0.460117    -10.873962


0.3391313E+03  0.6065091E+03   (MODE 5)

   0.048388    235.093948
   0.416707    144.303619
   0.168255    -81.337791
   0.327439     26.131439
   1.000000      0.000000
   0.273034    169.836227


0.3391308E+03 -0.6065106E+03

   0.048388   -235.093948
   0.416707   -144.303619
   0.168255     81.337784
   0.327439    -26.131439
   1.000000      0.000000
   0.273034   -169.836212
```

0.8106963E+03 0.0000000E+00   (OVERDAMPED MODE 3)

1.000000	0.000000
0.010714	-180.000000
0.005185	-180.000000
0.002059	0.000000
0.002909	0.000000
0.002614	-180.000000

0.1525654E+03 0.0000000E+00

1.000000	0.000000
0.551585	0.000000
0.570056	0.000000
0.004520	180.000000
0.045965	180.000000
0.351140	0.000000

MODEL 1
STAGE 5
MODE SHAPE DATA USED FOR PLOTTING THE MODE SHAPES OF HAV MODELS

```
0.5639008E+02 -0.8135683E+02   (MODE 1)

   0.354817
   0.979689
   1.000000
  -0.740103
  -0.014240
  -0.154531


0.5638998E+02  0.8135707E+02

  -0.354817
  -0.979689
  -1.000000
   0.740103
   0.014240
   0.154531


0.1548614E+03 -0.9483437E+02    (MODE 2)

   0.058417
   0.483689
   0.511520
   0.681848
  -0.039535
   1.000000


0.1548614E+03  0.9483437E+02

  -0.058417
  -0.483689
  -0.511520
  -0.681848
   0.039535
  -1.000000
```

```
0.9502402E+03 -0.5359056E+03    (MODE 4)

   0.023690
  -0.177745
   1.000000
  -0.474711
  -0.604860
   0.451855


0.9502404E+03  0.5359060E+03

  -0.023690
   0.177745
  -1.000000
   0.474711
   0.604860
  -0.451855


0.3391313E+03  0.6065091E+03    (MODE 5)

  -0.027689
  -0.338416
   0.025341
   0.293970
   1.000000
  -0.268750


0.3391308E+03 -0.6065106E+03

   0.027689
   0.338416
  -0.025341
  -0.293970
  -1.000000
   0.268750
```

0.8106963E+03 0.0000000E+00 (OVERDAMPED MODE 3)

1.000000
-0.010714
-0.005185
0.002059
0.002909
-0.002614

0.1525654E+03 0.0000000E+00

-1.000000
-0.551585
-0.570056
0.004520
0.045965
-0.351140